The risk of secondary screw perforation in plate osteosynthesis of unstable proximal humerus fractures: prediction and the effect of screw length

Master thesis

by Daniel Ciric

Industry Supervisor: Dr. Peter Varga

Academic Supervisor: Associate Professor John Costi

Submitted to the College of Science and Engineering in partial fulfilment of the requirements for the degree of Master of Engineering (Biomedical) at Flinders University – Adelaide, Australia.

Declaration

I certify that this work does not incorporate without acknowledgment any material previously submitted for a degree or diploma in any university and that to the best of my knowledge and belief it does not contain any material previously published or written by another person except where due reference is made in the text.

Daniel Ciric  (signed 27th May 2019)

First and foremost, I would like to thank Dr. Peter Varga and Associate Professor John J. Costi for supporting me prior to and during my thesis. Without the guidance of these two excellent researchers and mentors, all my work would not have been possible.

I would also like to thank Dominic Mischler for being an amazing long-time friend who has supported me both professionally and personally.

For their surgical expertise, I would like to thank Lisa Wenzel and Feras Qawasmi who brought such valuable components to the projects, those of which could only be realised with their knowledge and talents.

For their support in the work place and technical knowledge, I would like to thank the members of the Biomedical Development department at the AO Research Institute who helped with the project. Boyko Gueorguiev, Ivan Zderic, Dieter Wahl, Usri Eberli and Markus Windolf.

Last but not least, I would like to thank my extended international family who I closely worked and lived with during the project. Ben Burkard, Jan Barcik, Clemens Schopper, Chresche Wapp, Philippa Jörger, Naomi Pötter, Frederick Westbrock, Vicky Panagiotopoulou, Igor Escalante, Yann Ladner, Phillippe Hatt, Guillermo Sanchez, Celine Jana, Despina Stefanoksi, Karen Mys, Bernardo Atunes, and Tino Jucker. I will always treasure my memories with you, from the hiking, skiing and extended coffee breaks.

If I had more time, I would have written a shorter thesis.

Abstract

Proximal humeral fractures (PHF) are the third most common joint fracture and have high rates of mechanical type failures following plating treatment. Secondary screw perforation through the joint is a prominent mechanical type failure requiring reoperation. Identifying what factors influence this, along with pre-operative prediction, could help avoid complications. The work within this thesis investigates the influence that screws tip to joint distance (TJD) has on the biomechanical risk of secondary screw perforation in PHF. Furthermore, a model was established to predict the failure based on bone mineral density and content (BMD) (BMC) and finite element analysis (FEA).

Ten pairs of cadaveric proximal humeri were scanned with high peripheral quantitative computed tomography (HR-pQCT). Specimens were osteotomised and instrumented with the PHILOS plate, simulating a highly unstable 3-part fracture. Bones were randomised into a long screw group (LSG) with 4mm TJD, or a short screw group (SSG) with 8mm TJD. Instrumented specimens were scanned with a clinical computed tomography (CCT) scanner. A custom biomechanical screw perforation setup tested the samples to failure cyclically with a constant valley load and an increasing peak load. Two key cycle events were identified, the screw loosening and the failure event. The cycles to the initial screw loosening event were significantly higher for the LSG compared to the SSG ($p<0.01$). The number of cycles to the failure event was not significantly different between groups ($p=0.5$). Screws with a smaller TJD have better initial stability and resistance against loosening. Longer screws, within limits dictated by the surgical guide, are expected to decrease the risk produced by secondary perforation failures in unstable PHF.

Specimen-specific prediction computer models of the plated humeri were generated from co-registered pre- and post-instrumentation computed tomography (CT) scans and meshed with linear tetrahedral elements using ScanIP. Materials were assumed to be elastic and isotropic. The implant was modeled as titanium; the elastic moduli of bone elements were mapped from the HR-pQCT-based BMD. The experimental setup was mimicked, and quasi-static linear elastic simulations were performed using Abaqus. BMC and average minimum compressive strain were evaluated in cylindrical bone regions around the screw tips. These parameters were correlated with the cycle events to assess their predictive potential. Density-based measures of BMC around the screw tips predicted well the screw loosening and perforation and thus has a high potential for future clinical application and pre-operative planning. The simple strain-based measures computed with linear FE models predicted well the screw loosening, better than BMC. These measures for pre-operative planning are expected to aid in decreasing the failure rate of complex PHF plate fixations. Future studies shall investigate if the BMC data available in CCT scans provides similar prediction strengths. Additionally, non-linear modelling approaches will be applied to improve FE-based predictions.

Table of Contents

List of Figures

List of Tables

Glossary of Terms

AO/OTA – AO Foundation and Orthopeadic Trauma Association

CCT- Clinical computer tomography

CT – Computed tomography

DXA – Dual-energy x-ray absorptiometry

GT – Great tuberosity

HR-pQCT – High-resolution quantitative computed tomography

PHF – Proximal humerus fracture

QCT – Quantitative computed tomography

SD -Standard deviation

SE – Standard error of estimate

TJD – Tip-to-joint distance

List of Publications

Daniel Ciric, Dominic Mischler, Feras Qawasmi, Lisa Wenzel, Boyko Gueorguiev, Markus Windolf, Peter Varga, submitted April 10th, 2019, Secondary perforation risk in plate osteosynthesis of unstable proximal humerus fractures: a biomechanical investigation of the effect of screw length, Journal of Orthopaedic Research, manuscript under review

Conference Abstracts

Daniel Ciric, Dominic Mischler, Feras Qawasmi, Lisa Wenzel, Boyko Gueorguiev, Markus Windolf, Peter Varga, Longer screws do not increase perforation risk in the plating of complex proximal humerus fractures in vitro, 25th Congress of the European Society of Biomechanics, Vienna, Austria, 2019, accepted for podium presentation

Daniel Ciric, Dominic Mischler, Feras Qawasmi, Lisa Wenzel, Boyko Gueorguiev, Markus Windolf, Peter Varga, Predicting cyclic screw perforation in complex proximal humerus fracture plating, 25th Congress of the European Society of Biomechanics, Vienna Austria, 2019, accepted for podium presentation

Lisa Wenzel, Daniel Ciric, Dominic Mischler, Feras Qawasmi, Geoff Richards, Boyko Gueorguiev, Markus Windolf, Peter Varga, Biomechanical investigation of the effect of screw length on screw perforation in unstable 3-part osteoporotic proximal humerus fractures, Deutscher Kongress für Orthopädie und Unfallchirurgie, Berlin, Germany, 2019, accepted for podium presentation

1. Thesis introduction

Proximal humerus fractures (PHF) are the third most frequent fracture related to osteoporosis with an expected increasing incidence due to the ageing population[1–3]. Complex and unstable fractures are the most challenging to treat and are performed conventionally with locking plates[4–10]. However, the rate of mechanical failure of plating is high[6,11,12]. A commonly reported mechanical failure type is secondary screw perforation, where locking head screws in plates puncture the humeral head subchondral bone as a result of the post-operative humeral head collapse. The secondary screw perforation mechanical failure type has been reported commonly in clinical studies as a significant contributor to current challenges faced surgically[12–17]. The studies detailed in this thesis attempt to understand the mechanisms behind secondary screw perforation and the factors that contribute to its occurrence. In this thesis, a thorough literature review was conducted to identify the factors that contribute to secondary screw perforation. Gaps in the currently available research were identified and used to develop the study design. Two complementary studies were conducted: an experimental in vitro biomechanical study that explored the effect of screw length on the perforation, and a computational study. The computational study was validated from the experimental study to develop a prediction model for the mechanical failure type. Finally, the outcomes of the two complementary studies were seperately discussed, compared and the required future works were considered.

1.1 Thesis outline

This thesis investigated factors that influence the mechanical complication of secondary screw perforation associated with plating of PHF. This work was achieved through two major sub-studies (sub-study 1 and sub-study 2) (**Figure 1**).

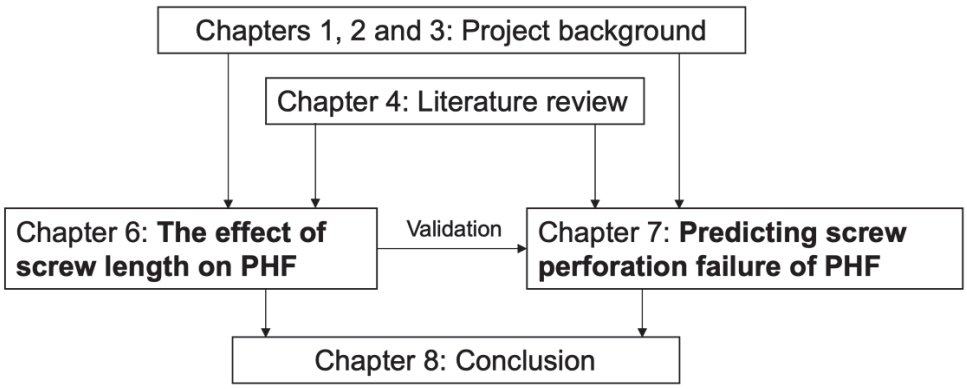

Figure 1. *Master thesis outline and the relation of chapters to each other. Chapters 1, 2 and 3 describe the necessary background information required for the thesis. Chapter 4 describes the existing literature. Chapter 6 and 7 are the two complmentary studies. Chapter 8 concludes the findings of the two complementary studies.*

1.1.1 Sub-study 1: Secondary perforation risk in plate osteosynthesis of unstable proximal humerus fractures: a biomechanical investigation of the effect of screw length

The goal of this sub-study was to understand the influence of screw length on secondary screw perforation of unstable PHF via experimental testing. The methods and results collected from sub-study 1 were used in sub-study 2 to develop a prediction model for secondary screw perforation.

1.1.2 Sub-study 2: Predicting cyclic screw perforation in complex proximal humerus fracture plating

The goal of the sub-study 2 was to develop a validated prediction model for secondary screw perforation using the data collected in the sub-study 1. The prediction models of sub-study 2 are to be incorporated into a larger osteosynthesis toolkit for PHF under development at the AO Research Institute Davos, Davos Switzerland for optimising fracture fixation and surgical outcomes of unstable PHF.

2. Background

2.1 Bone anatomy

The bone of the body under investigation in this thesis is the proximal humerus. The main anatomical features of the proximal humerus are the (1) Humeral head, (2) Anatomical Neck, (3) Surgical Neck, (4) Greater Tuberosity, (5) Lesser Tuberosity, (6) Intertuberous Sulcus, (7) Humeral Shaft (**Figure 2**)[18].

Figure 2. *Anterior (a) and posterior (b) aspects of a left proximal humerus, including label numbers (1) – (7)* [18].

The articular surface is a half spheroid shape on the most medial side of the humeral head and humeral shaft. The surgical neck connects to the proximal end of the humeral shaft which further connects to the anatomic neck. The surgical neck is located distally to the tuberosities across the flare of the metaphyseal and represents

a common location of fractures[19,20]. Superiorly to the surgical neck lies the continuation of the metaphyseal flare and the tuberosities.

The proximal humerus resides within the glenohumeral joint which is lined with articulating cartilage allowing for smooth translation and rotation of the head of the humerus within the glenoid cavity (**Figure 3**).

Image removed due to copyright restriction.

Figure 3. *Radiographic examination of the glenohumeral joint*[21].

2.2 Ligaments and tendons

The glenohumeral joint capsule is composed of three main tissue layers: the inner and outer layer of fibers parallel to the frontal plane from the glenoid to the humerus and the middle layer which has fibers in the direction of the sagittal plane[22]. The greater tuberosity has 3 facets which tendons insert into the bone known as the supraspinatus, infraspinatus and teres minor insertion[23]. These tendons are apart

of the rotator cuff (**Figure 4**) which is complete by the subscapularis tendon inserting into the lesser tuberosity. The subscapularis and supraspinatus are fused with the capsule at the site of their insertion. The rotator cuff encapsulates the glenohumeral joint with a large surface area, twice the size of the humeral head, and contributes to the biomechanics and stability of the proximal humerus[22].

Image removed due to copyright restriction.

Figure 4. *The ligaments of the rotator cuff surrounding the proximal humerus*[23].

2.3 Biomechanics

The biomechanics of the shoulder joint involves complex and dynamic relationships between the articulating surfaces, constraints provided from the ligaments and the forces imposed by the muscles surrounding the glenohumeral joint[24]. The deltoid and rotator cuff muscle are muscles that cover the humerus from the anterior, lateral and posterior sides. The deltoid is the most important abductor of the shoulder joint[22]. The glenohumeral joint has six degrees of freedom, three translational and three rotational (**Figure 5**).

Image removed due to copyright restriction.

Figure 5. *The regions of functional shoulder motion, shaded in yellow, compared with the normal range of motion in (A) forward flexion and extension, (B) abduction, (C) cross-body adduction, (D) and external rotation with the arm abducted at 90 degrees*[25].

Simple descriptions of these motions for the proximal humerus are spinning, sliding and rolling. For motions of spinning, the contact point on the glenoid is the same while the contact point of the humeral head is changing with the rotation[24]. Sliding refers to the translation of the humeral head across the articular surface of the glenoid. The third action of rolling means a combination of humeral head translation and rotation with respect to the glenoid[24]. The glenohumeral joint is the most mobile joint in the body due to combinations of complex mechanical interactions between the humerus, surrounding muscles, and forces generated from the soft tissue[19]. The

main biomechanics of the shoulder joint is provided by ligaments and muscles adjacent from each other. The rotator cuff, both ligaments, and muscles are important in providing the stability of the glenohumeral joint[22]. The muscles will provide stability to glenohumeral joint through the passive muscle tension, contraction that applies compression to the glenohumeral joint. Motion of the glenohumeral joint tightens the ligament constraints and redistribution of forces to the surface of the glenoid through the coordination of the muscles in the shoulders[22].

2.4 Bone distribution

The proximal humerus has a heterogenous bone distribution and comprises of two types of bone, cortical and trabecular. The highest regions of bone mineral density (BMD) in the humeral head are located just beneath the articular cartilage surface of the medial side in the thin subchondral (quasi-cortical) bone[26,27]. The lowest BMD is located towards the central region of the humeral head within the trabecular bone[28]. The highest regions of bone strength are in the medial and dorsal aspects of the humeral head[27,28]. The bone distribution can be seen in tomographic slices of the proximal humerus (**Figure 6**), with the highest bone regions located under the articular surface and lesser regions located towards the centre of the humeral head. From a mechanical standpoint, screws that purchase in the denser bone will have a stronger bone screw interface as opposed to those in lesser bone stock[26].

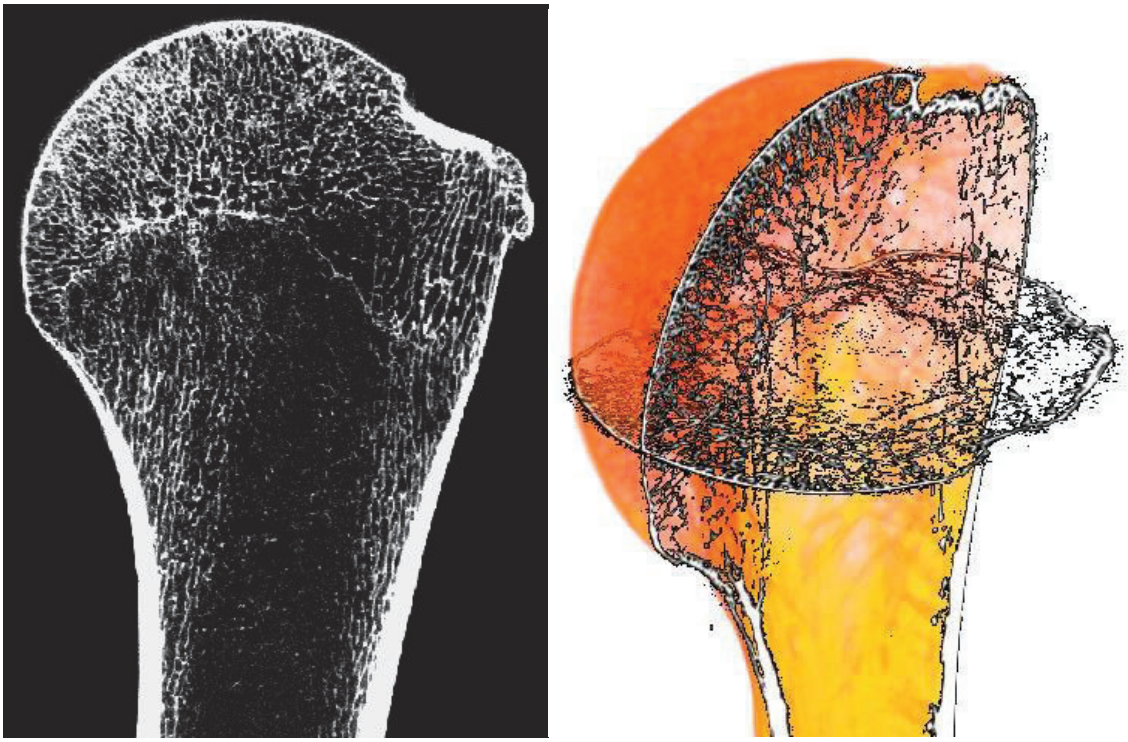

Figure 6. *Tomographic slices of proximal humerus taken on a high resolution peripheral quantitative computed tomography (HR-pQCT) scanner for this thesis and displayed by image processing software Amira.*

2.5 Principles of fractures and fixation of the proximal humerus

Fractures of the proximal humerus are typically classified using a system that Neer introduced in 1970[29]. This system works by identifying anatomical parts that have been displaced from the humerus. Classification of displaced fracture parts aid in surgical decision making and the level of invasiveness for treatment. These displaced fractures are categorised under 2-, 3- and 4-part fractures of the main anatomical features of the proximal humerus: anatomical neck, surgical neck, greater and lesser tuberosity, and articular surface.

Image removed due to copyright restriction.

Figure 7. *Diagram showing Neer Classification for fractures of the proximal humerus*[29].

Another classification system for PHF types is the AO Foundation and Orthopaedic Trauma Association (AO/OTA) fracture and dislocation classification established in 2018[30]. The AO/OTA classification system divides fractures into three groups. The three groups are A, B, and C that all include 2-, 3- and 4- part fractures by Neer classification. Group A fractures are extra-articular and unifocal type fractures, group B fractures are extra-articular, bifocal and 3-part fractures and group C are articular or 4-part fractures[30].

In 1958, the AO Foundation formulated four basic principles to guide internal fixation of fractures: anatomical reduction, stable fixation to provide absolute and

relative stability, early activation of mobilization and rehabilitation of the patient as a whole and preservation of blood supply to the soft tissue at the site of the trauma[31]. Ideally, implants should be further developed to uphold these principles. The Proximal Humeral Internal Locking System (PHILOS)[32] (DePuy Synthes, Zuchwil, Switzerland) (**Figure 8**) is an implant used for plating treatment of challenging PHF. The implant is a locking compression plate with screws that enable angular stability and grip into the osteoporotic bone in fractures with multiple fragments[32]. Self-tapping locking head screws purchase in the humeral head and in the humeral shaft while a self-tapping non-locking cortex screw is inserted into the surgical neck around the region of the medial hinge. Medial support and screw purchase in good bone stock is important for the success of the plate[17,33,34]. Screws that are projected in various angles allow for purchase in different distributions of the trabecular matrix on the humeral head.

Image removed due to copyright restriction.

Figure 8. *PHILOS plate implant from DePuy Synthes*[32].

2.6 Primary and secondary implant healing and stability

Primary stability refers to the level of stability achieved during the surgery and depends on the contact between the fractured bone and the implant[35]. Restoration to the original anatomical form, also known as anatomical reduction, with bone fragments contacting each other is known as contact healing and is important for primary healing phases of a fracture[36,37]. Small fracture gaps typically benefit from primary bone healing, which is also known as absolute stability or the primary stability[37]. Along with implant design, the quality of primary stability is important for the success of an implant. Complex fractures types involve multiple bone fragments and typically do not benefit from primary healing and heal via a delayed healing type known as bone resorption[37]. Multi-fragmentary healing relies on secondary bone healing and callus formation. Secondary healing is divided into four stages and occurs post-operatively; known as the relative stability or secondary stability. Healing and bone formation are first successful when the vascular networks support the fracture site with blood supply (**Figure 9**).

Image removed due to copyright restriction.

Figure 9. *Vascular supply to the callus area of a fracture, supplied from the surrounding soft tissue*[37].

Hematoma that forms during the inflammatory process has a network of fibrin and collagen fibrils[37]. The hematoma is slowly replaced by granulated tissue in which osteoclasts remove the necrotic bone at the end of the fracture fragments. Following granulated tissue formation, the formation of soft callus starts, in which progenitor cells in the periosteum and endosteum stimulate the activity of osteoblasts. At the fracture lines, mesenchymal progenitor cells build up the extracellular matrix and replace the hematoma. This occurs while proliferating and moving through the callus, differentiating into fibroblasts and chondrocytes (**Figure 10**).

Image removed due to copyright restriction.

Figure 10. *Secondary bone healing: the inflammation stage and formation of hematoma that resolves the granulated tissue*[37].

The hard callus is then formed by endochondral ossification where soft tissue in the fracture is replaced by woven bone, joining the cortex (**Figure 11**).

Image removed due to copyright restriction.

Figure 11. *Secondary bone healing: hard callus formation and conversion of callus into calcified tissue*[37].

Secondary stability of an implant is the level of stability during bone regeneration and remodelling phases[38]. The implant aims to maintain the reduction while surrounding bone contact provides mechanical stimulation for fracture repair and hard callus formation. Devices for internal fixation, such as the PHILOS plate, provide the primary and secondary stability in PHF and ensure healing through hard callus formation. Fractures of the proximal humerus that involve multiple fragments (3- and 4- part fractures) typically produce unstable situations for bone healing and therefore place the post-operative outcomes at a high risk of complications. In high risk implant failure scenerios, the order of priority for stabilisation is as follows: achieve anatomical reduction, restore stiffness to the fracture and minimise the pain at the fracture[38]. The primary stability highly influences the outcome of secondary healing and therefore the quality of secondary stability. Therefore, the term primary screw perforation relates to screws that perforate during the operation and reduction stages of fixation[39]. The term secondary

screw perforation relates to screws which penetrate the articular surface of the humeral head as a result of the loss of initial stability after the operation. The factors which influence the stability of the implant are summarised in the flowchart in **Figure 12**.

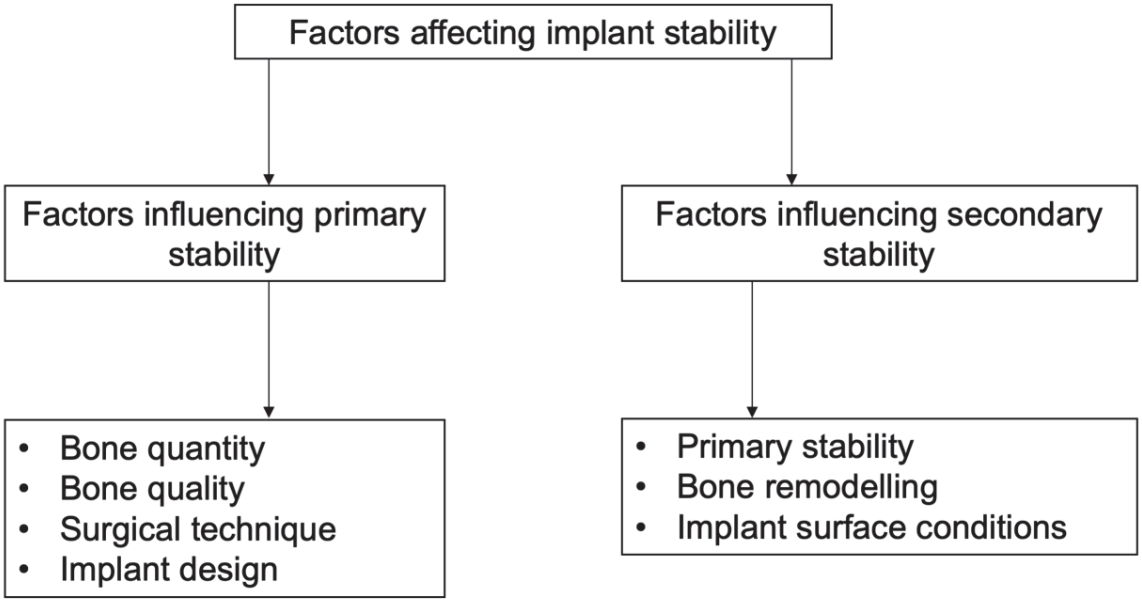

Figure 12. *Factors influencing implant stability, flowchart adapted from Javed et al.*[38].

Mechanical and biological factors of bone healing are inseparable, which makes PHF troublesome. Healing and bone formation are first successful when the vascular networks support the fracture. The perfusion which occurs in the proximal humerus is predominately from the axillary artery and circumflex artery from posterior and anterior sides[18,40]. These vessels may be injured if they are within close proximity to the fracture due to displacement and dislocations of head and neck fragments. Injured vessels can result in inadequate blood supply to the fracture site that leads to necrosis. Necrosis, accompanied by poor primary stability, increases the chances of secondary stability loss.

2.7 Finite element analysis

Finite element analysis (FEA) is a mathematical tool that simplifies the complex interaction of several discrete problems by solving a system of partial differential equations. Using FEA, approximate solutions of complex problems can be computed via a collection of nodes and elements that form geometries, dictated by predefined material properties; i.e. stiffness and Poisson ratio. The collection of nodes and elements form the basis of a mesh that can be in many forms such as triangular, tetrahedral and cubic. Numerous FEA examples are present in the field of orthopaedics and it is a valuable tool for guiding implant design, optimising surgical procedures and describing biomechanical behaviour[22–28]. The main components of an FE model for consideration are model definition, geometry, and mesh, material properties, boundary and loading conditions. The main components factor into the following concepts: discretisation, validation, verification, and interpretation of the results.

2.7.1 Discretization

An FE model is comprised of elements and nodes to form the connectivity of different geometries. The connectivity types include but are not limited to, triangles, squares, and tetrahedrons. The solution to the FE model is divided amongst partial differential equations which govern the behaviour of the model. Element selection and geometries can have a direct effect on the numerical solution and on whether the prediction of the model is acceptable or not. Common element formulations include isoparametric quadratic elements and triangular elements. The performance of these two elements are commonly compared and their relative complexity for a problem are analysed and weighted against the extraction and error estimate they produce.

2.7.2 Validation

Engineering design decisions are based on the information which is provided from computational models with the expectation that the models are accurate and reliable quantitative estimates of the attributes of physical systems[48]. The assurance and reliability of the information provided from computer models have two key components; the selection of suitable mathematical models and the approximation of the solution which corresponds to the mathematical problem. Obtaining the approximate solution of a mathematical model with a guaranteed accuracy is a primary goal of FEA. Through proper design of an FE mesh and assignment of polynomial degrees, the exponential rates of convergence to a real solution and validity of a model can be determined. Validation is the process in which the computational model's predictive capabilities can be compared against experimental or previously published data[48]. This is a primary concern with models of solid mechanical systems, to ensure the reliability of an FE model. The validation of a model is heavily dependent on the initial design specifications and the assumptions made. For many materials, the boundary conditions are known to predict outcomes of controlled experiments because loading constraints typically reflect the influence of the environment that it coincides.

2.7.3 Verification

Verification is concerned with the assurance that the input data is correct and the code, which the FE model is run with, is functioning correctly. The errors in the data of interest must meet the necessary conditions of the design problem and reside within the permissible tolerances to be considered a valid solution. In biomechanical related FEA, there is a large error percentage due to high variability in models.

Verification and validation can only be confirmed when the model has correctly formed with respect to the initial problem and clearly defined goals of computation.

2.7.4 Results interpretation

A major challenge when modelling orthopaedic or biomechanical conditions is achieving an accurate recreation of anatomy and physiological loads[48]. Biomechanical FEA may take simplified approaches in loading and boundary conditions with a specific clinical question in mind and the desired output. There is typically a clinically oriented question involved with biomechanical FE modelling, which decides upon the complexity of the FE model required and the results used to answer the said question[49]. For example, in a proximal humerus study, Varga et al. used an FE model validated from experimental data to predict screw cut-out type failure in PHF based on the compressive strain around the screws[50]. Another example is from Murdoch et al. who tested a new intramedullary nail for PHF with FEA and showed the mechanical superiority it had against other solutions by outputting the average compression and torsion forces generated[51]. Additionally, a study from Clavert et al. showed the stress distribution in multiple bone specimens and the effect osteoporosis has on deformation when implants are purchased in lower bone density[52]. The given examples of FEA on the PHF all had a clinical question which defined the study and the output parameters. A clinical motivation that defines a problem and a need is paramount for FEA studies to have valuable output that can be used and interpreted by engineers, clinicians, and surgeons.

3. The clinical problem

3.1 Proximal humerus fractures

There are high morbidity and mortality rates associated with fracture types of osteoporotic bone, making implant design and surgical guidance important for patient care[53]. Extended hospital stays and post-operative complications are usually associated with osteoporosis fractures of hip, wrist, and shoulder. Studies suggest that PHF is the third most frequent fracture related to osteoporosis with an expected increasing incidence due to the ageing population[1–3]. Given the increase of fracture frequency, morbidity, mortality and cost, osteoporotic PHF require just as serious consideration as hip fractures[54]. In the United States, this fracture occurrence has been reported to be increasing at 13% per year for the past 30 years[6]. Several non-conservative surgical treatments are available for PHF. These include, open reduction and internal fixation (ORIF), closed reduction and percutaneous pinning, hemiarthroplasty, intramedullary nailing and reverse total shoulder arthroplasty[6]. Surgical intervention of PHF is becoming more popular according to some reports, specifically regarding methods of ORIF[3,6,12,15,55], also known as plating. Treatment of complex and unstable fractures is the most challenging and is performed conventionally with locking plates. However, the rate of mechanical failure of locking plates is high. A clinical study by Gupta et al. reported a complication rate of 15% for plating. Their study involved management of 92 patients with a reoperation rate of 12.7% for the patients treated with plates; versus hemiarthroplasty which had a complication rate of 4.9% and reverse arthroplasty which had a complication rate of 5%[6]. Plating had the highest complication rate in the study compared to the other surgical methods. The difficulties reside in the case that plating has more optimal functional outcomes for complex fracture types than other surgical solutions,

returning the most range of motion[6,15,39,40,56], is less invasive and preserves blood supply to humeral head[57]. Crosby et al. reported in a study that 70 patients with a mean follow up of 34 months had no change in post-operative outcomes after plating, demonstrating the potential benefit of successful fixation plating can have[40]. The final follow-up concluded that a mean range of motion of elevation was 140° (100°-175°), external rotation in the abducted position was 77° (45°- 95°), external rotation at the side was 49°- 85° and internal rotation was restored. All fractures reportedly healed with no loss of reduction at the final follow up[40].

Plating is typically more favourable over more invasive methods, such as reverse arthroplasty because it returns a wide range of motion to patient. However, the high complication rates associated with plating show that it is a challenging fracture to treat and determine post-operative outcomes.

3.2 Secondary screw perforation

A study by Charalambous et al. assessing the PHILOS plate for treating PHF reported that 41% of their study cohort with acute fractures and 50% of the non-union fractures experienced complications[15]. The high complication occurrence was predominately due to the difficulty of treating PHF and the high level of surgical technique demanded. In 4 cases, they found screws protruding into the glenohumeral joint, which could likely have been due to the early post-operative collapse of the humeral head (**Figure 13**).

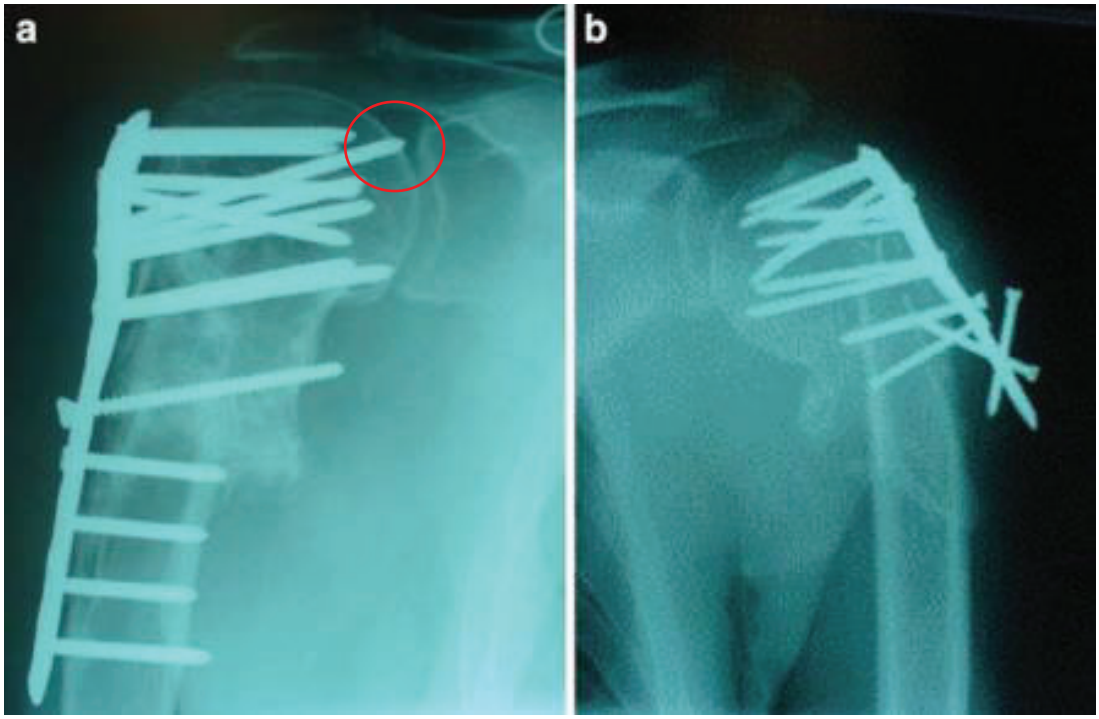

Figure 13. *a) Screw protrusion into the glenohumeral joint. b) Shaft screw loosening and backing out*[15].

The occurrence of post-operative screw perforation, also known as secondary screw perforation, is a commonly reported mechanical failure type of plating systems used for treating complex and unstable PHF. Secondary screw perforation occurs when reduction has been lost post-operatively, and the greater tuberosity and humeral shaft do not support the humeral head fragment. The plate is fixed to the shaft of the humerus and is substantially rigid while the humeral head is only fixed at the screw tips and can, therefore, move whenever the shoulder joint is loaded. The humeral head, if lacking medial support, will collapse in a varus rotation combined with inferolateral displacement and the screws perforate through to the articular surface and penetrate the medial cortex. Once penetrated through the humeral head, the screws can strip and damage the articular cartilage of the glenohumeral joint[5,16,39,56].

A study by Südkamp et al. encountered a complication rate of 34% amongst a study cohort of 155 patients with a one year follow up[12]. Eleven patients had a loss of

reduction (7%), which resulted in secondary screw perforation and ultimately in humeral head necrosis. Wang et al. reported secondary screw perforation occurring in 13.8% of their patients in their study cohort of 189 patients[16]. From the patients who had secondary screw perforation, 8 had humeral head necrosis, and 14 patients had severe shoulder pain as a result of the joint penetration and had their implants removed (**Figure 14**). Each patient received conservative treatment following implant removal. Fracture types that involve multiple fragments (3-part and 4-part) are at the greatest risk of secondary perforation due to instability and complexity of the multi-fragmentary fracture[16].

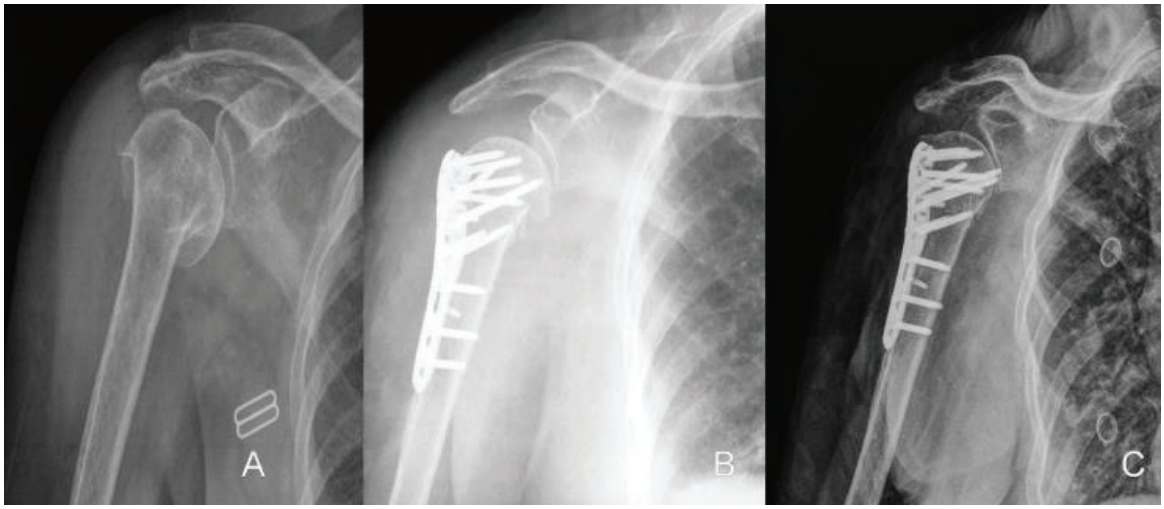

Figure 14. *A) Anteroposterior shoulder radiograph of an 81-year-old sustaining a 4-part (AO type C) PHF. B) Initial fixation after surgery. C) Two months post-operative radiograph show screws from PHILOS plate perforated into the joint as a result of humeral head collapse*[16]*.*

The mechanical failure type of secondary screw perforation is found to be one of the most frequently reported failures in PHF plating. A study from Gardner et al. who investigated the importance of the medial support on the stability of the humeral head report the failure type of 29% occurence[17]. Königshausen et al. reported in their clinical study that screw perforation was their most prominent complication type, contributing to 41.6% of the study's complications. Furthermore, 60% of the observed screw perforations occurred due to secondary reduction loss[58].

3.3 Screw selection and configuration

The surgical guidelines from DePuy Synthes recommend that the tips of their titanium locking head screws used for their PHILOS plate should anchor in bone 5-8 mm from the joint surface[32]. Previous studies and chapters of this thesis have shown that bone becomes stronger closer to the subchondral bone on the medial side of the humerus[26,27,59]. When the head is unsupported by the greater tuberosity and the humeral shaft, then mechanical stability resides predominately on the purchase of the screw tips into the humeral head[39]. The strength of the anchorage is the level of primary stability achieved during the surgery and will determine the initial stability until secondary fracture healing can occur. If the anchorage of screws is not sufficient, then they may loosen in the humeral head, and the humeral head is free to rotate and collapse via inferolateral displacement and in varus rotation. Some reports mention that some surgical techniques involve using shorter superior screws to avoid penetrating the joint post-operatively if reduction and alignment of the proximal humerus have been lost[12,20,60–62]. Using shorter screws, however, decreases the mechanical stability and therefore reduces the medial support of the humeral head, increasing the likelihood of screw cut-out type failure. Compromising the initial stability and medial support of a fracture fixation might not be worth compromising to avoid perforation. From a mechanical standpoint, the benefit of medial support against screw cut-out type failure has been shown in biomechanical studies[33,34,50,63]. Gardner et al. published the mechanical benefit of inferomedial support from calcar screws, stating that the addition of more medial support can help prolong the varus collapse of the humeral head[17]. A published paper from the AO Research Institute by Fletcher et al. found that longer screws provide a reduced risk of cut-out type failure in PHILOS plating of unstable 3-part fractures[50]. This

was assessed by conducting a parametric study in an FE model where multiple screw lengths were interchanged virtually for the same humerus specimens (N=25). The consensus of this study was that long screws prevent cut-out type failure; however, this is just one type of failure that can occur in proximal humerus fixations and does not consider the influence longer screws have on perforation characteristics. The different mechanical failure types of plating in PHF do not occur in isolation but are interlinked and changing; for example, the length of screws used may influence the chances of another failure type occurring[39,64]. To the knowledge of the author, there have been no studies, clinically, experimentally or computationally that directly report on whether screw perforation is influenced by using longer or shorter screws. Furthermore, an FE model that predicts this phenomenon has not been developed. Knowing the effect screw length has on perforation characteristics would be useful in guiding surgical decisions, when treating the most challenging unstable and complex PHF.

3.4 Failure prediction

Initial stability is predominately residing on the quality of the bone-implant interface rather than on the implant mechanical properties[41]. Pre-operative planning to avoid catastrophic events by optomising the initial stability could help avoid post-operative complications and improve patient outcomes. Different methods to determine fracture risk and implant failure before they occur exist clinically, such as dual-energy X-ray absorptiometry (DXA) based measurements, CT evaluation-based analysis. In vitro studies on CCT for FEA can show improved non-invasive assessments of bone strength, BMD and bone mass than quantitative CT (QCT) and DXA[42,45,65]. A study by Cody et al. compared the failure strength of femurs and attempted to correlate the failure from the displacement ramp test and along with

predicting ultimate load with QCT, DXA, and FE[42]. QCT measurements had an average linear predictive correlation (R^2=0.648), DXA had an average linear predictive correlation (R^2=0.556), and FE-based predictions were the best linear correlation (R^2=0.770). Cyclic cut-out failure in proximal humerus plating has been previously shown to be well predicted via bone mineral density measures[66] and even more accurately with FE simulations[67]. However, there is currently no method available to predict the occurrence of secondary screw perforation, via density-based measurements or FE simulations. Computer-based modelling can provide feedback on predicted implant performance in multiple simulated conditions and provide optimisation of surgical procedures. As clinical scanning technologies improve, the opportunity to implement patient-specific FEA becomes more realistic, and the benefit of models developed to predict specific failures before they occur becomes more valuable for optimal patient care.

4. Literature review

Studies considered for this literature review involve those that use in vitro experimental methods to investigate screw placement in the humeral head. The loading protocols and methods used were compared, and the aspects that were not investigated were considered. Furthermore, the overall key points of these studies were taken into consideration. Indicating gaps in previous research was important; it was also important to consider similar research but with different goals and methods such as computational compared to clinical studies. Similar studies and models in the form of FEA and experimental served as forms of validation, and when comparable papers were identified, a direct comparison was made. While current methods for surgical procedures and implants for the treatment of PHF are supported by scientific and clinical literature, there is still a need for research to be conducted to understand the mechanisms that cause secondary screw perforation. The main points to focus on to identify the gaps in currently available research are the following:

- Screw perforation both in vitro and clinical
- Screw placement and location
- Failure prediction-based papers
- FEA analysis of the proximal humerus

The literature review was divided into two sections which cover related literature first for sub-study 1 and then for sub-study 2. To the author's knowledge, there is currently no in vitro studies which experimentally test for the notion of whether purchase close to the glenohumeral joint results in early perforation or that have developed a prediction model for secondary screw perforation.

4.1 Screw length and perforation

Hepp et al. determined the most optimal locations for screws to purchase. These locations were found to be the medial and dorsal aspects of the humeral head, given that they have the highest bone strength[59]. Within regions of interest, they made histomorphometry analyses and mechanical loading tests to determine the densest locations. The loading regime consisted of ramp loading at 0.04 mm/sec in displacement control and measured the force response. They concluded that the strongest purchase for screws is in the medial and dorsal aspects of the humeral head[59]. The medial side of the humeral is located beneath the articular cap. The maximise screw purchase, they need to reside close to the joint. This study did not investigate whether perforation is affected by the different density locations.

A study by Liew et al. investigated the effect of screw placement on fixation in the humeral head[26]. In their study, they aimed to determine the most robust screw purchase locations within the humeral head. Their study consisted of two groups, the first group was a 6.5 mm fully threaded cancellous screw inserted flush with the subchondral cortex and the second group was an identical screw inserted 5 mm short of the subchondral cortex (**Figure 15**).

Image removed due to copyright restriction.

Figure 15. *Illustration of study groups for Liew et al. study on screw placement*[26].

They measured the pull-out forces at 7 locations in the humeral head and compared the two groups (**Figure 16**).

Image removed due to copyright restriction.

Figure 16. *Humeral head fragment. Locations: anterosuperior (AS), posterosuperior (PS), anterior (A), centre (C), posterior (P), anteroinferior (AI), posteroinferior (PI)*[26].

This study investigated how screw purchase distance from the joint surface affects the mechanical properties of screws; although they conducted this for pull-out force rather than screw perforation. They found the central region of the humeral head had the highest pull-out force; however, this was also the region with the most extended length of screw purchase (**Figure 17**). Based on their results they concluded that the most optimal locations for purchase in the subchondral and cancellous are in the centre of the head. By using a paired specimen study they could show that loosening of screw fixation is most reduced when purchased at the subchondral bone from more screw thread purchase and in denser bone.

Image removed due to copyright restriction.

Figure 17. *Absolute pull out force vs screw position for different screw locations, with and without subchondral abutment. Screw location significantly influenced the absolute pull out force (P < 0.01). Central pull out force was higher than that in any other location (P < 0.05). Subchondral abutment improved absolute pull out force (P = 0.004)*[26].

This study did not compare the cyclic axial loading and screw length effects on perforation characteristics in the humeral head. Furthermore, this study was focused more on the regional variation of screw purchase strength rather than how the screw length affects the perforation characteristics. Their study also recommends that for future studies, screw size should be investigated to optimise fixation of PHF.

The position and number of screws can influence whether screw perforation occurs[61]. A cadaver study conducted by Erhardt et al. showed that more screws in the humeral head significantly increases the mechanical stability in the PHF when loaded and unloaded multiple times[61]. To determine improved stability, they cyclically loaded proximal humeri instrumented with a polyaxial locking plate (NCB PH; Zimmer, Warsaw, IN) in a position of 30º flexion and abduction.

Image removed due to copyright restriction.

Figure 18. *The biomechanical set up of Erhardt et al. for cyclic screw perforation*[61].

Loading only the humeral head is a method that screw perforation can be induced in vitro. This testing set up is essential because it provides a proper and still relatively physiological loading of the humerus. A similar loading approach can be applied when investigating the effect that screw length has on the perforation. Despite the cyclic loading pattern, the testing remained relatively static compared with in vivo dynamics.

On the other hand, it is an easy and reproducible way to produce screw perforation events in a standardised manner. The main point to take from this study is that a minimum of 5 screws should be used for instrumentation, with at least one infero-medial screw to reduce the chances of screw perforation. However, more screws inserted remove more trabecular bone in the humeral. For osteoporotic patients, more screws may not be ideal due to limited bone quality and quantity; screw augmentation may be more desirable in this case. This study did not change the distance to the joint between groups, so the effect of purchasing away from the subchondral bone cannot be assessed. An important note, however, is that they mention that inhomogeneous bone strength distribution does not influence perforation and that they did not assess the density around the screws. A previous

study conducted by Röderer et al. has shown that density around the screw tip best correlates to cycles to failure, stronger than using the global BMD of the humeral[68]. A study was published by Katthagen et al. that investigated the influence of plate material and screw design have on the stiffness and ultimate load in osteoporotic PHF[69]. This study is valuable because they one of the few, along with Erhardt et al., that specifically biomechanically test for screw perforation[61]. The aim of this study was not directly on the effect of screw length or perforation prediction, but rather a comparison of implants. The experimental designs in their study could be used to develop a similar experimental test setup for screw perforation. They tested screw perforation by loading the humeral head statically until the screws perforated through. An 8 mm osteotomy was made on the anatomical neck of the humeral head. The articular surface is facing vertically and coupled with a transparent PMMA cylinder so that the screw penetration of the articular surface could be seen (**Figure 19**).

Image removed due to copyright restriction.

Figure 19. *Screw perforation experimental set up of Katthagen et al.* [69].

Their loading protocol involved constant displacement of 0.05 mm/s on the articular surface of the humeral head. The test was stopped once the screw tips penetrated the articular surface (**Figure 20**).

Image removed due to copyright restriction.

Figure 20. *A) sharp screw tip perforating the articular surface of the humerus B) bulge with a partial tear of cartilage layer*[69].

This study did not compare the effect screw length has on the perforation, nor was humeral head cyclically loaded in a manner that would be physiological. For their study, they compared PEEK and PHILOS plating between the study cohorts which makes it not comparable to our study. Furthermore, the fracture model is not comparable as they retested the specimens and re-osteotomised prior to perforation testing, so the results of the test are questionable.

A clinical study conducted by Qiang et al. assessed screw length in PHILOS plates for PHF using CT scans[20]. They agreed that screw perforation is a common complication in PHF and could be associated with the improper selection of screw length. The focus of their study was to select the ideal screw length of periarticular screws and to determine which factors influence the screw length and implantation of infero-medial support screws. Reported in this study, is that surgeons may practice in shortening the lengths of their screws to reduce the risk of screw

perforation; however, this can result in other implant failures such as early humeral head collapse. Mentioned in the study is that humeral head collapse can be decreased by using longer screws. However, they conjecture that longer screws paradoxically increases the chances of both primary and secondary screw perforation. Their study focused on the pre-operative planning that would influence surgical decisions rather than the actual effect of using different length screws.

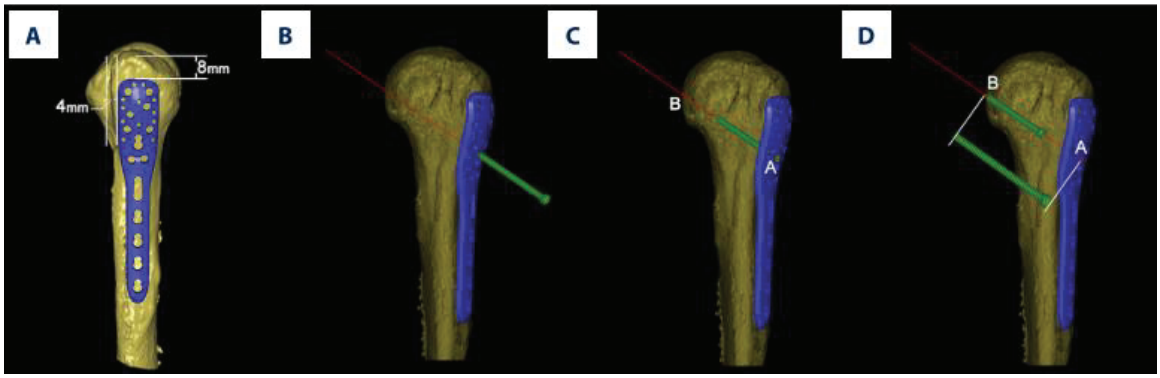

Figure 21. *Simulated implantation of the PHILOS plate and screw. (A) The plate is based on surgical guidelines. (B) The locking head screw (No. 7) positioned at the plate hole along its designed trajectory (red line). (C, D) The optimal screw length is equal to the distance between points A and B. Points A, and B are defined as the points on the screw cap and the intersection of the subchondral bone and screw tip, respectively*[20].

They based their optimal screw tip location off the study conducted by Liew et al. who was previously mentioned to investigate the effect of screw placement in the humeral head[26]. They do not directly quantify and compare the effect that using different screw lengths has on perforation in the humeral head.

The discrete nature of trabecular bone microarchitecture and its relation to the stability of an implant was investigated by Wirth et al.[70]. This was conducted for screws which purchase in the trabecular and the stress and strains around the screw that is produced. For this study, they used FEA to asses this with two groups with different boundary conditions; constrained and unconstrained (**Figure 22**).

Image removed due to copyright restriction.

Figure 22. *Two boundary conditions for the study, constrained on the left and unconstrained on the right*[70].

Within these two groups, they assessed different bone densities around the screw tip. This study is useful as it addresses the stresses and strains of different bone densities around screw tips for short, medium and long screws (**Figure 23**). This study is useful for analysing single screws purchased in different bone densities. The strain surrounding the screw tip was higher in low-density trabecular bone opposed to the high-density bone which exhibited considerably less strain for both constrained and unconstrained study groups. Shorter screws purchasing into trabecular bone also exhibited higher distributions of strain to the surrounding matrix; this was true for the constrained and the unconstrained model. This study indicates that FEA models with longer screws will produce substantially higher stiffness than models with shorter. However, the focus of this study is focused on the differences in trabecular for discrete and continuous models, which is not relevant to the FE model proposed to predict secondary screw perforation as the models will

not be constructed from micro-CT and the trabeculae will not be modelled to such detail.

Image removed due to copyright restriction.

Figure 23. *Peri-implant strain in the bone of a constrained model*[70].

Fletcher et al. conducted a parametric FEA study to identify the effect of screw length on prediction failure on screw cut-out in PHF[50]. They had 4 study groups, 4 mm, 8 mm, 12 mm and 16 mm and assessed the strain around the screw tip which had been shown to correlate to cyclic cut-out failure[67]. They simulated physiological loading protocols based on previously published loading data from in vivo measurements[71]. From their results, they found that longer screws have a reduced

risk of cut-out type failure with the effects seen most dramatically from varying the length of the calcar screws. This study addressed the effect that different screw length has in PHF; however, it only assesses it for cut-out type failure and not for screw perforation. This study addresses the initial implant stability and not the long term risks. A concluding statement from this study is that clinical judgment will be required to determine if extending the screws has a greater effect on cortex penetration[50].

In a clinical study, to prevent screw perforation, a study by Ricchetti et al. used a technique which had screw tips purchased further from the subchondral bone[62]. In 54 shoulder surgeries, they had no cases of screw perforation. They implanted patients with a screw ranging between 5-10 mm from the subchondral bone which reduced intraoperative perforation. However, this technique resulted in patients experience higher rates of varus collapse in the shorter screws, most likely due to a lack of medial support.

4.2 FEA and failure prediction

Krappinger et al. investigated the factors which contribute surgical fixation failure in PHF[72]. This study attempted to predict failure in a clinical setting. They used two surgical techniques for their study; treatment with the PHILOS plate from DePuy Synthes and the Humerusblock from Stryker. They treated 67 patients and for these, they assessed the following parameters: age, gender, BMD of cancellous bone in the humeral head, the complexity of the fracture, medial metaphyseal comminution and head extension, angulation, and anteversion of the humeral head and displacement of the fracture fragments relative to the humeral head. In their study, they found that the biggest contributors to failure were age, local BMD, quality of reduction and medial support restoration. The likelihood of these having poor properties increased

the chances of the failure occurring. Despite not reporting any occurrences of secondary screw perforation in their study, the proceedings indicate that an unstable fracture type with poor surgical reduction increases failure chances. Additionally, wide ranges of age and BMD are necessary for developing a prediction model. For their study, they did not develop a tool which could be implemented for pre-operative planning which may be used to predict future failures.

Density correlations are commonly used regarding cycles to fatigue failure for biomechanics[61,66,68]. A study by Varga et al. compared strain-based predictions of cycles to cut-out type failure from FE models with density-based measurements from different regions of the humeral head (**Figure 24**)[66].

Image removed due to copyright restriction.

Figure 24. *(a) the outer surface of the HR-pQCT of the proximal humerus shape. (b)(c)(d)(e) Four regions, the domain boundaries and the corresponding HR-pQCT-based densities (g)(h)(i)(j). For the instrumented humerus (e), the evaluation region was around the screw tips, restricted to the inner compartment of the head fragment to avoid subchondral bone*[66]*.*

It was found that the best predictor of cut-out type failure was using FEA-based measurements ($R^2 = 0.9$). The strongest density-based measurement was using the bone mineral content (BMC) in a cylindrical region around the screw on an HR-pQCT

scan (R^2 = 0.774) (**Figure 25**). The poorest performing correlation was for the clinically available CT scans.

Image removed due to copyright restriction.

Figure 25. *A summary of the correlations from study by Varga et al. (coefficient of determination, R^2) between experimental fixation cut-out type failure and BMC evaluated at the various regions on both CT data type and both sides*[66].

A study by Röderer et al. who investigated the local bone quality as a predictor for failure found that BMD surrounding the screw tips significantly correlates to failure (p=0.018) when regarding the mechanical failure type of screw cut-out[68]. This study along with prior mentioned studies shows that cut-out type failure has the strongest correlations when using the bone located around the screw, rather than the global bone content of the humeral head[66,68]. The method of measuring involved using a DensiProbe to determine the local bone quality in the regions of screws in the PHILOS plate. Correlating local bone content to experimental cycles to failure as

Varga et al. and Röderer et al. did in their studies could be used for developing prediction models for secondary perforation[66,68].

A study by Varga et al. found that the number of cycles to cut-out type failure had a strong logarithmic correlation ($R^2 = 0.90$) with the average minimum compressive principle strain around the screws in plated proximal humerus FE models (**Figure 26**)[66]. The study suggests that the average compressive strain around the screw tip can be a surrogate parameter for estimating the stability of a construct after the fracture has been fixed with a plate. A computationally cheap linear elastic model was used which could be an efficient solution for screening, optimising and improving surgical solutions. This study validated its model by conducting experimental testing and then aligning the boundary conditions of the FE model with the experimental. However, as previously mentioned, different mechanical failure types of plated PHF do not occur in isolation, the study by Varga et al. only assessed screw cut through and defined failure to be 2 mm plastic deformation. This study did not assess whether cyclic screw perforation could be predicted.

Image removed due to copyright restriction.

***Figure 26**. (a) The plot of the strains (μstrains) at 100 N compression. (b) The plot shows a strong logarithm correlation between the of the experimental number of cycles to cut-out type failure and the FE-based average compressive principal strain around the screws.*[67]

The same approach of this study could be applied to predicting screw perforation. New models would need to be generated and validated from an experimental screw perforation testing set up. Specimens would need to be biomechanically tested and using the new data, the model could be validated and a prediction curve for that failure type could be made.

5. Gap statement

Regarding post-operative outcomes, techniques of plating the proximal humerus are associated with the common occurences of secondary screw perforation. There currently remains a gap in research, for investigating the effect that screws length has on secondary screw perforation. The length of a screw could dictate whether there is strong purchase close to the subchondral bone or weak purchase away from the subchondral bone, and how this is related to failure mechanics of perforation, still remains unknown. Provided that longer screws have been previously reported to prevent cut-out type failure but may also increase the chances of secondary screw perforation occurring, makes the outcomes of screw selection valuable for optimising surgical procedures. Furthermore, to the best of the author's knowledge, the phenomenon of secondary screw perforation has yet to be predicted with FEA modelling or density-based measurements. Existing research shows that prediction based measurements and models are being developed. Failure prediction could potentially become a valuable tool in the future of clinical orthopaedics, especially for patient pre-operative screening before they undergo surgeries known to have high failure and complication rates.

5.1 Aim

The thesis aimed to investigate two aspects related to secondary screw perforation. For the sub-study 1, via biomechanical testing techniques, the effect that screws tip to articular surface distance has on secondary screw perforation failure in unstable and complex PHF. Using the experimental data acquired in sub-study 1, sub-study 2 was aimed at predicting the biomechanically observed cyclic screw perforation failure of locking plate fixations in PHF through methods of BMD and BMC

measurements and FE-based predictions. Both aims are reemphasised in their relative chapters.

5.2 Hypothesis

The hypothesis for sub-study 1 was that screw tip to joint distance does not have an influence on cyclic screw perforation. The hypothesis for sub-study 2 was that the average minimal compressive principle strain around the screw tip in a linear elastic FE model will correlate to the cycles to failure acquired in sub-study 1. Additionally, FE-based predictions will have stronger correlations than density-based measurements of BMD and BMC around the screw tips. Both hypotheses will be reemphasised in their relative chapters.

6. Sub-study 1: Secondary perforation risk in plate osteosynthesis of unstable proximal humerus fractures: a biomechanical investigation of the effect of screw length

Daniel Ciric[a,b], Dominic Mischler[a], Feras Qawasmi[a,d], Lisa Wenzel[a,c], Geoff Richards[a], Boyko Gueorguiev[a], Markus Windolf[a], Peter Varga[a]

[a] AO Research Institute Davos, Davos, Switzerland

[b] Flinders University, Tonesly, South Australia

[c]Department of Trauma Surgery, Trauma Centre Murnau, Murnau, Germany

[d]Hadassah Medical Centre, Jerusalem, Israel

6.1 Sub-study 1: Introduction

Fractures of the proximal humerus are the third most frequent injuries related to osteoporosis with an expected increasing incidence due to the ageing population[1–3]. Complex and unstable fractures account for a high portion of clinical cases observed and involve multiple fragment fixation with either locking plates, intramedullary nails or joint replacement via arthroplasty[6,55]. One of the most frequently applied joint-preserving approaches for the treatment of PHF is locked plating. However, this approach remains challenging, with complication rates ranging between 18-37%, indicating an urgency for improved surgical solutions[12,15,17,56]. PHF has a variety of causative factors, that could result in complications, progressing to a cascade of effects and debilitating the patient's post-operative recovery. Complications typically range from biological to biomechanical issues and are interlinked, usually leading from one into the other. For example, poor bone healing from disrupted blood supply to the humeral head in surgical neck fractures can result in implant failure and reoperation before the onset of necrosis[19,40].

On the other hand, primary osteosynthesis stability depends on the biomechanical fixation. The biomechanical failure in terms of intraoperative and post-operative screw perforation through the articular cartilage into the glenoid is one of the leading causes for reoperation in locked plating of PHF[6,12]. Secondary screw perforation with screws penetrating through the articular surface post-operatively results in intense pain and damage of the glenohumeral joint. Previous studies have reported secondary perforation at a rate of 7-29% within their cohorts, making it a significant contributor to current challenges faced surgically[12–17]. Osteoporotic patients are at an even higher risk of biomechanical fixation failure due to lack of support from screw purchase in poor bone quality[60,73]. The quality of humeral head bone at the location where the screw is purchased provides the initial level of stability post-operatively. Mainly, if anatomical reduction and alignment of the humerus are compromised, the stability relies entirely upon the anchorage of the screws in the humeral head. When fracture reduction is lost, the humeral head can subside and collapse. Locking screws cannot back out of the plate which causes them to perforate throughh the humeral head[15,39]. The distance between the tip of the proximal screws and the joint surface may affect the perforation risk; however, there remain discrepancies on whether the use of a closer or further distance is advantageous to avoid fixation failure[20,39,50,62,74]. The uncertainty of optimal screw tip location may cause surgeons to practice using shorter screws to avoid both intraoperative and secondary perforation[6,15,19,21,22]. However, the strongest bone to purchase in is known to exist medially in the subchondral region, and the lowest purchase strength exists in the central part of the humeral head[26,27,59,75].

Given that the distribution of bone stock is more robust towards the subchondral bone, using shorter screws may result in a weaker initial purchase and consequently

in biomechanical fixation failures such as early head collapse and screw cut-out[17,34,40,50]. Screw purchase location raises the dilemma of optimal screw tip to joint distance (TJD) when considering the risk of secondary screw perforation. It is not clear yet whether purchase away from the subchondral bone in lesser bone stock, but with the thicker bone layer in front of the screw tip, is advantageous over purchasing in the denser bone region closer to the joint surface but having a thinner bone layer to perforate through. Therefore, this biomechanical sub-study aims to investigate the effect of the distance between the screw tip and the articular surface concerning the secondary screw perforation failure in plated unstable PHF. The hypothesis is that the TJD does not have an influence on the cyclic screw perforation failure.

6.2 Sub-study 1: Material and methods

6.2.1 Specimens

Ten pairs of fresh-frozen human cadaveric proximal humeri of elderly donors (seven males and three females, 75 ± 16 years old (mean ± standard deviation (SD)), range: 46 – 100) were used. Donors gave their informed consent within the donation of anatomical gift statement during their lifetime. The specimens were stored at -20°C before preparation and subsequent biomechanical testing. The bones considered for inclusion in the study were pre-screened for pair symmetry based on both, BMD and radius of the humeral head, as well as an examination of any notable pathological features. The specimens were scanned with HR-pQCT (XtremeCT, Scanco Medical AG, Brüttisellen, Switzerland) with scan settings of 60 kV voltage, 900 µA current and 82 µm isotropic voxel size. These images were converted to BMD units ($HAmg/cm^3$) via the scanner's calibration function. Humeral head radius was evaluated by fitting a sphere on the joint surface of the head, and global trabecular

BMD was measured within a cap-shaped region under the articular surface, corresponding to the target location of the screw purchase[66]. The summary of the specimens for the study, along with the scanning protocols can be found in Appendix A. The checklist which ensures that each specimen received the same treatment can be found in Appendix D.

6.2.2 Fracture model, study groups and instrumentation

Specimens were left to thaw at room temperature before dissection of the tissue. The extraneous soft tissue was removed, and care was taken to prevent damage of the humeral head articular surface during dissection. A highly unstable 3-part fracture (AO/OTA 11-B1.1) was then simulated and plated applying a novel method developed to replicate a situation where the surrounding fragments do not support the humeral head fragment post instrumentation[76]. For this purpose, the cadaveric specimens were first osteotomised using an oscillating saw of 0.4 mm thickness, separating the humeral head from the greater tuberosity (GT) and the humeral shaft, following a standardised protocol to ensure osteotomy symmetry amongst paired specimens (**Figure 27**). Second, a CT scan of each osteotomised cadaveric GT fragment was acquired using a GE Revolution EVO scanner (GE Healthcare, USA) with scanning settings 120 kV voltage, 200 mA current and 0.625 mm slice thickness, followed by segmentation and generation of its external surface using Amira 6.4 (FEI, Hillsboro, USA) image processing software. Third, based on the Amira modelling, a specimen-specific surrogate GT fragment was 3D printed with water-soluble polyvinyl alcohol (PVA). Fourth, the osteotomised cadaveric humeral head, GT and shaft fragments were anatomically reduced, and a PHILOS plate (DePuy Synthes, Zuchwil, Switzerland) was positioned using anatomical landmarks and a Kirschner-wire passing through its guiding block's nose, touching the proximal

joint surface. Fifth, the plate position was temporarily fixed via a 3.5 mm cortex screw in the shaft fragment. Sixth, the cadaveric GT fragment was replaced with its 3D printed replicate; the two proximal fragments were then fixed using the K-wire holes of the plate's guiding block and a clamp. A typical clinical screw configuration by occupying rows A, B and E (surgical technical guide) was selected for all specimens during plating. Screws were inserted into rows A and B using guide sleeves and a limited torque screwdriver of 1.5 Nm, followed by removal of the humeral shaft fragment and screws insertion into row E. Finally, the 3D printed GT fragment equivalent was dissolved post instrumentation in warm phosphate buffered saline to remove the lateral support to the humeral head fragment. Only the printed piece submerged to ensure that no foreign particles entered the humeral head fragment during the dissolving process. Recalling that stability is predominately residing on the purchase of the screw tips into the trabecular bone of the humeral head fragment, such a procedure – performed by an upper extremity orthopaedic surgeon according to the manufacturer's surgical guide – was paramount to avoid damageing the peri-screw bone region with additional applied stress during plating. A summary of the instruments, surrogate GT image processing, and instrumentation protocols can be found in Appendix B.

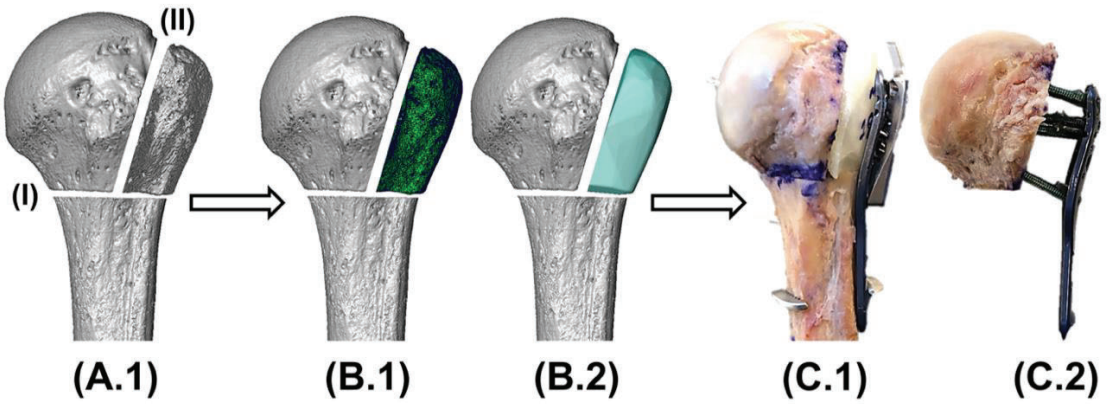

Figure 27. *Illustration of the osteotomy and instrumentation. (A.1) The osteotomy model, including a first cut (I) on the anteroposterior side of the humerus along the surgical neck, orthogonal to the humeral shaft and 5 mm below on the articular cartilage measured on the most medial point of the surgical neck; and a second cut (II) from the highest peak of the greater tuberosity over the lesser tuberosity, connecting with the cut along the surgical neck. (B.1) The GT segmented from CT scan (B.2) and a surface generated to 3D print a surrogate GT with water-soluble PVA material. (C.1) Surgical reduction of the humeral head, humeral shaft, and surrogate GT during instrumentation. (C.2) Final Instrumented specimen.*

The bone pairs were randomised into two study groups differing by the distance of the screw tip to the subchondral bone, i.e. TJD. The long screw group (LSG) had a TJD of 4 mm, whereas the short screw group (SSG) had a TJD of 8 mm, which represented the upper and lower limits recommended by the surgical guide of the implant manufacturer (5-8 mm). Each screw length was determined by measuring the plate-joint distance with a custom-made caliper and subtracting the approximated cartilage thickness of 2 mm and the TJD defined by the actual treatment group (4 mm or 8 mm)[77]. A drill with a custom-made depth gauge was used to ensure that the boreholes were not longer than the length of the intended screw. All specimens were CT-scanned with a CCT GE Revolution EVO scanner post instrumentation, and the achieved TJD was measured using Amira image processing software. A summary of measured TJD can be found in Appendix B.

6.2.3 Biomechanical testing

Biomechanical testing was performed using a custom screw perforation apparatus installed on a biaxial servohydraulic testing machine (Mini Bionix II 858, MTS Systems Corp, Eden Prairie, MN, USA) equipped with a 25 kN/200 Nm load cell (**Figure 28**). The test setup was based on previously published work testing screw perforation[61,69]. Each specimen was mounted on an XY table, alleviating shear forces during loading, with the PHILOS plate inclined at 20º to the machine base. An artificial glenoid, made from plastic and coated with a copper lining was used to load the humeral head. Based on a previously published loading protocol[66],the specimens were cyclically tested to failure under sinusoidal loading at 4 Hz. The valley load of each cycle was kept at a constant level of 25 N, the peak load increased progressively by 0.05 N/cycle, starting from 50 N. Each test was concluded when the first of any screw perforated through the joint surface. The perforation was detected by the electric contact between the screw and the encountered copper lining of the artificial glenoid, closing a 10 V circuit and triggering the testing machine to stop[78]. The experimental testing protocol can be found in Appendix C.

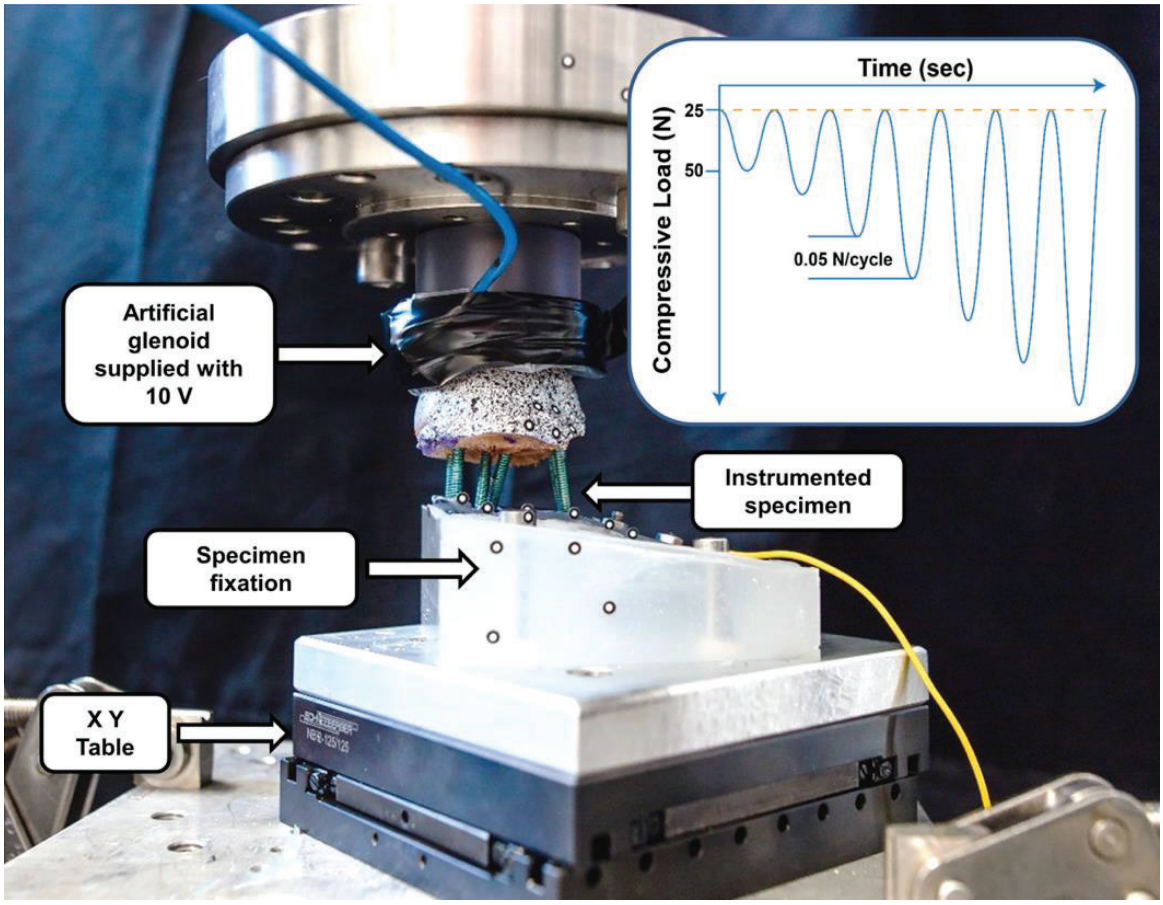

Figure 28. Biomechanical testing set up for screw perforation. Shearing of humeral head alleviated with the addition of an XY-table. Screw perforation detection with an artificial glenoid lined with copper. Motion tracking markers and spray on the humeral head were used for a different study and not for analysis in the present study.

6.2.4 Data acquisition and analysis

The system's controllers recorded machine data in terms of crosshead displacement and applied force at a sampling rate of 100 Hz. The displacement data was then extracted at the valley loads during cyclic testing, corresponding to residual specimen's deformation and used to identify screw loosening. The latter was defined by the first abrupt change in displacement under valley loads following the initial elastic behaviour, using Matlab software package (v. 2018a, Mathworks Inc., Natick, MA) (**Figure 29**). The corresponding cycle number indicating initial loss of stability of the screw's thread purchase in the trabecular bone defined the outcome cycles to screw loosening. Anteroposterior radiographic images were acquired using a C-Arm

(Arcadic Varic, Siemens, Medical Solutions AG, Munich, Germany) triggered every 500 cycles at peak load to monitor screw loosening and perforation during testing (**Figure 30**).

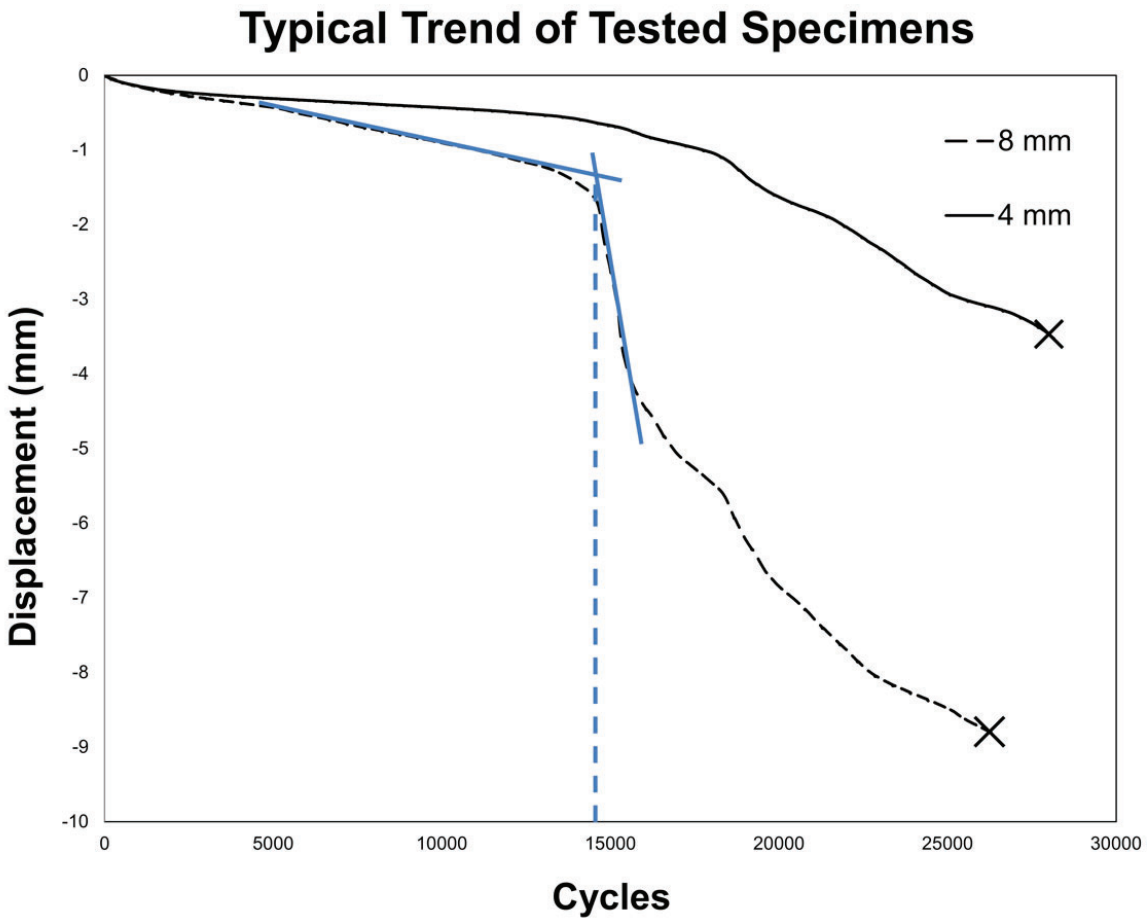

Figure 29 *Typical residual displacement vs the number of cycles curves for the two groups at unloaded state (valley load). Screw loosening event is highlighted from the annotated lines and failure event is marked with a cross.*

Moreover, the cycle number corresponding to the earliest screw perforation as a failure criterion defined the outcome cycles to failure. Also, the perforating screw was identified via visual inspection and noted. All specimens were re-scanned post testing with a GE Revolution EVO scanner to evaluate the mode of failure. Translational and rotational movements of the humeral head at failure were determined by co-registration of the CCT scans for each specimen post instrumentation and post-testing, based on the PHILOS plate using Amira image

processing software. Varus collapse was calculated as the rotation around the anterior-posterior axis at failure, while head tilting anterior (positive rotation) or posterior (negative rotation) was computed as the rotation around the longitudinal plate axis at failure. Additionally, the lateral-inferior head displacement was evaluated at failure.

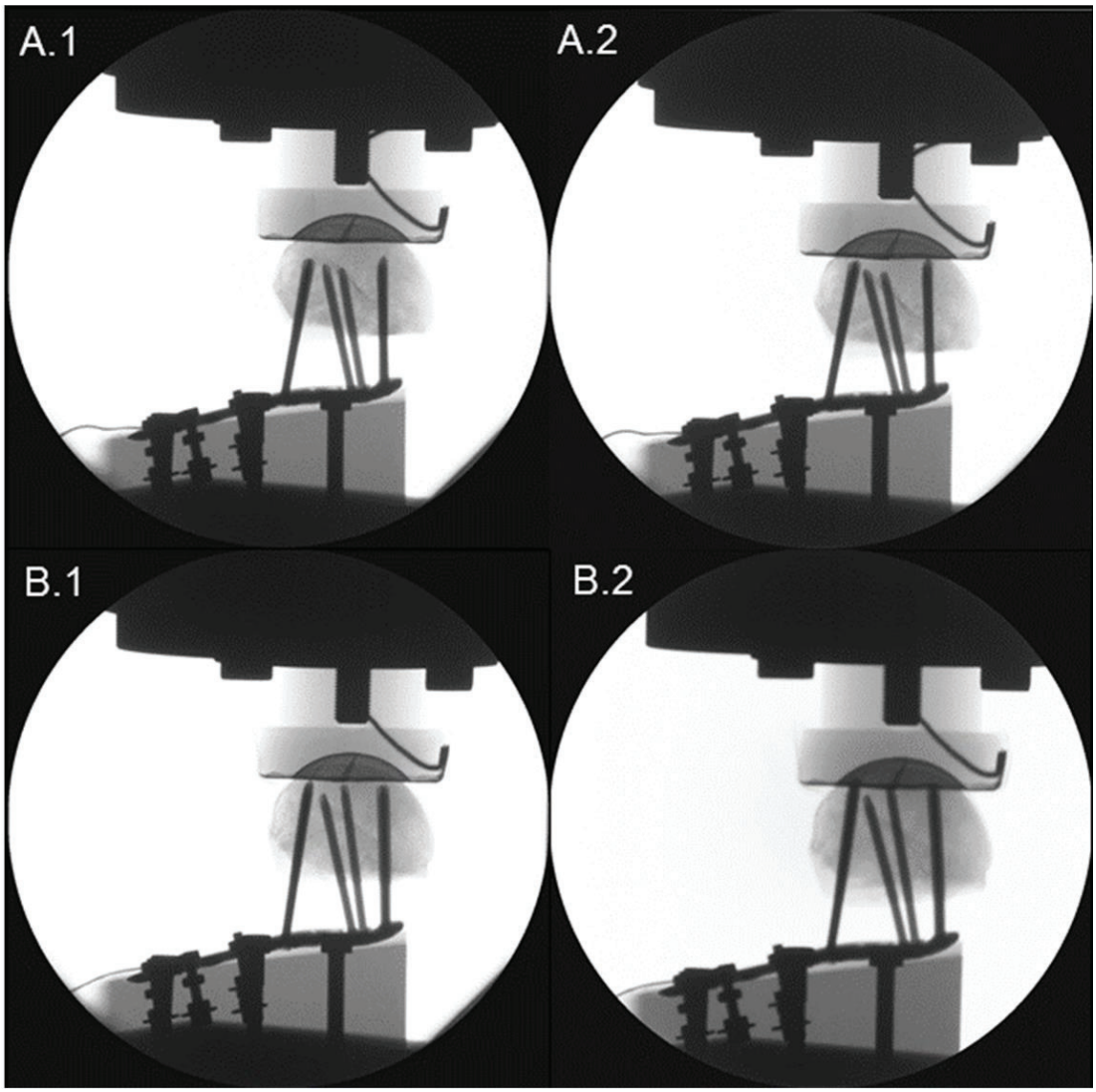

Figure 30. *Anteroposterior radiographs of instrumented pair at beginning of biomechanical testing (A.1: LSG 4 mm TJD) (A.2: SSG 8 mm TJD). Screw loosening event initiating head perforation of screws through to the articular surface for the two groups (B.1: LSG, B.2: SSG).*

6.2.5 Peri-screw BMD

The average BMD in cylindrical bone regions around the screw tips was evaluated with a previously developed methodology[66]. As the presence of metal caused image artifacts on the instrumented CCT images, the HR-pQCT scans of the intact specimens were used to determine the BMD by spatial co-registration with the instrumented CCT scans using Amira image processing software. The region of the head fragment on the intact HR-pQCT scan was isolated based on the segmented instrumented scan. Screw tip and head landmarks were defined on the instrumented CT scan and used to define cylindrical bone regions around the screw tip, with a cylinder diameter of 8 mm and length of 20 mm, with 5 mm towards the joint and 15 mm towards the screw head. The mean BMD was then evaluated in these bone cylinders using a GNU Octave 3.8.2 (www.gnu.org/software/octave/) script and averaged over the six proximal screws.

6.2.6 Statistical analysis

Statistical analysis was conducted using SPSS software (v21, IBM, Armonk, NY, USA). Normality of the data distributions was screened using a Shapiro-Wilk test. Potential differences between the two study groups in terms of head size and BMD, TJD, peri-screw BMD, cycles to screw loosening, cycles to failure, varus collapse, anterior and posterior head tilting, and lateral-inferior head displacement were evaluated with the Related-Samples t-test or the Wilcoxon Signed Rank test, for normally and non-normally distributed data, respectively. Level of significance was set at 0.05 for all statistical tests.

6.3 Sub-study 1: Results

Global trabecular humeral head BMD ranged between 79.80 and 166.90 HA mg/cm^3 (mean ± SD: 119.70 ± 28.81 HAmg/cm^3) and was not significantly different between the two groups (LSG: 122.07 ± 28.46 HAmg/cm^3, SSG: 117.31 ± 28.97 HAmg/cm^3), p=0.16. Head radius range was from 22.15 mm for the smallest to 25.32 mm for the largest specimen, with no significant difference between the groups (LSG: 24 ± 1.0 mm, SSG: 23.9 ± 1.03 mm), p=0.79. Average TJD, measured from instrumented CT scans, was significantly smaller for LSG (4.08 ± 0.86 mm, range: 1.50 – 6.16 mm) than SSG (8.40 ± 0.85 mm, range: 5.54 – 10.17 mm), $p < 0.01$. During instrumentation, no intraoperative perforation of the medial humerus head cortex was observed in any specimen. Peri-screw BMD was significantly different between the two groups for screw row A (LSG: 183.74 ± 41.76 HA mg/cm^3, SSG: 126.90 ± 34.24 HA mg/cm^3), p=0.027, screw row B (LSG: 134.54 ± 41.20 HA mg/cm^3, SSG: 92.11 ± 35.17 HA mg/cm^3), p=0.01, and screw row E (LSG: 136.14 ± 34.51 HA mg/cm^3, SSG: 96.78 ± 26.98 HA mg/cm^3), p=0.004. The number of cycles to screw loosening was significantly higher for LSG (17532 ± 6458, range: 9480 - 30192) compared to SSG (11002 ± 5440, range: 3999-19168), $p < 0.01$ (**Figure 31**) (59% difference between the two groups). Screw loosening on average occurred at a crosshead displacement of 0.88 ± 0.20 mm for both LSG and SSG with no significant difference between the groups, p=0.99. Number of cycles to failure for LSG (27849 ± 5648, range: 19929 - 39694) was not significantly different compared to SSG (28782 ± 7307, range: 19898 - 46549), p = 0.5. The magnitude of varus collapse at failure was 4.9 ± 3.2° for LSG and 3.5 ± 1.9° for SSG, with no significant difference between the two groups, p=0.16.

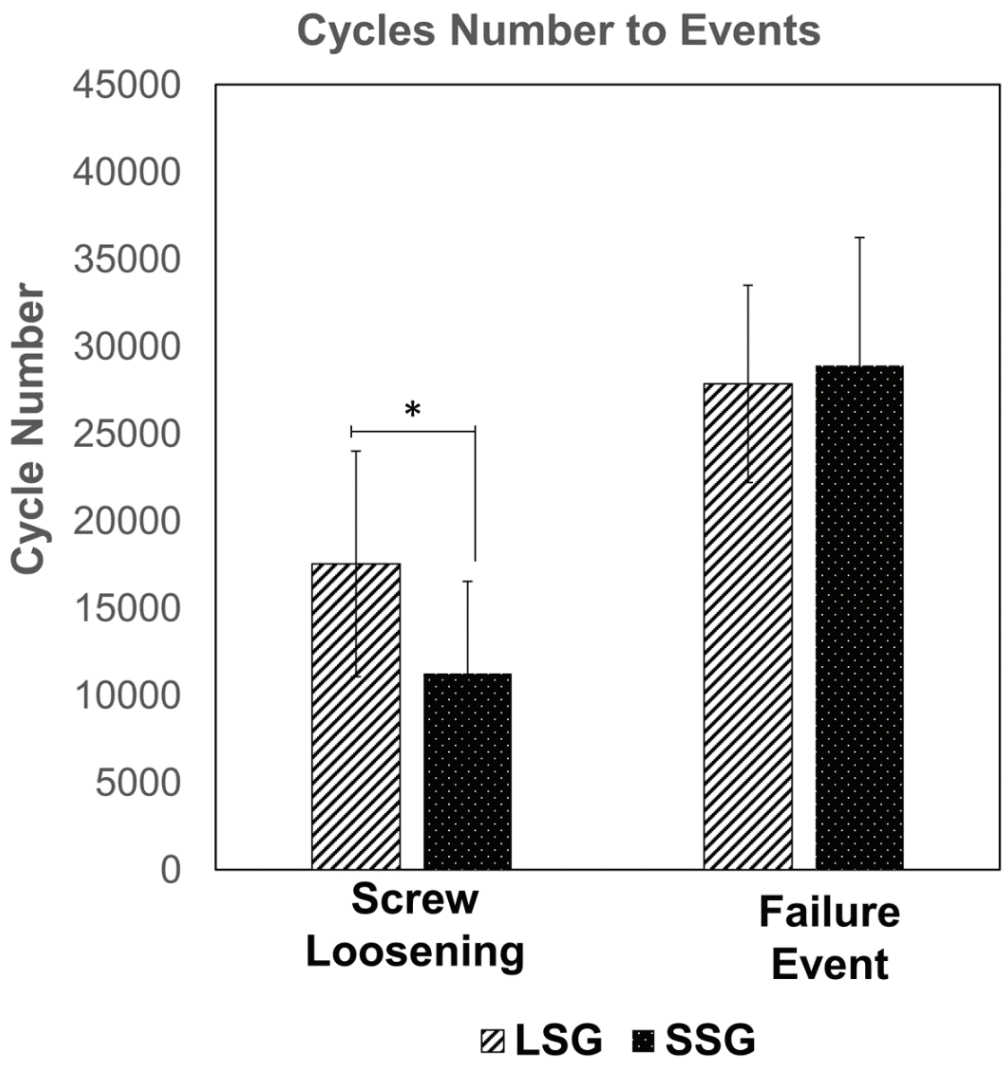

Figure 31. The cycle number at screw loosening and failure event for the two groups.

Head tilting at failure was not significantly different between the two groups (LSG: -2.6 ± 2.8°, range: -5.9 – 1.2°) (SSG: 2.6 ± 4.6°, range: -4.6 – 11.4 °), p = 0.074. The magnitude of lateral-inferior humeral head displacement at failure was significantly smaller for LSG (5.7 ± 1.1 mm) compared to SSG (10.2 ± 3.9 mm), $p<0.01$. In both groups, a screw from row E was the first one to perforate the joint surface (**Figure 32**) except a single case where a screw from row A perforated at the same time as another screw from row E. Individual specimen results and summaries can be found in Appendix C.

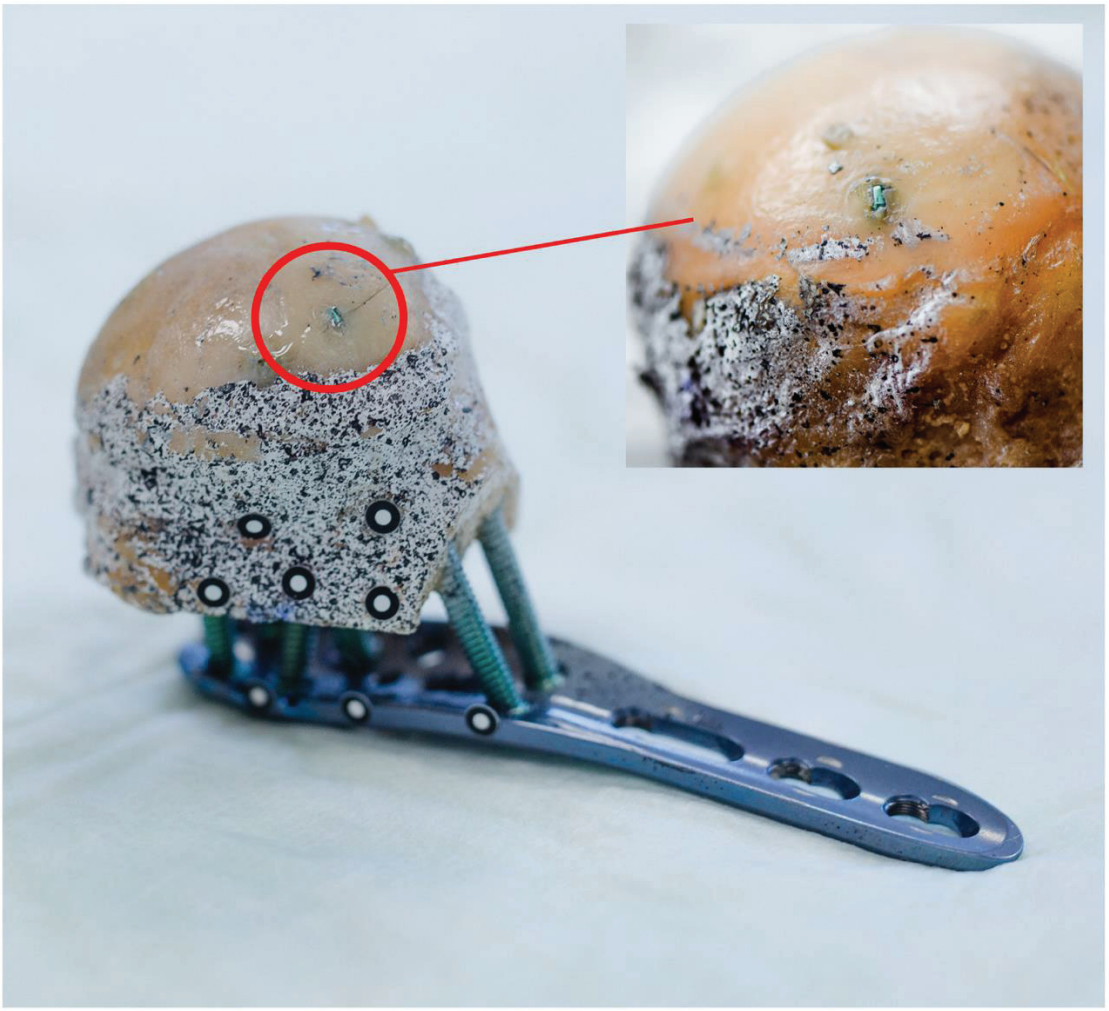

Figure 32. *A post-failure photograph showing the perforated calcar screw protruding through the articular cartilage of the joint.*

6.4 Sub-study 1: Discussion

This study aimed to investigate whether screw purchase closer to the joint surface would result in an earlier secondary perforation than purchase away from it. Bone stock quality determines the initial fixation stability[41], with the strongest bone to purchase located medially in the subchondral bone, and the weakest bone located within the central region of the humeral head[26,59]. The challenge resides in the case that longer screws have their tips closer to the joint and thus may increase the chances of secondary screw perforation. The most important outcome was that there was a superior screw purchase of longer screws regarding initial loosening with no significant difference in the cycles to failure between the two groups with different TJD. The study hypothesis could be accepted. These biomechanical findings suggest that, when using longer screws within the boundaries of the surgical guidelines, i.e. purchasing closer to the joint, the risk of secondary perforation is not increased.

Considering that screws purchased adjacent to the subchondral bone are crucial in preventing other mechanical failure types such as screw cut-out and humeral head varus collapse, screw length selection is, therefore, a crucial component in fixation success[12,39,60]. Indeed, a previous computer simulation study reported that longer screws were beneficial for decreasing the cut-out failure risk[50], but remained inconclusive considering screw perforation. The biomechanical evidence from the present study implies that the occurrence of secondary screw perforation failure was not influenced by the screw length, indicating no increased risk of placing the screw tips closer to the joint. We conjecture that the stronger purchase of the LSG in the denser subchondral bone cancels out the effect of the SSG perforating a greater distance. These suggest that placing longer screws, within limits dictated by the surgical guide, is expected to decrease the risk of screw cut-out while not increasing

the risk of secondary perforation failures in the surgically challenging, complex and highly unstable PHF. Some previous reports have commented that surgeons may practice choosing short screws over long screws to avoid intra-articular penetration of the joint[12,20,60,62]. These reports are not supported by our study; in contrary, shorter screws may increase the risk of the above mentioned other mechanical failure types[17]. Our findings are consistent with Hymes et al. who recommended that surgeons should maximise the depth of screw insertion to decrease the chances of failure, particularly in the case of osteoporotic bone[74]. However, they recommended that this must be weighed against the risk of using screws which are too long, and risks associated with joint penetration. Our biomechanical results indicate that secondary joint penetration is not increased by utilising longer screws.

Nevertheless, realising optimal screw length in a clinical setting is challenging, and the risk of primary perforation is higher when drilling and inserting screws close the joint. In poor bone quality, tactile drill feedback is weak and may result in boreholes drilled too far. Ideally, methods and devices guaranteeing that the planned TJD can be achieved are required, so that screw length selection is guided[60,79]. Surgical guidance for screw selection is essential to avoid both intraoperative penetrations of the medial cortex and placement of too short screws risking the chances of early screw loosening and varus collapse of the humeral head.

6.4.1 Previous studies

To the best of the author's knowledge, there is no previous work investigating the effect of screw length on the perforation risk in PHF. Katthagen et al. and Erhardt et al.[61,69] tested for screw perforation by loading the humeral head. The primary focus of their study was not the same as the investigation in sub-study 1 on screw length so that they did not report on differences in TJD and the effect they have on

perforation characteristics. Furthermore, a study by Liew et al. reported the most robust screw purchase locations within the humeral head for different TJD[26]. However, their study investigated how TJD affects the mechanical properties of screws for pull-out force rather than screw perforation. The results from our study bare resemblance with a study from Acklin et al. who did not necessarily compare screw length but compared gliding screw concepts against standard PHILOS plating in PHF[80]. They found that even though more optimal subchondral anchorage was targeted, there was no influence on screw perforation biomechanically, and commented on screw sharpness influencing the rate of perforation. Screw tip sharpness was not assessed in our study but was addressed by Freude et al. who conjected that lower rates of perforation occurred when using dynamic locking screws because of their blunt screw tips[81]. Stress concentration can become prominent when there are abrupt changes in cross-sectional areas of screws and plates. The stress concentration places the bone-implant interface under a higher risk of anchorage loosening and eventual failure due to an increase of stress surrounding purchase region. Provided that our results show that TJD has no significant influence on secondary screw perforation failure event, tip sharpness or methods of surgical procedures, such as boreholes drilled too far, could be more influential factors on this prominent mechanical failure type.

6.4.2 Screw loosening

The key finding of our study was that longer screws were beneficial against initial screw loosening. The initial construct stability – in relation to the cycles to screw loosening – was significantly different between the two groups. Initial stability and screw fixation are essential because if they are compromised, the onset of head collapse commences. Implant loosening as a result of weak anchorage in poor bone

quality is a still commonly reported complication with adverse effects on the recovery of a patient[15,64,82,83]. In this study, the screw loosening event could be identified by the initial loss of stability before the onset of perforation accompanied by the head varus collapse. The possible explanation for the significant difference regarding the screw loosening event in the two groups is twofold: screws in the LSG had more threads purchasing in the humeral head and the additional threads – compared to SSG – were in the relatively denser subchondral bone. The difference between groups in terms of screw loosening resides in the difference of TJD but also in the different BMD surrounding the threads of the screw, which we found to be significantly lower for SSG compared to LSG for all rows. The study by Liew et al. reported that the effect of screw placement in the humeral head improves the absolute pull-out force by purchasing in the subchondral opposed to the cancellous bone, even if normalising for the length of purchase. These results coincide with the consensus from this study that screws, which purchased at different depths in the humeral head, loosen after a significantly different number of cycles[26].

6.4.3 Limitations

The findings from this study were obtained via biomechanical testing of a highly unstable fracture type, where the reduction is not correctly achieved intraoperatively, and the humeral head is free to collapse, and screws perforate. With this model, we attempted to replicate a worst-case scenario, knowing that secondary screw perforation is a common complication in PHF and occurs when the humeral head subsides from a lack of medial support and poor anatomical reduction[15,17,39,58]. Königshausen et al. recognised the secondary loss of reduction as a contributor to secondary screw perforation, which was one of the most prominent complications, contributing to 41.6% of the study's complications, and 60% of screw

perforations[58]. The anatomical reduction is the most critical factor of providing medial support as this reduces the bone implant stresses[17]. When anatomical reduction cannot be achieved, such as in the case of medial comminution, then the humeral head is supported only by the screw purchase and hence free to rotate, and screws can perforate through to the joint surface[5,17,39,56].

Limitations should be considered as this was an in vitro study and some aspects are not directly translatable to in vivo situations. The load cell used for testing would have experience a loss of accuracy at lower loads of the humeral head, however, the system used was designed for biomechanical applications and failure loads were in order of the 10% capacity of the load, which is within the accepted performance range of the device. Freezing and thawing of cadaveric bones can lead to changes in tissue stiffness. The specimens underwent two freezing and thawing cycles to reduce the post-freezing effects. The first cycle consisted of tissue removal and preliminary CT scanning and the second included osteotomy, instrumentation and biomechanical testing. Despite achieving the desired TJD between the two groups, human error and only commercially available screw lengths and oblique joint surfaces, e.g. at the calcar region, made achieving an accurate TJD challenging. Such as in the case of one specimen from the LSG, which had a TJD of 1.5 mm for a calcar screw. However, the overall difference in TJD was significant between the two groups. This study was conducted on humeri without any soft tissue, with muscle forces and ligamentous stabilisation disregarded. Although the way perforation occurs in the humeral head is known, the physiological loading of the humerus, which results in perforation, remains relatively unknown. Loading only the humeral head is a limitation to the study as there are currently no available in vivo studies, describing screw perforating from such a perspective, but only from in vitro testing[61,69]. On the basis

of in vivo loading data[71], biomechanical testing setups that load from 25° lateral angulation have been developed, inducing primary varus bending. However, the related failure mode was screw cut-out type failure rather than screw perforation[7,67,68,84]. Testing for screw cut-out type failure is clinically relevant, as it is reported in high rates[39,84]. However, previous reports have shown that secondary screw perforation is also occurring at alarming rates[5,12,15,16]. In a study that investigated early complications of PHF with locked plating, Egol et al[5]. reported screw perforation as their most prevalent complication, more so than screw cut-out type failure, from improper hardware placement. Problem-based testing setups are designed for specific mechanical failure types; the setup of this sub-study 1 was based on those of previous studies by Katthagen et al. and Erhardt et al.[61,69]. Complex complications of the proximal humerus do not occur in isolation but are interlinked with other factors, including biology, surgical procedures, and complex shoulder biomechanics. In vitro testing that only quantitively defines an aspect of PHF can only be a potential replication for in vivo performance of implants. Despite achieving clinically relevant mechanical failure types, these findings may be limited to the investigated fracture model and require clinical confirmation.

6.5 Sub-study 1: conclusion

The results suggest that placement of longer screws within limits dictated by the surgical guidelines does not increase the biomechanical risk of secondary perforation failures in the surgically challenging, complex and highly unstable PHF. In turn, smaller tip to joint distance may improve initial stability by delaying screw loosening and, based on findings of previous studies, can decrease the risk of screw cut-out. Clinically, these results should be interpreted with care, with the utmost importance, that this biomechanical study stands true when operating within the

surgical guidelines. Closer purchase to the joint can increase the chances of primary screw perforation, which occurs in higher rates than secondary perforation.

7. Sub-study 2: Predicting biomechanical cyclic screw perforation in complex proximal humerus fracture plating

Daniel Ciric[a,b], Dominic Mischler[a], Feras Qawasmi[a,d], Lisa Wenzel[a,c], Boyko Gueorguiev[a], Markus Windolf[a], Peter Varga[a]

[a] AO Research Institute Davos, Davos, Switzerland

[b] Flinders University, Tonesly, South Australia

[c]Department of Trauma Surgery, Trauma Centre Murnau, Murnau, Germany

[d]Hadassah Medical Centre, Jerusalem, Israel

7.1 Sub-study 2: Introduction

Early failure of locking plates in PHF is predominately due to poor primary reduction, a lack of medial support, level of osteoporosis and the rehabilitative protocol[5,64,85]. Studies have reported that fixation failure rates of plate osteosynthesis of unstable PHF can range up to 35% in the first post-operative year [72,86]. Secondary screw perforation through the articular surface of the glenohumeral joint is a prominent mechanical failure type which may be one of these early complications. Mechanical failure types are more likely to occur in the early post-operative stages because secondary stability has not yet been provided from hard callus formation. Prolonging the secondary healing phase from good primary stability is important to avoid these early mechanical type implant failures. The complexity of displaced PHF surgery for reduction achieving good primary stability makes pre-operative planning important. Displaced fractures accompanied by poor anatomical reduction places patients at the greatest risk of early fixation failure due to the instability that leads to greater bone fragment displacement[6,64,72,76]. Furthermore, if a surgeon is unable to achieve adequate reduction and fixation, then more invasive adjustments, such as

augmentation, reverse arthroplasty or other changes in post-operative rehabilitative protocols should be considered. Preserving the joint is the primary goal of many surgeons. In any case, the primary aim is to avoid fixation failure and the need for reoperation; as this is the worst case scenario for the patient. To avoid reoperation, strategies should be implemented to determine the risk associated with surgical fixation.

Defined in the investigation of sub-study 1, the cyclic failure event via secondary screw perforation is first initiated when initial stability is lost, and the screws loosen within the trabecular bone of the humeral head. Screw loosening is challenging to diagnose in a clinical setting because only large implant migrations are directly obvious from X-Ray and CT evaluation. Prolonging the initial stability before screw loosening is important for the patient outcome. Predicting the initial stability and the failure outcome for unstable fractures prior to surgery crucial for early patient intervention[44,47,56,72]. BMD measures and FEA simulations have been used previously to predict implant failure and success in plating osteosynthesis[11,41,43–47,50,65,66,68,72]. A previously published computational study predicted cyclic cut-out type failure in proximal humerus plating by correlating average compressive strain around the screw tips with experimental results to form strong prediction curves for the success the implant fixation[66]. An in vitro study by Röderer et al. investigated local bone quality for predicting cut-out type failures in PHF[68]. The strong correlation between peak torque and number of cycles to failure in this biomechanical model provide local bone quality as a suitable tool for improving the stability of fixation. To the best of the author's knowledge, there is currently no method available to predict the occurrence of secondary screw perforation. Prior to clinical implementation, the effectiveness of the convergence of predictive models

needs to be assessed. To develop a model that predicts the phenomenon of secondary screw perforation, cross-validation by comparing the predictive outputs to the experimental ex vivo results from sub-study 1 needs to be made, i.e. correlation to the number of cycles for screw loosening and perforation failure was made. Additionally, prediction models should be practical for clinical implementation i.e. simple and computationally cheap. Therefore, sub-study 2 aimed to determine whether cyclic screw perforation failure of locking plate fixations could be predicted in highly unstable and complex PHF using bone density and FEA modelling. The hypothesis is that, in analogy with previous prediction studies, simple linear elastic FE models using peri-screw bone strain will have a strong predictive power for the different fixation failure events.

7.2 Sub-study 2: Materials and Methods

7.2.1 Specimen preparation and medical imaging

CT scans were required for developing the prediction models. As detailed in 6.2.1 Specimens section of sub-study 1, ten pairs of fresh frozen human cadaveric proximal humeri (seven males and three females, 75 ± 16 years old), range: 46 – 100) were selected for the study. Subsequent to thawing for 12 hours and prior to tissue dissection, the proximal part of each intact humerus was scanned with HR-pQCT with scanning settings of 60 kV voltage, 900 µA current, 82 µm isotropic voxel size. Specimens osteotomised with a highly unstable 3-part fracture (AO/OTA 11-B1.1) and scanned with CCT with scan settings 110 kV voltage, 114 µA current, 0.63 mm slice thickness. The osteotomised scans were used to 3D print a polyvinyl alcohol water-soluble surrogate bone fragment for instrumentation. The osteotomised fragments were surgically reduced and instrumented with the PHILOS plate using row A, B, and E. Following instrumentation and dissolving the lateral surrogate

bone fragment, specimens were scanned with CCT with the same scan settings as the osteotomised scan.

7.2.2 BMD conversion

The HR-pQCT were converted to units of BMD (HAmg/cm^3) using the calibration function of the Xtreme CT scanner.

$$s = slope = 1422.86$$

$$i = intercept = -36221$$

$$m_w = 0.25170$$

$$m = \mu = linear\ attenuation\ coefficient$$

$$h = HU\ (Hounsefield\ unit\ available\ in\ DICOM\ image)$$

$$BMD = ms + i$$

$$h = \frac{m - m_w}{m_w} \times 100$$

$$m = m_w\left(1 + \frac{h}{1000}\right)$$

$$\therefore BMD = h\left(\frac{m_w s}{1000}\right) + m_w s + i$$

$$\therefore BMD = 0.358133h - 4.07916\ \left[\frac{HAmg}{cm^3}\right] \qquad (1)$$

CCT scans were converted to units of BMD in HAmg/cm^3 using a density calibration phantom. The Phantom of the scanner was segmented (**Figure 33**) in image processing software Amira, and the greyscale of each rod was determined to derive the linear attenuation conversion equation seen in **Figure 34**.

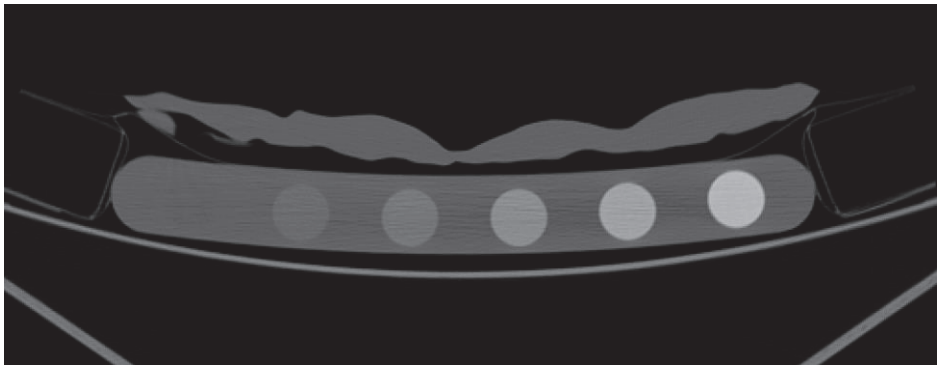

Figure 33. CCT of calibration phantom of GE Revolution CT scanner.

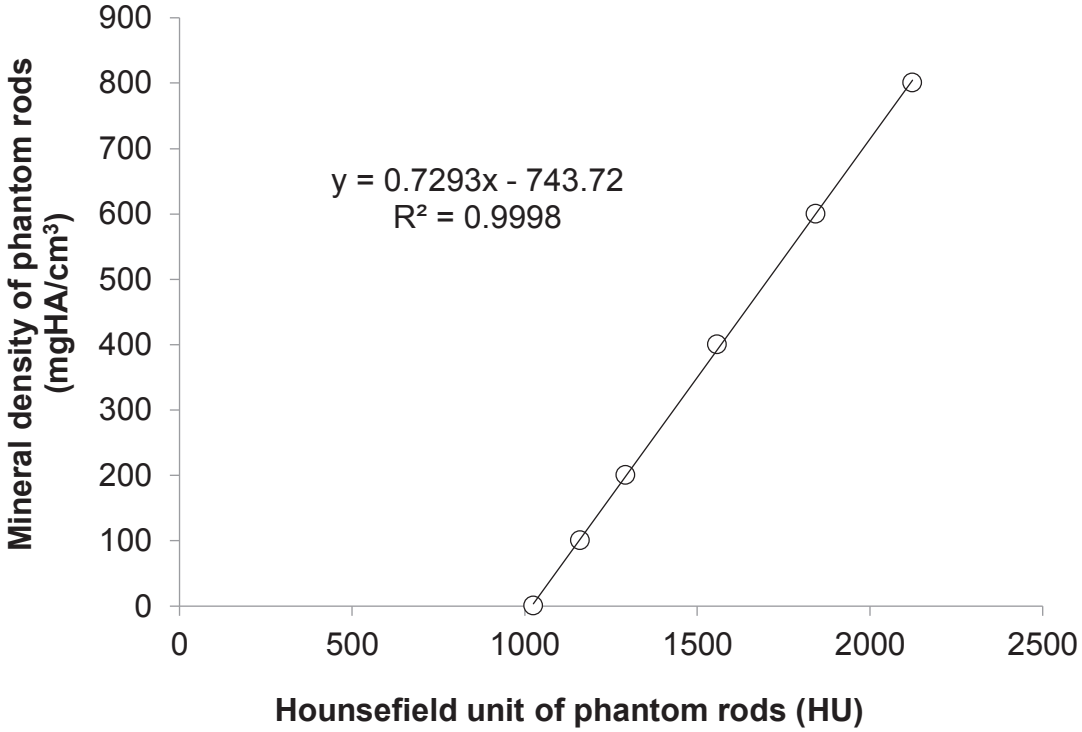

Figure 34. BMD conversion for CCT scans.

$$\therefore BMD = 0.7293h - 743.72 \left[\frac{HAmg}{cm^3}\right] \qquad (2)$$

7.2.3 Image processing

Specimen-specific (N=20) prediction models of the plated humeri were image processed using image processing software Amira 6.4 (**Figure 35 (A)**). Model components were defined by co-registering pre-instrumentation CCT and HR-pQCT scans within the spatial coordinates of the post-instrumented CCT scan. Prior to

developing the models, all scans were converted to BMD range in Amira software using the previously derived equations (1) and (2). Firstly, an iso-surface was generated on the PHILOS and screws of the implant and the surface geometry extracted (**Figure 35 (B)**). On the generated surface, screw tip and head landmarks were defined (**Figure 35 (C)**). Following landmark definition, an STL of the PHILOS plate was registered with the generated surface by aligning the faces of the geometry mesh (**Figure 35 (D)**).

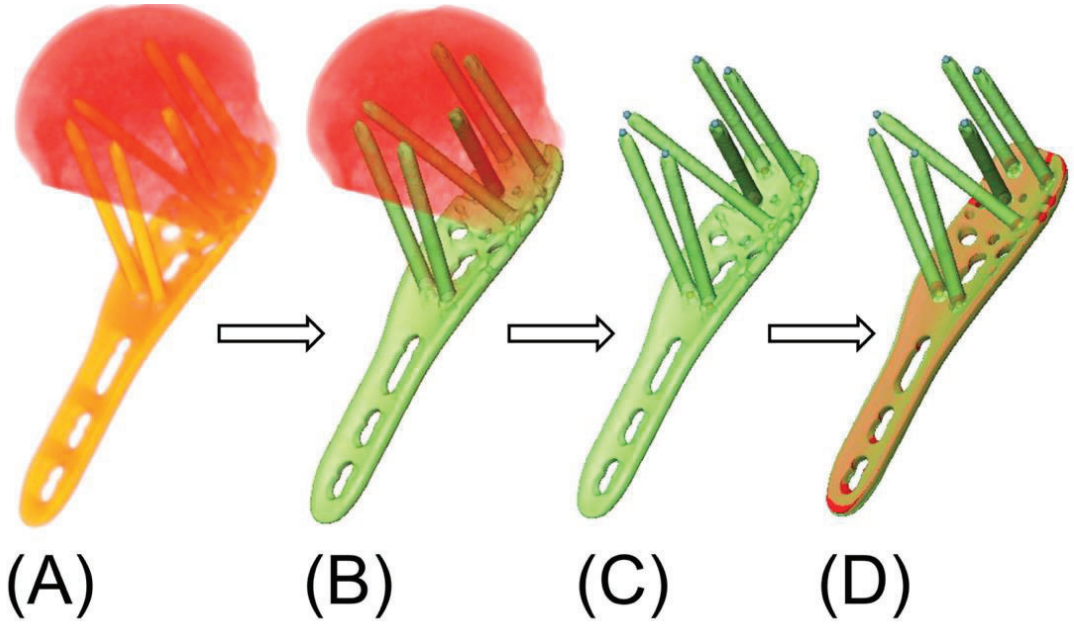

Figure 35. *(A) Instrumented CCT scan (B) Iso-surface generated on the plate and screws (C) Screw tip and head landmark definition (D) Registered STL of PHILOS to instrumented CCT scans.*

The humeral head of the osteotomised CCT scan was registered with the humeral head of the instrumented CCT. The HR-pQCT of the intact proximal humeri was then registered to the osteotomised humeral head (**Figure 36 (A)**). Metal artifacts in the instrumented CCT scans do not allow for BMD to be extracted, which meant that intact HR-pQCT scans needed to be registered. The cortical and trabecular bone was segmented using a special filling algorithm from software Medtool 3.8 (Medtool, 2014)[87]. From the segmentation, a combined compartment mask of the two bone

regions was generated and it was registered with the instrumented CCT scan (**Figure 36 (C)**). Following registration, all scans were resampled to an isotropic voxel size of 0.3 mm. The humeral head of the osteotomised CCT scan was segmented, including cortical and trabecular so that a virtual osteotomy could be made on the HR-pQCT scan and the combined compartment bone mask (**Figure 36 (B)(D)**).

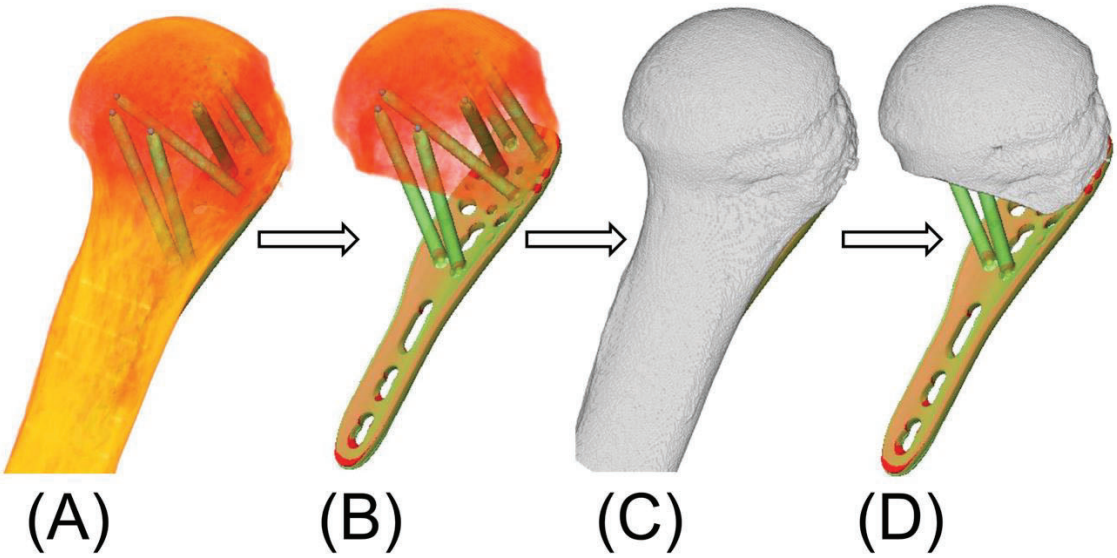

Figure 36. *(A) Registered HR-pQCT scan with the instrumented clinical CT scan (B) Virtual osteotomy of the HR-pQCT scan (C) Registered bone compartment mask scan with the instrumented CCT scan (D) Virtual osteotomy of the bone compartment mask.*

A combined compartment mask was generated from all the previously specified components (**Figure 37**) using a custom written script with GNU Octave 3.8.2 (www.gnu.org/software/octave/) with the iso2mesh 2013 toolbox[88]. The masked image was output with the following domains: (1) osteotomised head trabecular mask, (2) osteotomised head cortical mask, (3) PHILOS Plate STL, (4) Screw 1 STL, (5) Screw 2 STL, (6) Screw 3 STL, (7) Screw 4 STL, (8) Screw 8 STL, (9) Screw 9 STL, (10) Articular cartilage mask. Screw number configuration can be seen in Appendix B on the specimen instrumentation sheet. The virtually osteotomised HR-pQCT scans, instrumented CCT scan and the compartment mask of the cortical and trabecular bone registered with the instrumented CCT scan was imported. The STL

of the registered PHILOS plate and the screw head and tip landmarks were imported. The articular cartilage was approximated by dilating the outer surface of the cortical bone mask. The screw tip and head locations were used to position a simplified threadless screw STL file with its length was adjusted based on the cartesian coordinates and the normal axis between the screw head and tip landmarks. An iPython script is then output at the end of the code which contains the parameters required for the meshing.

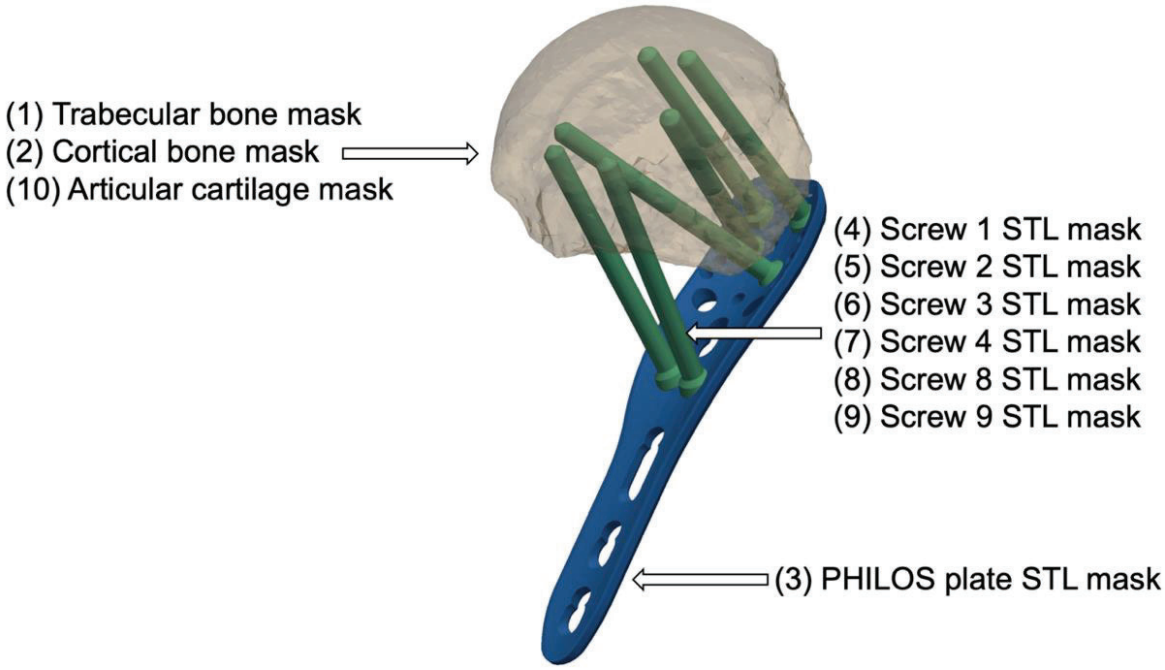

Figure 37. Mask domain regions labelled with a number corresponding mask layer.

7.2.4 Numerical modelling

Specimen-specific FE models of the bone and implant fixation were generated from CT scans. The boundary conditions of the experimental setup in the 6.2.3 Biomechanical testing section of sub-study 1 were recreated and linear elastic analyses were performed. The main output assessed for the FE model was the average minimal compressive principle strain (μstrain) around the proximal end of the screws[67].

7.2.5 Meshing and material properties

Linear tetrahedrons were used to mesh the combined compartment masks (**Figure 38**). A default mesh density was established for all models with an average length of edges in the mesh of 0.77 ± 0.48 mm and containing approximately 909943 ± 88760 elements within the mesh. The convergence of mesh density for the course and fine mesh was assessed for the following edge lengths 1.09 ± 0.75 mm and 0.66 ± 0.35 mm and element amount of 301147 ± 30554 and 1630859 ± 165383 respectively. The results of the convergence study can be found in Appendix E.2. A custom iPython script was used to batch mesh the masks through ScanIP software (Simpleware Ltd.; Exeter, UK) which assigned element connectivity and material properties. The PHILOS plate and locking head screws were modelled with titanium material properties with Young's modulus of 105 GPa, linear elastic behaviour and Poisson's ratio of 0.3. The material properties of the bone elements were assigned based on the co-registered HR-pQCT BMD values. The material properties were assigned based on a relationship from Dragomir-Daescu et al. where ρ is the elements ash density in units of g/cm^3, as seen in equation (3)[89].

$$E = 14664\rho^{1.49} \qquad (3)$$

The bone implant interface, as well as the screw-plate interface, were modelled as tied.

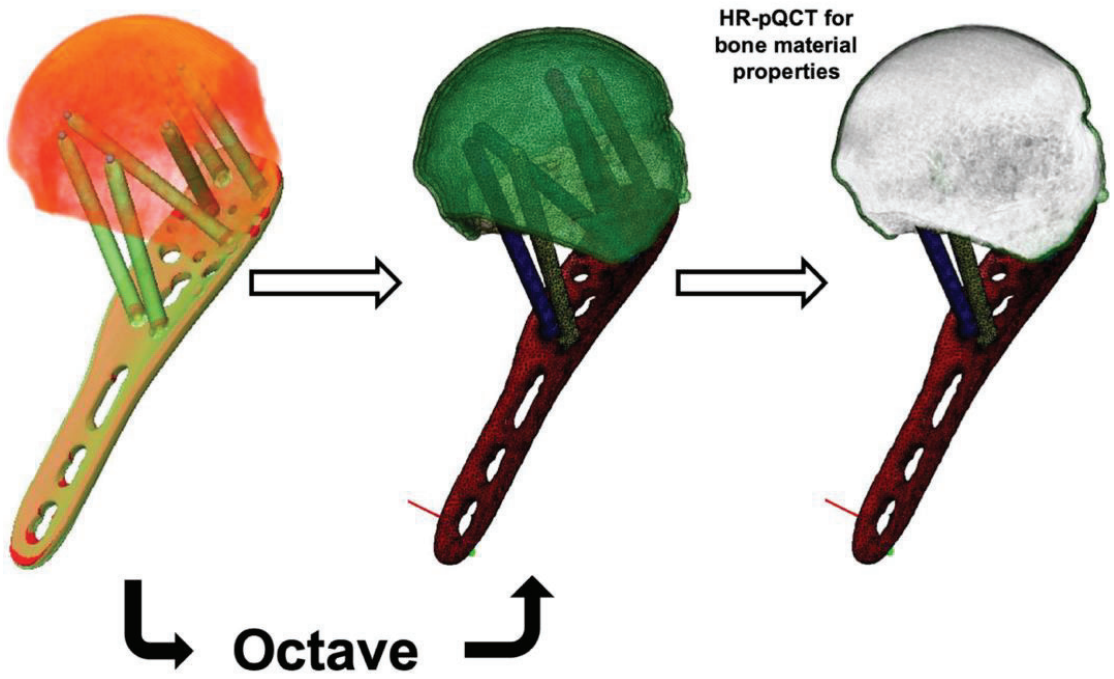

Figure 38. Image processing components, run with a custom octave script to generate mask to mesh and assign material properties in ScanIP software.

7.2.6 Biomechanical testing and boundary conditions

The prediction models were validated by correlating the results with the screw loosening and failure defined from the testing in sub-study 1. The FE model was aligned with the boundary conditions of the experimental testing set up (**Figure 39**). The 3D model of the mesh was transformed by creating a coordinate system on the plate component. A custom-made Python script was used to pre-process and align the humerus to the global coordinate system of Abaqus v6.13 (Simulia, Dassault Systemes, Velizy-Villacoublay, France). The model was aligned with the same angulation as the experimental setup. All models were imported into Abaqus and aligned using coordinate systems created on the landmarks of the screw tip and head and two landmarks defined on the combi-hole of the PHILOS plate.

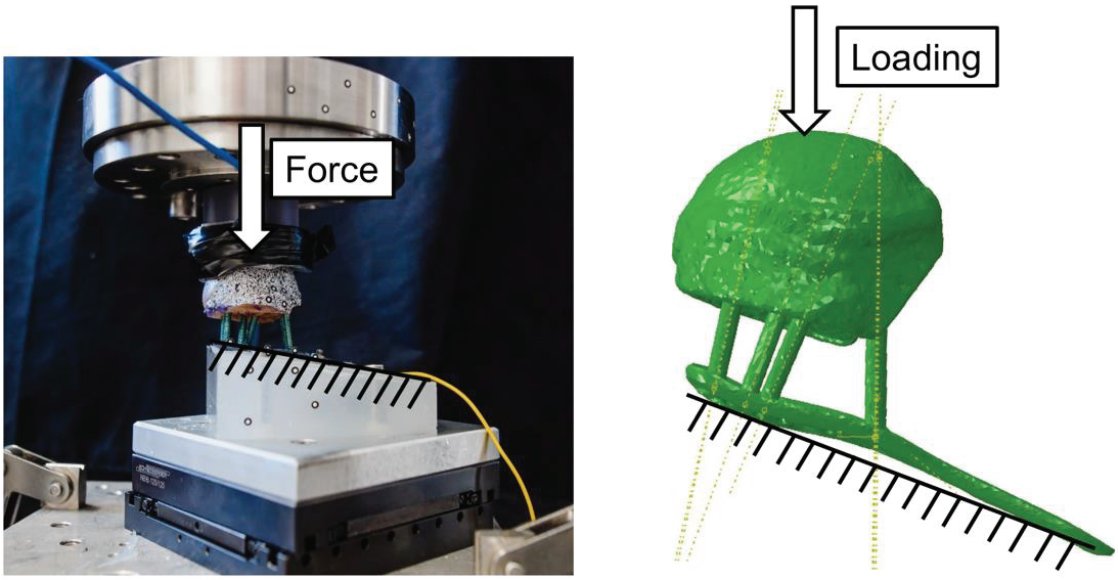

Figure 39. CAD model aligned in Abaqus with the experimental setup, screw axis is shown on the Abaqus model.

The pre-processing script generated an input file for each specimen which was required to run the simulation. Simulations were batch run and result files were produced for post-processing analysis.

7.2.7 FE Simulations and post-processing

A Linux server equipped with 192 GB of RAM and 24 Intel Xeon X5690 CPUs having a clock speed of 3.47 GHz was used to perform the FE analysis with standard implicit solver on Abaqus. A custom written Python script batch ran the input files containing the boundary and loading configurations. Three different models were generated that simulate the boundary conditions of the experimental procedure. The first was a 100 N Gaussian load (The Gaussian model) as a function of distance, distributed over the surface nodes of the head fragment, with a radius of 15 mm applied onto the highest vertical node on the humeral head, with respect to the global coordinate system of Abaqus. The second was an analytical rigid surface with a cup shape that mimicked the contour of the testing drop head and loaded onto the

humerus model (The cup loaded model). The cup loaded the humerus model with 3 steps:

1. The cup displaced vertically to contact the humeral head, all the degrees of freedom constrained except for the vertical translation
2. The cup balanced above humeral head to simulate X Y slider table, all the degrees of freedom constrained except for the horizontal translation
3. A 100 N load applied from the cup to surface of the humerus model, all rotational degrees of freedom constrained, vertical and horizontal translation degrees of freedom unconstrained

The last simulation type was a pseudo perforated model in which all the STL screw components were virtually extended to the subchondral bone (The extended screw model). The extended screw model was loaded with Gaussian distribution due to the convenience of simulation time and model convergence.

The default model was the 100 N Gaussian loaded model and the other models acted as a reference to this. The results were post-processed using a custom-written Python script. A cylindrical region around the screw tip was used for the evaluation. Within the cylindrical region, the main output was the volume weighted average minimal compressive principal strains (μstrain) of the elements within the cylindrical region[67]. A parametric study was conducted assessing different cylinder sizes. The cylinder sizes assessed in the parametric study along with the output correlation are summarised in Appendix E. The most optimal cylinder size was determined from the model output with the highest correlation to the experimental number of cycles to screw loosening and failure. The cylinder size with the highest correlation to screw loosening had a radius of 4 mm, a length in front along the trajectory of the screw tip of 5 mm and length behind the screw tip of 15 mm. The

average strains of the elements within the trabecular and cortical bone were analysed and averaged over all head screws. This cylinder size was applied to the cup loaded model, the pseudo perforated model and the models with different mesh density.

7.2.8 Density-based measurements

A custom-made Octave GNU script was used to analyse a domain around the screws in the instrumented humeri CCT scan. For each proximal screw, a cylindrical region was defined around each of the screw tips (**Figure 40**) using the screw tip landmarks defined in the Image processing section. The method to calculate the BMD (HAmg/cm^3) and BMC (mg) around the screw tips was using a previously developed method evaluated by Varga et al.[66]. The imaged voxels within the cylindrical region at the screw tip landmark are identified. The average BMD and total BMC were computed for the regions of all head screws based on the BMD-scaled co-registered HR-pQCT image of the head fragment. A parametric study was conducted which measured the BMD and BMC at different cylinder sizes around the screw tip. The correlations from the parametric study of the density measures can be found in Appendix F. Cylinder sizes were selected based on the strongest correlation. The selected cylindrical region for the screw loosening event was a radius of 3 mm, a length above the screw tip of 5 mm and a length below the screw tip of 20 mm. The selected cylindrical region for the failure event was a radius of 1.5 mm, a length above the screw tip of 15 mm and a length below the screw tip of 30 mm. Both the cortical and trabecular bone compartments were included for the measurements. A summary of the methods and code langeuges used to develop the two types of prediction models is summarised in **Figure 41**.

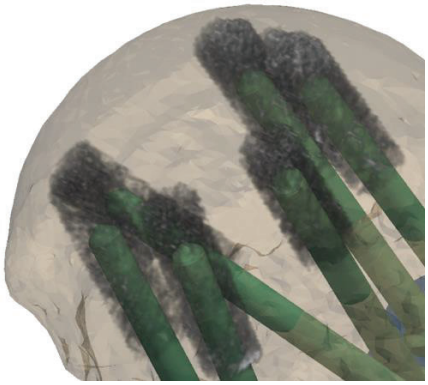

Figure 40. The bone cylindrical region around screw tip.

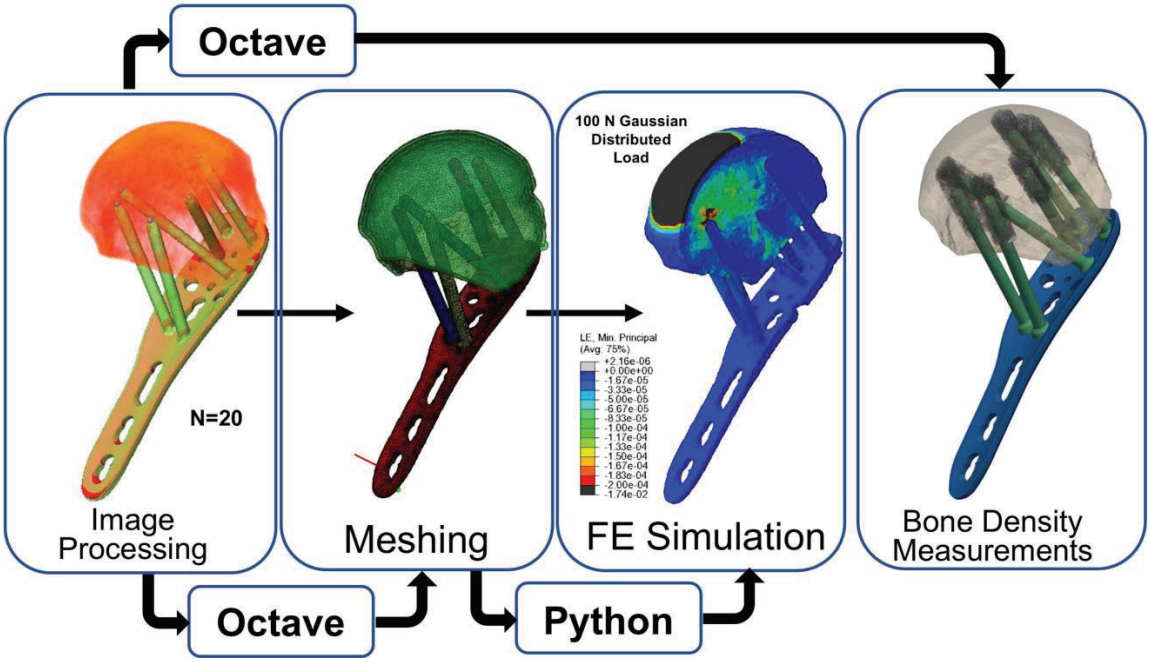

Figure 41. Summary of components required to develope the FE model and density-based measurement prediciton models.

7.2.9 Statistics

Analogous with previous studies predicting cut-out type failure, average BMD, total BMC, and average compressive principle strain were evaluated in cylindrical bone regions around the screw tips. These parameters were then correlated with the experimental number of cycles to screw loosening and failure event to assess predictive potential. Linear regression Pearson correlation was performed in Microsoft Excel (2014) and the R^2 coefficient of determination and standard error of estimate (SE) was used for prediction strength and validation of the model.

7.3 Sub-study 2: Results

7.3.1 Screw loosening correlations and results

The experimental number of cycles to initial screw loosening ranged between 4'000 and 30'200 (mean ± SD: 14391 ± 6681 cycles). The average minimum compressive principle strain around the screws for the default Gaussian model was -59.9 ± -32.3 μstrain (range: -1.53 to -22.7 μstrain). The Gaussian loaded model had a strong logarithmic correlation between peri-screw strain to the cycles to screw loosening (R^2=0.84) (SE: ± 4128 cycles). The average minimum compressive principle strain around the screws for the cup loaded model was -52.1 ± -20.1 μstrain (range: -10.6 to -2.23 μstrain). The cup loaded model had a moderate logarithmic correlation between peri-screw strain to the cycles to screw loosening (R^2=0.61) (SE: ± 4306 cycles). The average minimum compressive principle strain around the screws for the extended screw model was -34.2 ± -14.7 μstrain (range: -70.2 to -17.5 μstrain). The extended screw model had a weak logarithmic correlation between peri-screw strain to the cycles to screw loosening (R^2=0.41) (SE: ± 5385 cycles). The average total BMD around the screws for the selected cylinder size was 128.4 ± 36.4 HAmg/cm^3 (range: 66.8 – 203.2 HAmg/cm^3). The average BMD around the screws had a strong linear correlation to the cycles to screw loosening (R^2=0.79) (SE: ± 3260 cycles). The total BMC around the screws for the same cylinder size was 475.5 ± 122.7 mg (range: 252.3 – 737 mg). The total BMC around the screw had a strong linear correlation to the cycles to screw loosening (R^2=0.83) (SE: ± 2920 cycles).

7.3.2 Failure results correlations and results

The number of cycles to the failure event ranged between 19'900 – 46'500 (28316 ± 6547 cycles). The default Gaussian loaded model had a weak logarithmic correlation

between peri-screw strain to the cycles to failure (R^2=0.19) (SE: ± 6290 cycles). The cup loaded model had a weak logarithmic correlation between peri-screw strain to the cycles to failure (R^2=0.12) (SE: ± 6971 cycles). The extended screw model had a moderate logarithmic correlation between peri-screw strain to the cycles to failure (R^2=0.55) (SE: ± 4993 cycles). The average BMD around the screw had a moderate linear correlation to the cycles to failure (R^2=0.56) (SE: ± 4590 cycles). The total BMC in front of the screw to the surface of the humeral head had a strong linear correlation to the cycles to failure (R^2=0.75) (SE: ± 3444 cycles). Coarsening the mesh approximately increased the simulation time by a factor of four whereas finer mesh resulted in approximately five times longer simulation when compared to the default mesh density. The difference in correlations to the default Gaussian loaded model can be seen in **Figure 42**. Summaries of the FEA and density correlations can be found in Appendix E and F respectively.

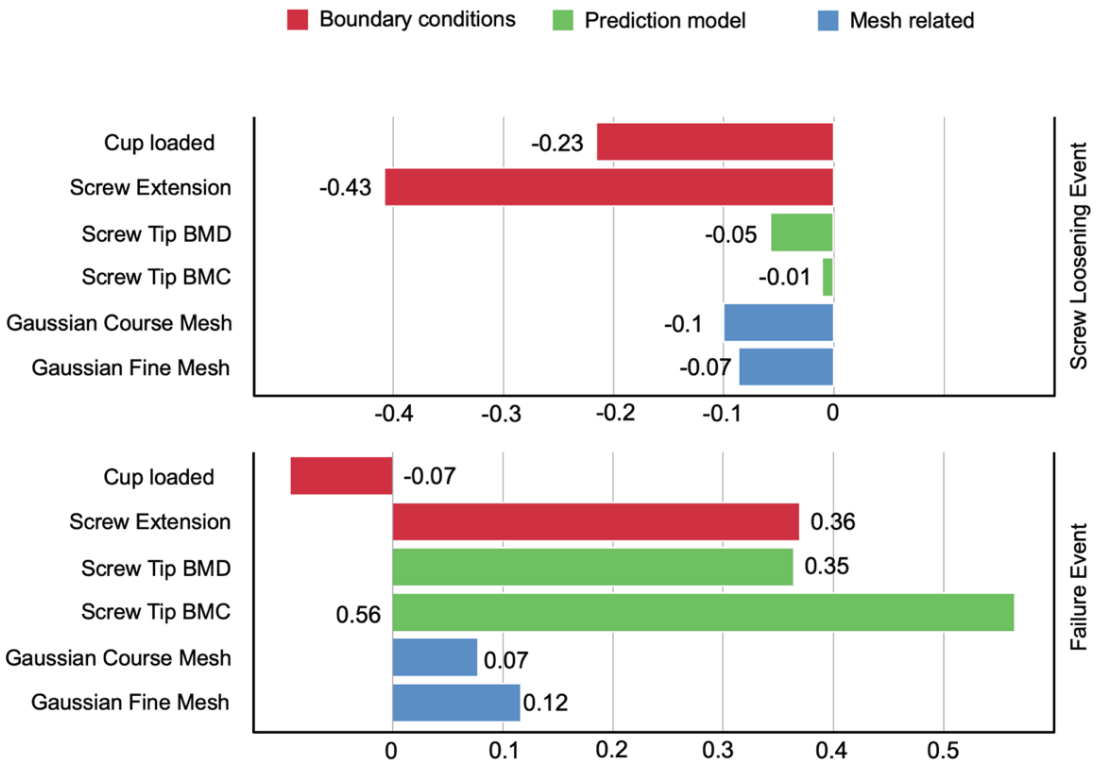

Figure 42. The difference in correlation coefficient R^2 compared to the default Gaussian loaded model.

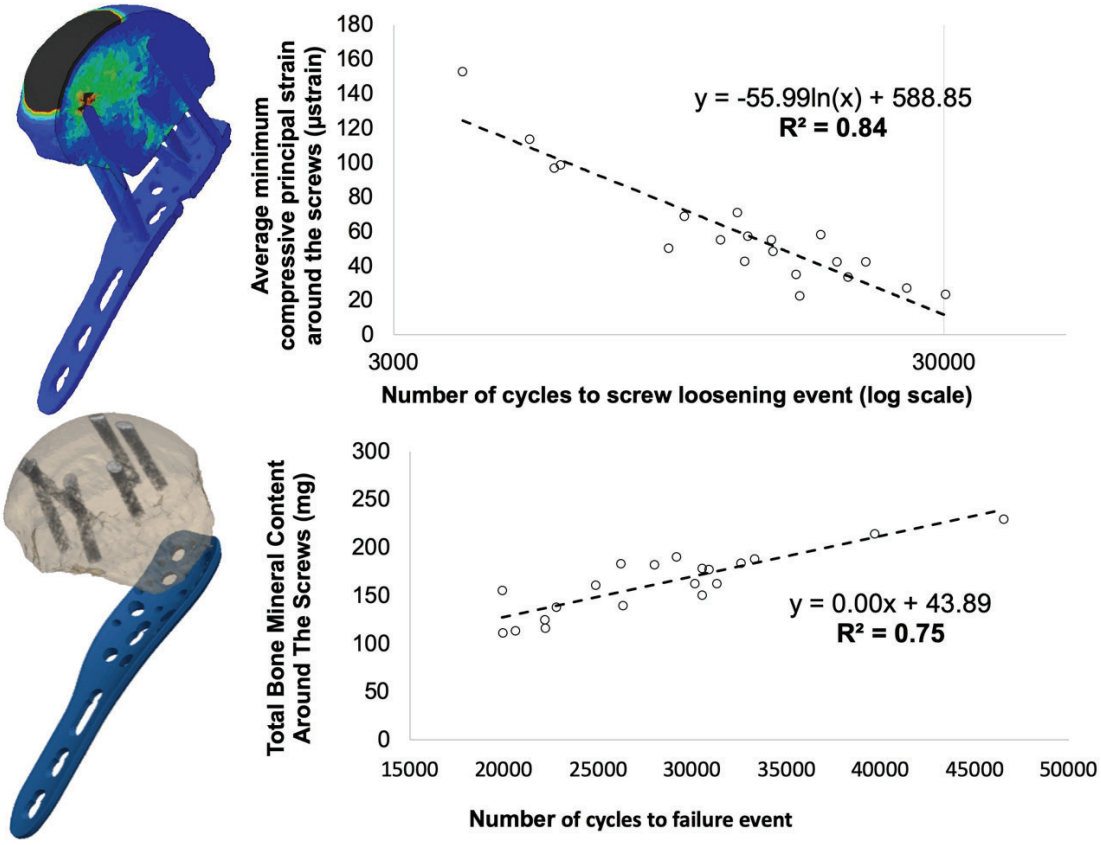

Figure 43. The strongest correlation amongst all models for screw loosening and failure number of cycles.

7.4 Sub-study 2: Discussion

This sub-study investigates whether a prediction model could be developed for secondary screw perforation in complex and unstable PHF. Post-operative outcomes are challenging to determine due to the surgical complexity in treating PHF. Challenges vary depending on mechanical factors of bone quality, implant placement, screw purchase and the quality of anatomical reduction; all contributing to fixation success in the early post-operative stages[37,64]. The most important outcome from the study is a strong correlation to screw loosening (FE model) and failure (BMC measures). The strongest correlation to initial screw loosening was average minimum compressive principle strain in the Gaussian loaded FE model (R^2=0.84). The strongest correlation to failure was total BMC leading the screws (R^2=0.75). The study hypothesis was not accepted because the best predictor of failure was not the FE model. These prediction findings suggest that density-based measurements are the most optimal method for predicting the number of cycles to failure in complex and unstable PHF. Conversley, screw loosening is better predicted with simple linear elastic FE models.

7.4.1 Framework

This study is intended to contribute to a larger framework under development at AO Research Institute Davos, Davos Switzerland. Studies have already been published that contribute to components of this framework[44,50,66,67]. The studies have been developed with the intention to benefit patients who have fractured their proximal humerus. The framework looks at providing optimal parameters for implant position, screw configuration, screw length and reduction can be chosen for individuals to reduce early PHF fixation failure. The pre-screening process will involve segmenting and reconstructing fractured bone fragments from a CCT scans

and virtually placing the plate and screws. Results from the pre-screening would fit patients on the prediction curve for screw loosening and failure. Prediction models used in clinics should have low computational power, complexity, prediction time while maintaining an accurate output. Despite FEA having poorer failure predictions than the density-based measurements, it was the most accurate tool for predicting screw loosening. The advantages of FEA is that alterations can be made in loading protocols and boundary conditions to account for different physiological motions. Furthermore, there is more effort required for FEA than density-based assessments due to more image processing, simulation time and pre- and post-processing. Density-based measurements shoud save surgical preparation time and costs. The assessment scripts and frameworks for the density-based measurements have an automated calculation. The automated process includes landmark identification and density evaluation algorithms, which makes clinical implementation possible due of simplicity. This paper considers HR-pQCT for bone material properties and density measurements rather than clinically available scanners. Prediction strength by using CCT scans instead of HR-pQCT requires investigation before clinical implementation. Furthermore, clinical studies should be conducted to verify the predictions derived in this sub-study.

7.4.2 Correlations to the cyclic screw loosening event

Both density-based measures and FE modelling have a strong correlation to screw loosening and are valuable for pre-operative planning. From sub-study 1, it was found that screw loosening is the first onset of screw perforation. High stresses placed on the bone-implant interface as a result of the poor reduction can lead to loosening of the screw's bone anchorage[57]. Screw loosening is difficult to analyse with a post-operative radiograph because only large implant migrations are detectable.

Radiographic assessment during the secondary healing phase reflects past tissue events and may not be helpful in predicting outcomes when critical decisions need to be made[90]. A study by Shim et al. developed patient-specific FEA failure prediction models for pelvic ring fractures[91]. They commented that due to low scanner resolution, the initiation of implant loosening of the internal fixation system was not detected. Prescience of when screw loosening occurs could aid in avoiding complications that follow it; both biological and mechanical. Loose screws that perforate through the trabecular of the humeral head destroy bone and can prevent healing from taking place[57].

Secondary stability and healing is highly dependent on the primary stability established during a surgical procedure. By prolonging the initial stability after surgery, fractures have a longer secondary healing phase that allows hard callus formation[37]. The results from sub-study 1 and literature shows that purchase in most dense humeral head bone is important for prolonging the initial stability[26,28,59,92]. However, reduction quality though is more important to consider for osteoporotic patients that do not have dense regions of trabular for screws to purchase. Maddah et al. reported that fixation loss does not result from screw placement but predominately from secondary reduction loss, and, that this should not be disregarded[57]. The biomechanical model used to validate our prediction curves mimicked the worst case scenario of secondary reduction loss. The model is a scenario most susceptible to varus collapse that results in screws perforating to the articular surface or cutting through the trabecular matrix. If early screw loosening has been predicted in a patient, the importance of good quality reduction to avoid this is re-emphasised. High risk failure scenerios require the order of priority for stabilisation: achieve anatomical reduction, restore stiffness to the fracture and

minimise the pain at the fracture[38]. Predicting whether screw loosening will occur early after fixation could guide the surgical decisions and the rehabilitative protocols to achieve these principles.

7.4.3 Correlations to the cyclic failure event

A key finding of the study was that BMC is the best predictor for the failure. The most catastrophic screw perforation effects are experienced when the screw protrudes out of the articular surface of the humeral head and into the glenoid. When this occurs, patients can experience pain and require revision surgery[16]. Identifying a factor can be used to predict this failure is already an advantage for patient care and implant success. Density-based measurement has the advantage of straight forward evaluation and overall would make for a relatively simple pre-operative screening tool compared to FE modelling. However, FE-based analyses, in general, are more advantageous than density-based measurements because post-processing can provide displacement, stress, strain and forces from simulations, which provides a more diverse analysis. Despite FE having more benefits over density, mechanical interactions which result in plastic deformity require more complex FE modelling. Simple linear elastic models that are computationally cheap were correlated to a non-linear event, which indicates why the failure events correlated so poorly with the default Gaussian loaded model (R^2=0.19). Screw loosening occurred at the end of linear elastic deformity. When the screws loosened, the construct entered plastic deformity and the screws began perforating through the trabecular. Using linear elastic models meant that screw loosening could be predicted but not the failure event.

The screw extended model, despite achieving a moderate correlation to the failure (R^2=0.55) and the strongest regarding the FE models, does not accurately represent

the physical experiment. Extending all screw lengths creates no difference between the two study groups. Ultimately, the difference between donors, when the screws are extended to the surface is age, and local and global BMD. This alludes to the case that density and quality of bone remain the best currently available predictor of implant success. Krappinger et al. reported that factors of age, local BMD, quality of reduction, medial support restoration are the most significant prediction of failure in plated PHF[72]. All fracture models of our specimens imitate inadequate medial support and secondary reduction loss. This then leaves local BMD and age as being the biggest contributors to failure. Röderer et al. and Varga et al. strongly correlated the number of cycles to screw cut-out type failure for BMD and BMC measurements[66,68]. This is in line with the results of sub-study 2 as local total BMC was the strongest predictor of failure. The total BMC around the screws was stronger predictor than averaged BMD, which coincides with previously reported data[66]. The differences between these two parameters would require further investigation involving larger sample sizes to fully determine the predictive power of total BMC compared to average BMD.

7.4.4 Comparison of different loaded FE model types

The loading type that performed most optimally for predicting screw loosening was the 100 N Gaussian loaded model. Due to linearity, potentially any magnitude of load could have been selected for the analysis. However, investigation would be required on how this influences correlation strength. The optimal performance of the Gaussian loaded model was not only regarding screw loosening correlation but also the simplicity and the convenience of simulation time. The simulation time is essential to consider when developing a prediction model to be used for pre-operative planning. The cup loaded model, although accurately modelling the reality of the

experiments, has a much longer simulation time relative to the Gaussian, and less accurate predictions. The longer simulation is due to the model convergence when modelling contact between two surfaces. Not all specimens fully converged, even despite running a parametric study that varied the displacements of the loading cup contacting with the humeral head. Overall, the Gaussian loaded model was the most optimal FE model.

7.4.5 Limitations

A Limitation to consider is that this model is validated for in vitro, uni-axial loading of the proximal humerus. To develop a more realistic model, six degrees of freedom biomechanical testing that simulates everyday activities is required to validate the model. Currently there are in vivo measurements that investigate the loading on the humerus from everyday activities[71]. However, the direct in vivo motions that directly lead to secondary screw perforation remains unknown. The FE model was simple and linear elastic, not modelling the full failure procedure and thus remaining a surrogate measure for failure. Screw loosening can lead onto cut-out type failures and perforation, so despite not prediciting the final failure, screw loosening prediction measures are still useful. Furthermore, the model developed only reflects the failure via screw perforation and does not consider other mechanical failure types, i.e. screw cut-out type failure and biological complications that affect the fixation success and the secondary healing phase. Disrupted blood supply of the bone is one of these biological complication that is the initiation at a tissue level, for potential problems in healing, perfusion and the vitality of the fracture bone fragments[90].

Despite achieving a strong prediction strength for both key events, the findings are limited to the study, and real clinical cases need to be considered. The analysis

conducted in this study only considered one plate type, one screw configuration, and one standardised fracture pattern. In a clinical setting these factors, along with physiology and biological processes are changing between patients. This study is limited as it did not consider all these factors and their resultant predictive outcomes. The actual predictive power will not be realised until incorporated into the framework for improving plating of unstable and complex PHF.

The FEA models used in orthopaedics are generated from CT images. Modern CT scanners scan with slices that generate matrices of voxels within a volume. Fitting a CAD model into a CT scan creates a partial volume effect where the voxels in the region of an edge have a value either too high (bone) or low (air) when compared to the original attenuation value of the scan[48]. Porous structures forming trabecular bone become less obvious with lower resolution scanners as a result of flatter step functions, resulting in frayed edges. Lower resolution scans lose finer details and approximate attenuation values higher than that of a higher resolution scanner. The partial volume effect is reduced by increasing the spatial resolution of a scanner, which increases the matrices that store the voxel data. Despite this study using Xtreme CT scans that are a gold standard for research applications, the level of partial volume effect on the model lowers the accuracy of the FEA model. This study was conducted on high-resolution scans with low partial volume effect, which are not able to scan PHF clinically. A limitation of this study is that the level of partial volume effect on the prediction strengths was not investigated for scan qualities used clinically. Furthermore, the influence that the partial volume effect had on the prediction strengths for the HR-pQCT scans used was not investigated.

The cartilage which lined the articular surface of the humeral head was not segmented from the HR-pQCT scans. Due to segmentation challenges, the cartilage

was approximated by dilating a sphere from the outer cortical bone mask. The dilation does not take into account varying thickness of the cartilage layer in the specimens or any damage done to the cartilage either during mechanical testing, specimen preparation or during the donors lifetime. Furthermore, the validation method is recognised as a limitation in this study. The loading of the humerus model in the FEA study was only a quasi-static 100 N and not simulating the cyclic loading. Quasi-static testing was not conducted on the experimental model so a direct validation could not be conducted for the FEA models. Indeed, the models developed in this thesis serve as surrogates for prediction and future works would be to simulate a quantifiable aspect of the experimental and acquire the same output from the FE models.

7.4.6 Future work

Future work and development on the FE prediction includes using non-linear approaches to model the progression of the screws through the humeral head. Non-linear approaches are very computationally expensive. Computationally expensive models lose clinical application due to complexity. Pre-operative planning requires quick decision making and simple to use screening tools that aid surgeons without delaying them. Increasing the sample set to produce stronger prediction curve could be an alternative to developing a complex FE model. For a clinical setting, the current scanning technology available for analysis is CCT scanners with a lower spatial resolution to scanners used for our study. The XtremeCT HR-pQCT scanners used in this study are typically only used for distal fractures of the arm such as the distal radius due to the small entry to the scanner. Scanning a PHF of a patient is not possible due to the limited scanning space. Lower resolution scanning technologies may inhibit the predictive potential of both FEA and density-based

measurement. Future work for the study would involve re-running the analysis of the study but interchanging the HR-pQCT scan used for the FEA material properties and density measurements with a CCT scan. Accuracy of FEA in orthopaedics is currently hindered by the assumptions made for CT scan data and loading estimations[48]. As scanning technology develops, so does the potential for FEA and implant failure prediction become a reality. Ideally, future solutions will be tailored to individual patients, which allow for personalised implants and procedures.

7.4.7 Sub-study 2 conclusion

The simple strain-based measures computed by the linear FE models could predict well the initial screw loosening event. This is in accordance with a previous study demonstrating that this measure well predicts cyclic cut-out failure with similar accuracy. The parameters used for the FE-based predicting can be used as surrogate measures for primary fracture fixation stability. However, screw perforation failure could not be predicted by these simple simulations. Non-linear FE techniques could be used to appropriately describe the complex process of screw perforation through the subchondral bone of the humeral head. The simple density-based measure of BMC around and in front of the locking screw tips predicts well the screw cut-out, loosening, and perforation, and thus have a high potential for future clinical application and pre-operative planning. These measures are expected to eventually aid in decreasing complications for surgically challenging PHF plate fixations. Future studies shall investigate if the BMC and FEA data available in CCT scans provide similar prediction strengths.

8. Thesis conclusion

Complications associated with surgical fixation of proximal humerus fractures are prominent and commonly reported. This thesis investigated factors that contribute to secondary screw perforation. One factor identified as contributing to secondary screw perforation was the fixation screw length. Sub-study 1 investigated the effect of screw length on perforation characteristics in complex and unstable proximal humerus fractures. Two major secondary screw perforation events identified were screw loosening and final perforation failure. Findings from sub-study 1 show that longer screws, biomechanically, prolong the number of cycles to screw loosening and do not increase the risk of the failure occurring earlier. The literature indicates longer screws are preferential for preventing cut-out type and perforation failures. Sub-study 1 was conducted within surgical guideline limits and screw tip to joint distance outside of these limits was not investigated. Future work for sub-study 1 is to determine clinical relevancy of these findings. Methods and data acquired in sub-study 1 were used to develop a prediction model for secondary screw perforation for sub study 2. The FE-based peri-screw bone strain was a good predictor for screw loosening, in line with previously published studies on screw cut-out. Density-based bone mineral content measurements correlated most strongly to failure, whereas FE modelling weak correlation. Sub-optimal correlations of FE-based modelling predominately result from using a linear elastic model to predict plastic deformity failure; non-linear approaches may be required for improved accuracy. Results of this thesis are preliminary for optimising failure outcomes of proximal humerus fractures and further verification requires clinical corroboration to inform decision making in pre-operative planning. This study reinforces previous literature on preventing cut-out type failure; that using longer screws within the surgical

guidelines may prolong initial stability due to stronger initial purchase. Prolonged initial stability increases recovery time and improves secondary implant stability. Improved secondary implant stability should prolong the secondary healing phase and can reduce the likelihood of early medial cortex penetration resulting from humeral head collapse. Sub-study 2 showed screw loosening and perforation failure can be predicted using simple measures and models. Further development and verfication is required before realising the full potential for clinical application.

Bibliography

1. Lauritzen JB, Schwarz P, Lund B, McNair P, Transbøl I. Changing Incidence and Residual Lifetime Risk of Common Osteoporosis-Related Fractures. *Osteoporos Int*. 1993;3(3):127-132.

2. Seeley DG, Browner WS, Nevitt MC, Genant HK, Scott JR, Cummings S. Which Fractures Are Associated With Low Appendicular Bone Mass in Elderly Women? *Obstet Gynecol Surv*. 1991;115(11):424-425.

3. Launonen AP, Lepola V, Saranko A, Flinkkilä T, Laitinen M, Mattila VM. Epidemiology of proximal humerus fractures. *Arch Osteoporos*. 2015;10(2):1-5.

4. Bjorkenheim J, Pajarinen J, Savolainen V. Internal fixation of proximal humeral fractures with a locking compression plate. *Acta Orthop Scand*. 2004;75(6):741-745.

5. Egol KA, Ong CC, Walsh M, Jazrawi LM, Tejwani NC, Zuckerman JD. Early complications in proximal humerus fractures (OTA types 11) treated with locked plates. *J Orthop Trauma*. 2008;22(3):159-164.

6. Gupta AK, Harris JD, Erickson BJ, et al. Surgical Management of Complex Proximal Humerus Fractures-A Systematic Review of 92 Studies Including 4500 Patients. *J Orthop Trauma*. 2015;29(1):54-59.

7. Jabran A, Peach C, Ren L. Biomechanical analysis of plate systems for proximal humerus fractures：a systematic literature review. *Biomed Eng Online*. 2018:1-30.

8. Kettler, Biberthaler, Braunstein Z, Kroetz M, Kettler M. Treatment of

proximal humeral fractures with the PHILOS angular stable plate. Presentation of 225 cases of dislocated fractures. *Unfallchirurg*. 2006;109(12):1032-1040.

9. Kristiansen B, Christensen SW. Plate fixation of proximal humeral fractures. *Acta Orthop Scand*. 2009;6470(1986):320-323.

10. Lau TW, Leung F, Chan CF, Chow SP. Minimally invasive plate osteosynthesis in the treatment of proximal humeral fracture. *Int Orthop*. 2007:657-664.

11. Kralinger F, Blauth M, Goldhahn J, et al. The influence of local bone density on the outcome of one hundred and fifty proximal humeral fractures treated with a locking plate. *J Bone Jt Surg*. 2014;96(12):1026-1032.

12. Südkamp N, Bayer J, Hepp P, et al. Open reduction and internal fixation of proximal humeral fractures with use of the locking proximal humerus plate. Results of a prospective, multicenter, observational study. *J Bone Jt Surg*. 2009;91(6):1320-1328.

13. Röderer G, Gebhard F, Erhardt J, Al-Agha S, AbouElsoud M, Kinzl L. Die Non-Contact-Bridging (NCB) Platte: Ein neues winkelstabiles system zur minimal-invasiven versorgung von frakturen des proximalen humerus - Technik und erste ergebnisse. *Unfallchirurg*. 2007;110(6):505-512.

14. Kettler M, Biberthaler P, Braunstein V, Zeiler C, Kroetz M, Mutschler W. Die winkelstabile osteosynthese am proximalen humerus mit der PHILOS-platte. Darstellung von 225 dislozierten frakturen. *Unfallchirurg*. 2006;109(12):1032-1040.

15. Charalambous CP, Siddique I, Valluripalli K, et al. Proximal humeral internal

locking system (PHILOS) for the treatment of proximal humeral fractures. *Arch Orthop Trauma Surg*. 2007;127(3):205-210.

16. Wang Q, Zhu Y, Liu Y, Wang L, Chen Y. Correlation between classification and secondary screw penetration in proximal humeral fractures. *PLoS One*. 2017;12(9):1-9.

17. Gardner MJ, Weil Y, Barker JU, Kelly BT, Helfet DL, Lorich DG. The importance of medial support in locked plating of proximal humerus fractures. *J Orthop Trauma*. 2007;21(3):185-191.

18. Bain G, I I, Eiji D, Giacomo G, Sugaya H. *Normal and Pathological Anatomy of the Shoulder*. 1st ed.; 2015.

19. Galatz LM, Iannotti JP. Management of surgical neck nonunions. *Orthop Clin North Am*. 2000;31(1):51-61.

20. Qiang M, Jia X, Chen Y, et al. Assessment of Screw Length of Proximal Humerus Internal Locking System (PHILOS) Plate for Proximal Humeral Fractures Using Three-Dimensional Computed Tomography Scan. *Med Sci Monit*. 2018;24:1158-1165.

21. Andy C. Imaging Fractures of the Acromion. http://www.wikiradiography.net/page/Imaging++Fractures+of+the+Acromion. Published 2010. Accessed May 2, 2019.

22. Haldera A, Itoi E, An K-N. ANATOMY AND BIOMECHANICS. *Orthop Clin North Am*. 2000;31(April):159-176.

23. KIPPE M. Functional Anatomy of the Shoulder. *Orthop Phys Ther Secrets*. 2009:321-330.

24. Park JY. *Sports Injuries to the Shoulder and Elbow.*; 2015.

25. Namdari S, Yagnik G, Ebaugh DD, et al. Defining functional shoulder range of motion for activities of daily living. *J Shoulder Elb Surg*. 2012;21(9):1177-1183.

26. Liew ASL, Johnson JA, Patterson SD, King GJW, Chess DG. Effect of screw placement on fixation in the humeral head. *J Shoulder Elb Surg*. 2000;9(5):423-426.

27. Tingart MJ, Bouxsein ML, Zurakowski D, Warner JP, Apreleva M. Three-Dimensional Distribution of Bone Density in the Proximal Humerus. *Calcif Tissue Int*. 2003;73(6):531-536.

28. Saitoh S, Nakatsuchi Y, Latta L, Milne E. Distribution of bone mineral density and bone strength of the proximal humerus. *J Shoulder Elb Surg*. 1994;3(4):234-242.

29. Neer C. Displaced Fractures of the Proximal Humerus. *Clin Orthop Relat Res*. 1970;81:183-184.

30. Kellam JF, Meinberg EG, Agel J, Karam MD, Roberts CS. *AO/OTA Fracture and Dislocation Classification Compendium - 2018*. Vol 32.; 2018. www.jorthotrauma.com.

31. Smith R. AO Principles of Fracture Management. *J Bone Jt Surg*. 2002;84(7):1293.

32. Synthes D. *PHILOS and PHILOS Long: The Anatimic Fixation System for the Proximal Humerus*.

33. Jung W, Moon E, Kim S, Kovacevic D, Kim M. Does medial support decrease

major complications of unstable proximal humerus fractures treated with locking plate ? *BMC Musculoskelet Disord*. 2013;14(1):1.

34. Zhang W, Zeng L, Liu Y, et al. The mechanical benefit of medial support screws in locking plating of proximal humerus fractures. *PLoS One*. 2014;9(8):3-10.

35. Baftijari D, Benedetti A, Kirkov A, et al. Assessment of Primary and Secondary Implant Stability By Resonance Frequency Analysis in Anterior and Posterior Segments of Maxillary Edentulous Ridges. *J IMAB - Annu Proceeding*. 2018;24(2):2058-2064.

36. Gallinaro P, Brach del Prever E. Biology of primary fracture healing. From experimentation with animals to clinical application. A review. In: *Materials Sciences and Implant Orthopedic Surgery*. 6th ed. Kluwer Academic Publishers; 1986:55-65.

37. Ito K, Perren SM. Biology and biomechanics in bone healing. In: *AO Philosophy and Basic Principles Vol. 1: Principles*. 1st ed. Thieme; 2018:8-30. https://cms.aot-start.org/assets/Uploads/Biology-and-Biomechanics-AOPrinciplesOfFractureManagement.pdf?

38. Javed F, Ahmed HB, Crespi R, Romanos GE. Role of primary stability for successful osseointegration of dental implants: Factors of influence and evaluation. *Interv Med Appl Sci*. 2013;5(4):162-167.

39. McMillan TE, Johnstone AJ. Primary screw perforation or subsequent screw cut-out following proximal humerus fracture fixation using locking plates: a review of causative factors and proposed solutions. *Int Orthop*. 2018;42(8):1935-1942.

40. Crosby LA, Neviaser RJ. *Proximal Humerus Fractures: Evaluation and Management.*; 2015.

41. Steiner JA, Ferguson SJ, van Lenthe GH. Computational analysis of primary implant stability in trabecular bone. *J Biomech*. 2015;48(5):807-815.

42. Cody DD, Gross GJ, Hou FJ, Spencer HJ, Goldstein SA, Fyhrie DP. Femoral strength is better predicted by Finite element models than QCT and DXA. *J Biomech*. 1999;32:1013-1020.

43. Dahan G, Trabelsi N, Safran O, Yosibash Z. Verified and validated finite element analyses of humeri. *J Biomech*. 2016;49(7):1094-1102.

44. Varga P, Inzana JA, Gueorguiev B, Südkamp NP, Windolf M. Validated computational framework for efficient systematic evaluation of osteoporotic fracture fixation in the proximal humerus. *Med Eng Phys*. 2018;57:29-39.

45. Zysset PK, Dall'Ara E, Varga P, Pahr DH. Finite element analysis for prediction of bone strength. *Bonekey Rep*. 2013;2(AUGUST):1-10.

46. Jabran A, Peach C, Zou Z, Ren L. Parametric Design Optimisation of Proximal Humerus Plates Based on Finite Element Method. *Ann Biomed Eng*. 2019;47(2):601-614.

47. Johannesdottir F, Allaire B, Bouxsein ML. Fracture Prediction by Computed Tomography and Finite Element Analysis: Current and Future Perspectives. *Curr Osteoporos Rep*. 2018;16(4):411-422.

48. Roberts GL, Pallister I. Finite element analysis in trauma & orthopaedics - an introduction to clinically relevant simulation & its limitations. *Orthop Trauma*. 2012;26(6):410-416.

49. Herrera A. Applications of finite element simulation in orthopedic and trauma surgery. *World J Orthop*. 2012;3(4):25.

50. Fletcher J, Windolf M, Grünwald L, Richards RG, Gueorguiev B, Varga P. The influence of screw length on predicted cut-out failures for proximal humeral fracture fixations predicted by finite element simulations. *Arch Orthop Trauma Surg*. 2019:1-6.

51. Murdoch AH, Shepherd DE, Mathias KJ, C. ES. Design of a retractable intramedullary nail for the humerus. *Biomed Mater Eng*. 2003;13(3):297-307.

52. Clavert P, Kempf JF, Kahn JL, Mille P, Krier J, Zerah M. Finite element analysis of the strain distribution in the humeral head tubercles during abduction: comparison of young and osteoporotic bone. *Surg Radiol Anat*. 2006;28(6):581-587.

53. Nazrun AS, Tzar MN, Mokhtar SA, Mohamed IN. A systematic review of the outcomes of osteoporotic fracture patients after hospital discharge: Morbidity, subsequent fractures, and mortality. *Ther Clin Risk Manag*. 2014;10:937-948.

54. van Eck CF, Klein CM, Rahmi H, et al. Morbidity, mortality and cost of osteoporotic fractures—should proximal humerus fractures be taken as seriously as hip fractures? *Ann Jt*. 2019;4(January):4-4.

55. Bahrs C, Tanja S, Gunnar B, et al. Trends in epidemiology and patho-anatomical pattern of proximal humeral fractures. *Int Orthop*. 2014;38(8):1697-1704.

56. Silverstein MP, Yirenkyi K, Haidukewych G, Koval KJ. Analysis of Failure with the Use of Locked Plates for Stabilization of Proximal Humerus Fractures. *Bull Hosp Jt Dis*. 2015;73(3):185-189.

57. Maddah M, Prall WC, Geyer L, Wirth S, Mutschler W, Ockert B. Is loss of fixation following locked plating of proximal humeral fractures related to the number of screws and their positions in the humeral head? *Orthop Rev (Pavia)*. 2014;6(2):85-89.

58. Königshausen M, Kübler L, Godry H, Citak M, Schildhauer TA, Seybold D. Clinical outcome and complications using a polyaxial locking plate in the treatment of displaced proximal humerus fractures. A reliable system? *Injury*. 2012;43(2):223-231.

59. Hepp P, Lill H, Bail H, et al. Where Should Implants Be Anchored in the Humeral Head? *Clin Orthop Relat Res*. 2003;(415):139-147.

60. Bengard MJ, Gardner MJ. Screw depth sounding in proximal humerus fractures to avoid iatrogenic intra-articular penetration. *J Orthop Trauma*. 2011;25(10):630-633.

61. Erhardt JB, Stoffel K, Kampshoff J, Badur N, Yates P, Kuster MS. The Position and Number of Screws Influence Screw Perforation of the Humeral Head in Modern Locking Plates: A Cadaver Study. *J Orthop Trauma*. 2012;26(10):e188-e192.

62. Ricchetti ET, Warrender WJ, Abboud JA. Use of locking plates in the treatment of proximal humerus fractures. *J Shoulder Elb Surg*. 2010;19(2):66-75.

63. Osterhoff G, Ossendorf C, Wanner GA, Simmen H, Werner CM. The calcar screw in angular stable plate fixation of proximal humeral fractures - a case study. *J Orthop Surg Res*. 2011;6(1):50.

64. Gueorguiev B, Lenz M. Why and how do locking plates fail ? *Inj Int J Care Inj*.

2018;49(June):56-60.

65. Engelke K, Khosla S, Lang T, et al. Clinical Use of Quantitative Computed Tomography–Based Finite Element Analysis of the Hip and Spine in the Management of Osteoporosis in Adults: the 2015 ISCD Official Positions—Part II. *J Clin Densitom*. 2015;18(3):359-392.

66. Varga P, Grünwald L, Windolf M. The prediction of cyclic proximal humerus fracture fixation failure by various bone density measures. *J Orthop Res*. 2018;36(8):2250-2258.

67. Varga P, Grünwald L, Inzana JA, Windolf M. Fatigue failure of plated osteoporotic proximal humerus fractures is predicted by the strain around the proximal screws. *J Mech Behav Biomed Mater*. 2017;75(June):68-74.

68. Röderer G, Brianza S, Schiuma D, et al. Mechanical Assessment of Local Bone Quality to Predict Failure of Locked Plating in a Proximal Humerus Fracture Model. *Orthopedics*. 2013;36(9):e1134-e1140.

69. Katthagen JC, Schwarze M, Warnhoff M, Voigt C, Hurschler C, Lill H. Influence of plate material and screw design on stiffness and ultimate load of locked plating in osteoporotic proximal humeral fractures. *Injury*. 2016;47(3):617-624.

70. Wirth AJ, Müller R, Harry van Lenthe G. The discrete nature of trabecular bone microarchitecture affects implant stability. *J Biomech*. 2012;45(6):1060-1067.

71. Bergmann G, Graichen F, Bender A, Ka M. In vivo glenohumeral contact forces — Measurements in the first patient 7 months postoperatively. 2007;40:2139-2149.

72. Krappinger D, Bizzotto N, Hengg C, Riedmann S, Kralinger FS, Kammerlander C. Predicting failure after surgical fixation of proximal humerus fractures. *Injury*. 2011;42(11):1283-1288.

73. Spross C, Zeledon R, Zdravkovic V, Jost B. How bone quality may influence intraoperative and early postoperative problems after angular stable open reduction–internal fixation of proximal humeral fractures. *J Shoulder Elb Surg*. 2017;26(9):1566-1572.

74. Hymes RA, Levine MJ, Schulman JE, Westbrook RD, Li J. Mechanisms of failure of locked-plate fixation of the proximal humerus: Acoustic emissions as a novel assessment modality. *J Orthop Trauma*. 2013;27(7):392-398.

75. Kamer L, Noser H, Popp AW, Lenz M, Blauth M. Computational anatomy of the proximal humerus: An ex vivo high-resolution peripheral quantitative computed tomography study. *J Orthop Transl*. 2016;4:46-56.

76. Schneider K, Oh JK, Zderic I, et al. What is the underlying mechanism for the failure mode observed in the proximal femoral locking compression plate? A biomechanical study. *Injury*. 2015;46(8):1483-1490.

77. Blazejak M, Hofmann-Fliri L, Büchler L, Gueorguiev B, Windolf M. In vitro temperature evaluation during cement augmentation of proximal humerus plate screw tips. *Injury*. 2013;44(10):1321-1326.

78. Stoffel K, Zderic I, Gras F, et al. Biomechanical Evaluation of the Femoral Neck System in Unstable Pauwels III Femoral Neck Fractures: A Comparison with the Dynamic Hip Screw and Cannulated Screws. *J Orthop Trauma*. 2017;31(3):131-137.

79. Knierzinger D, Buschbaum J, Konschake M, Richards RG, Blauth M, Windolf

M. Ex-vivo evaluation of a novel system for implant positioning assistance at the proximal humerus using angular stable plates. *Kongress Dtsch Gesellschaft für Biomech Hann*. 2017.

80. Acklin YP, Zderic I, Inzana JA, et al. Biomechanical evaluation of a new gliding screw concept for the fixation of proximal humeral fractures. *Bone Joint Res*. 2018;7(6):422-429.

81. Freude T, Schroeter S, Plecko M, et al. Dynamic-locking-screw (DLS)-leads to less secondary screw perforations in proximal humerus fractures. *BMC Musculoskelet Disord*. 2014;15(1):1-6.

82. Röderer G, Erhardt J, Graf M, Kinzl L, Gebhard F. Clinical Results for Minimally Invasive Locked Plating of Proximal Humerus Fractures. *J Orthop Trauma*. 2010;24(7):400-406.

83. Vijayvargiya M, Pathak A, Gaur S. Outcome Analysis of Locking Plate Fixation in Proximal Humerus Fracture. *J Clin Diagnostic Res*. 2016;10(8):1-5.

84. Jost B, Spross C, Grehn H, Gerber C. Locking plate fixation of fractures of the proximal humerus: Analysis of complications, revision strategies and outcome. *J Shoulder Elb Surg*. 2013;22(4):542-549.

85. Wu JW, Shen HL, Liu LM, Gao ZH. Analysis of early failure of the PHILOS in proximal humerus fractures. *J Peking Univ Heal Sci*. 2016;48(1):683-685.

86. Urgery S, Ncorporated I, Kralinger F, Blauth M, Kurt K, Voigt C. The Influence of Local Bone Density on the Outcome of One Hundred and Fifty Proximal Humeral Fractures Treated with a Locking Plate. *J Bone Joint Surg Am*. 2014;96(12):1026–1032.

87. Ingenieurs DP. Medtool. 2014:Medtool User's Manual V3.8.

88. Fang Q, Boas D. Tetrahedral mesh generation from volumetric binary and gray- scale images. In: Proceedings of IEEE International Symposium on Biomedical Imaging 2009. 2009:1142-1145.

89. Dragomir-Daescu D, Op Den Buijs J, McEligo S, et al. Robust QCT/FEA models of proximal femur stiffness and fracture load during a sideways fall on the hip. *Ann Biomed Eng*. 2011;39(2):742-755.

90. Lambert SM. Ischaemia, healing and outcomes in proximal humeral fractures. *EFORT Open Rev*. 2018;3(5):304-315. doi:10.1302/2058-5241.3.180005

91. Shim V, Höch A, Grunert R, Peldschus S, Böhme J. Development of a patient-specific finite element model for predicting implant failure in pelvic ring fracture fixation. *Comput Math Methods Med*. 2017:1-11.

92. Tingart MJ, Lehtinen J, Zurakowski D, Warner JJP, Apreleva M. Proximal humeral fractures: Regional differences in bone mineral density of the humeral head affect the fixation strength of cancellous screws. *J Shoulder Elb Surg*. 2006;15(5):620-624.

Appendix A: Specimens

Table A.1. Summary of specimen details used for the study

AO Serial No:	Study Group TJD (mm)	Alter age	Length (mm)	Head radius CCT (mm)	Head radius HR-pQCT (mm)	Global BMD CCT (HAmg/cm³)	Global BMD HR-pQCT (HAmg/cm³)	Pathological conspicuousness
f07-1762r	8	46	120	22.15	21.95	165.21	166.93	No
f07-1763l	4	46	115	22.22	21.90	163.01	166.50	No
f07-1766r	4	56	240	24.74	25.59	119.19	147.76	No
f07-1767l	8	56	260	25.32	25.64	112.37	128.89	No
f10-1047l	8	100	180	22.15	21.93	67.46	85.61	Cystic structure in
f10-1047r	4	100	160	22.16	21.99	71.47	88.66	No
m07-1800r	4	82	240	24.74	24.51	119.90	109.41	No
m07-1801l	8	82	285	24.19	24.02	125.14	118.14	No
m07-1810r	8	63	290	24.03	24.81	132.55	106.13	No
m07-1811l	4	63	270	24.57	24.27	123.16	115.02	No
m07-1812r	4	66	225	24.16	24.07	168.34	159.92	No
m07-1813l	8	66	225	24.52	23.88	154.18	150.72	No
m10-1044l	4	93	155	24.37	24.58	72.68	80.92	No
m10-1044r	8	93	175	24.67	25.19	72.09	79.80	No
m11-3000l	8	82	330	24.11	24.56	87.36	82.38	No
m11-3000r	4	82	335	24.66	24.47	96.85	93.29	No
m12-2200l	4	78	330	23.83	23.97	140.84	135.47	No
m12-2200r	8	78	335	24.32	24.15	146.71	146.27	No
m12-2208l	4	89	345	24.63	24.27	126.08	123.76	No
m12-2208r	8	89	345	24.44	24.58	117.46	108.20	No

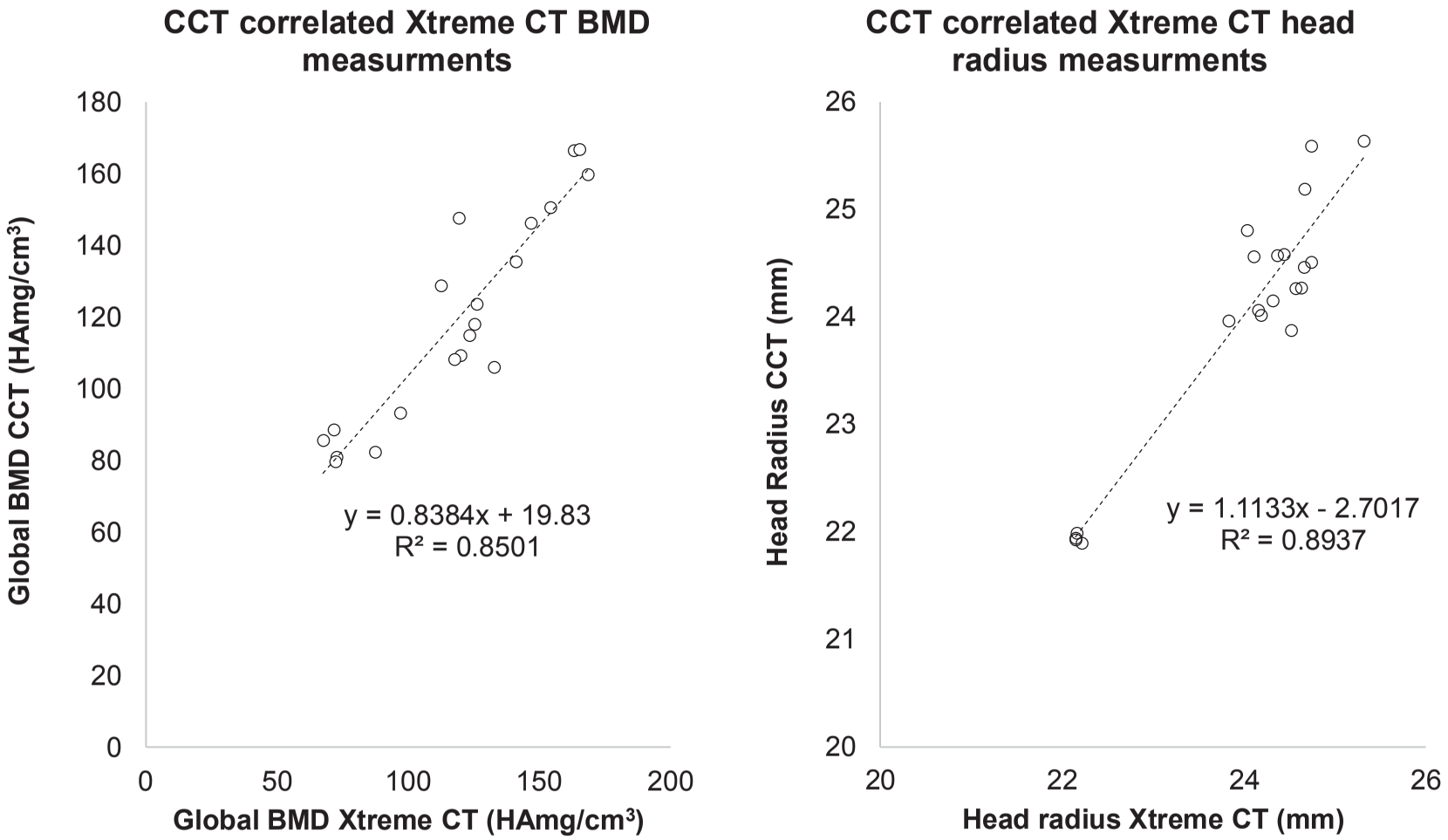

Figure A.1. Correlation between two scanner types used to assess BMD and humeral head size, each point represents a specimen.

XtremeCT scanning protocol

1. Take specimens to be scanned out the freezer
2. Ensure specimens being scanned are double bagged
3. Scan all specimens with Clinical CT (CCT) Scan
    a. Scan Settings
    b. KVP: 120
    c. X-Ray Tube Current: 200
    d. Slice Thickness: 0.625
4. All available specimens are scanned with CCT for selection based on BMD and Head Size
5. All intact specimens are then to be scanned with Xtreme CT
6. Take double packed specimens to Pre-Clinic
7. Quality Control procedure (QC1 and QC2), if the procedure has been made, skip to next step
    a. Login on the machine SC3305 next to Xtreme CT with account name and password
    b. Open the tomography program by typing operator name and selecting the Xtreme CT icon
    c. Type QC1 for density control (Daily) or QC2 for geometry control (Weekly) in pop up window
    d. Press RECALIBRATE
    e. Press START CALIBRATION
    f. Wait for the program to finish
    g. Load phantom into machine ensuring it is properly connected
    h. Close door and lead shield
    i. Press SCAN
    j. Press START MEASUREMENT
    k. Wait till scanning finishes
    l. Wait for quality control measures to be reconstructed
        i. QC1 = 5 mins
        ii. QC2 = 30 mins
    m. Check final ISQ size "Views > Data"
        i. QC1 = 299, 264 blocks
        ii. QC2 = 921, 856 blocks
    n. Start evaluation software by selecting evaluation icon
    o. Click File > Select Measurement and open most recent QC1 or QC2
    p. Select "T…" and select script number 2 (QC1) or 79 (QC2)
    q. Start Evaluation of phantom
    r. In the file "UCT_LIST_3DLOG_QC1.txt" or "UCT_LIST_3DLOG_QC2.TXT" within the RESULTS folder ("Views > Login Directory")
    s. Compare obtained values with reference values, if they do not match repeat

Mean 1:	-7	±	8	mgHA/cm^3
Mean 2:	94	±	8	mgHA/cm^3

Mean 3:	199	±	8	mgHA/cm^3
Mean 4:	405	±	8	mgHA/cm^3
Mean 5:	**793**	**±**	**8**	**mgHA/cm^3**

t. Enter outcome in XtremeCT Logbook

Intact scanning XtremeCT

1. Scanning a Specimen
    a. Write down in the Xtreme Logbook as well in the project forms
    b. Login on SC3305 with account and password
    c. Start tomography program by typing operator name and select the XtremeCT icon
    d. Click NEW in specimen section and enter specimen name
    e. Naming "SystemFixII_[study number]_specimenID"
    f. Save and exit
    g. Define new measurement parameters in a new control file
    h. Pre-calibrate Xtreme CT
        i. Push empty carrier to the back of machine hull
        ii. Close door and lead shield
        iii. Click RECALIBRATE
        iv. Click START CALIBRATION
        v. Wait for the program to finish
        vi. Repeat every hour of scanning
    i. Place specimen in centre of the holder using spacers to ensure it is secure
    j. Place sample in the machine, make sure to tape end of the specimen so it does not move during the scan
    k. Click SCOUT MODE
    l. In scout, view define the start and end of the scan and angle
        i. By selecting REFERENCE LINE the ROI can be defined
    m. Press OK when the region is defined
2. Press SCAN
3. Press START MEASUREMENT
4. Wait for the scan to finish
5. Repeat for all specimens
6. When finishing
    a. Remove Sample from the machine and push carrier to back
    b. Close tomography program (File > Exit)
    c. End Session (Session > End Session)

Appendix B: Instrumentation

Table B.1. Screw lengths used for instrumentation.

AO Serial No:	Screw 1 (mm)	Screw 2 (mm)	Screw 3 (mm)	Screw 4 (mm)	Screw 8 (mm)	Screw 9 (mm)
f07-1762r	35.36	34.53	44.5	40	44	40.4
f07-1763l	42	41.97	48.53	46.64	48.5	48.5
f07-1766r	48.5	48.5	54.5	52.3	54.54	54.05
f07-1767l	42.5	44.5	46.5	48.36	48.5	48.5
f10-1047l	32.3	32.3	40.53	40.51	42.3	42.5
f10-1047r	44.5	44.9	50.4	48.4	50.51	48.4
m07-1800r	44.4	45.55	49.9	50.48	50.5	52.54
m07-1801l	38.53	37.9	44.51	42.38	44.5	44.5
m07-1810r	41.94	40.5	46.53	46.54	46.54	46.55
m07-1811l	42.44	42.24	48.25	47.9	48.02	48.48
m07-1812r	46.54	45.56	50.58	50.5	52.1	52.05
m07-1813l	40.49	40.39	45.57	44.39	44.51	44.99
m10-1044l	44.99	44.51	48.4	50.5	48.36	48.13
m10-1044r	40.48	40	45.07	42.51	44.95	44.52
m11-3000l	38.3	34.54	44.99	41.79	44.99	42.31
m11-3000r	44.5	44.5	48.4	50.5	48.32	50.5
m12-2200l	40	40.4	46.3	46.54	46.5	46.6
m12-2200r	40	40.4	46.3	46.54	46.5	46.6
m12-2208l	42.33	42.32	48.36	48.39	50.49	50.49
m12-2208r	40.52	40.4	44.4	45.27	46.26	46.27

Table B.2. Measured tip to joint distance.

AO Serial No:	Screw 1 (mm)	Screw 2 (mm)	Screw 3 (mm)	Screw 4 (mm)	Screw 8 (mm)	Screw 9 (mm)	Average (mm)
f07-1762r	9.15	8.47	7.73	8.71	6.97	7.50	8.09
f07-1763l	2.63	3.19	2.65	5.20	2.51	3.14	3.22
f07-1766r	3.60	4.14	2.93	4.50	1.50	2.67	3.22
f07-1767l	10.16	7.73	8.79	9.23	7.03	8.51	8.57
f10-1047l	8.66	9.30	9.43	9.39	7.49	6.10	8.39
f10-1047r	6.16	4.75	3.77	3.67	3.32	3.17	4.14
m07-1800r	4.93	4.58	4.89	4.77	2.99	4.52	4.45
m07-1801l	9.02	8.83	9.38	10.17	8.62	8.70	9.12
m07-1810r	7.30	8.74	8.64	9.36	8.88	9.48	8.73
m07-1811l	4.81	4.25	5.70	4.58	4.70	3.93	4.66
m07-1812r	4.49	5.18	4.60	5.45	2.84	3.84	4.40
m07-1813l	8.08	7.43	9.29	8.95	9.21	8.79	8.63
m10-1044l	4.01	4.56	5.25	3.14	3.03	4.54	4.09
m10-1044r	8.39	8.08	8.68	10.03	5.97	6.37	7.92
m11-3000L	6.65	8.97	9.33	7.28	9.20	7.88	8.22
m11-3000R	2.50	3.52	4.39	5.38	4.92	4.87	4.26
m12-2200l	4.85	4.90	3.55	5.25	2.79	4.43	4.29
m12-2200r	8.60	7.79	7.97	8.90	8.01	7.79	8.18
m12-2208l	4.13	3.89	5.63	4.98	3.03	2.49	4.02
m12-2208r	8.52	8.65	8.81	9.50	5.43	7.38	8.05

Table B.3. Mean ± standard deviation (SD) tip to the joint distance between two groups.

Study Group	Screw 1 (mm)	Screw 2 (mm)	Screw 3 (mm)	Screw 4 (mm)	Screw 8 (mm)	Screw 9 (mm)
4 mm (Mean ± SD)	4.22 ± 1.05	4.34 ± 0.59	4.19 ± 1.03	4.66 ± 0.72	3.18 ± 0.95	3.90 ± 0.80
8 mm (Mean ± SD)	8.45 ± 0.92	8.40 ± 0.58	8.80 ± 0.56	9.15 ± 0.76	7.68 ± 1.27	7.85 ± 1.01

Table B.4. Material checklist for instrumentation.

Amount	Material	Details	Material company and number if relevant
1	Scalpel	Soft tissue dissection	
1	Forceps	Soft tissue dissection	
1	X-Ray C Arm	Checking screw position	Siemens Cios Select
1	Portable Laptop	Recording instrumentation measurements	
1	Metal vice clamp	Fixing humeral shaft	
20	PHILOS plate	Titanium, 3 shaft holes, 90 mm length	DePuy Synthes (241.901)
1	PHILOS plate guide	PHILOS Aiming Device Stardrive, with Nose	DePuy Synthes (0.3.122.066)
1	PHILOS drill sleeve	LCP Drill Sleeve 3.5, for Drill Bits Ø 2.8 mm	DePuy Synthes (323.027)
1	PHILOS screw sleeve	Outer Sleeve 6.0/5.0 for PHILOS Aiming Device	DePuy Synthes (03.122.053)
3	Kirschner wire	Fixing fragment position and checking plate height	
1	Drill	Compact Air Drive II, Air Driven power tool	DePuy Synthes (511.701)
1	Drill chuck	keyless	DePuy Synthes (511.731)
1	Kirschner wire chuck	Quick Coupling for Kirschner Wires	DePuy Synthes (511.791)
2	Drill bit	Drill Bit Ø 2.8 mm, with Stop, for Quick Coupling	DePuy Synthes (03.122.051)
120	Titanium locking head screw	Locking Screw Ø 3.5 mm, length 12-60 mm, self-tapping, hexagonal head	DePuy Synthes(413-010S-070S)
20	3D printed surrogate GT	Printed from PVA for water dissolving	
11	Hand screwdriver	Ø 3.5 mm, hexagonal head	
1	Torque limiter chuck	Limited to 1.5 Nm	DePuy Synthes (511.770)
1	Custom designed drill depth gauge	Ensuring boreholes drilled to correct depth	Custom developed at, ARI Davos Switzerland

Table B.5. Instrumentation protocol.

Step Number	Check	Steps
1		Defrost humerus pair for 3 hours or night before
2		Get 3D-fragments and glue sandpaper on them to prevent plate sliding
3		Use protocols to write down specifications
		Protocol for one side always starting with the right humerus
4		Preparation: Start X-ray
5		Mount vice so C-Arm can be adjusted for X-in-One (lateral view-position in relation to X-in-One holes)
6		Mount humerus shaft in vice vertically (use tissue between the shaft and grabbing part of vice)
7		Attach the aiming device to plate
8		Fracture reduction by hand
9		Adjustment of the plate along the humerus shaft axis
10		Adjustment of the plate with K-wire (joint surface contact)
11		Temporary fixation of the distal part of the plate with a clamp
12		Drill the middle of the combi-hole (2,5 mm)
13		Fix plate with a non-locking screw (3,5 mm), allow for movement of the plate up and down

14		Insert a screw into most distal hole to leave room for head fragments (if necessary)
15		Check again adjustment of the plate with K-wire (joint surface contact)
16		Temporary fixation with a clamp
17		Insert K wire into lateral fragment proximally and into the head fragment ensuring not to puncture the articular surface
18		Fix fragments with point clamps
19		Using the 60 mm drill bit, measure the distance from the plate to the articular surface
20		From the caliper, reading add 3 mm to account for screw head and subtract 70 mm and distance of caliper end on the articular surface (should be 1 mm)
21		Write down values on instrumentation sheet
22		measure all holes 1, 2, 3, 4, 8 and 9 and note down lengths before drilling
23		Select the screw length and write down on instrumentation sheet (round the parameters to the 2mm-steps)
24		calibrate Auto-gauge
25		Place drill guide in auto-gauge, place laser piece on drill and aim
26		Use outer sleeve and drill (2,8 drill bit) the whole way using Auto-gauge for length control
27		Drill in this order 1-2-3-4 (drill 8 and 9 with shaft)
28		Of each recognise maximal depth displayed on Auto-gauge and write down
29		Remove drill sleeve and insert the screw most of the way using the outer sleeve
30		Alternatingly tighten all screws with torque limiter 1,5 Nm

31		remove k wires and fragment clamps
32		Attach x-in-one device
33		After insertion of all screws: take X-in-One FROM ORIGINAL X-RAY POSITION
34		Write down values and any notes of interest
35		Release clamps and shaft screw
36		Remove shaft fragment
37		Fix the distal end of plate in the clamp
38		In the calcar screws, use auto-gauge to drill depth from initial x-in-one
39		Insert screws 8 and 9 using a torque limiter of 1,5 Nm
40		Release plate from the clamp
41		Dissolve fragment and release sandpaper
42		Wrap specimen in PBS gauze once fragment has been removed
43		Double pack specimen in preparation for Clinical CT

AO Foundation

Specimen-No: Group (tip-apex distance): 4 mm / 8 mm Side: Left / Right

Treatment-No: Date:

Treatment:

	Measured calipers (averaged)	Selected screw length/aimed drill depth
1		
2		
3		
4		
8		
9		

Actual Drilling depth (Auto-gauge)	Measured physically measured screw length (electronic calipers)
1	
2	
3	
4	
8	
9	

Achieved plate position? Yes / No

Documented Photos? Yes / No

Corrected plate position: _____ mm

Post instrumentation X-in-One: Good / Bad

Additional Comments:

AO Research Institute Davos
Clavadelerstrasse 8, 7270 Davos, Switzerland
Phone: +41 81 414 22 11, Fax: +41 81 414 22 88
ari@aofoundation.org, www.aofoundation.org

Pre-Instrumentation planning (Image processing and 3D printing)

Lateral fragment

1. Import DICOMS from HR-pQCT Osteotomy
2. Duplicate imported file
3. Crop duplicated file to the fragment of interest
4. Resample
    a. Mode: Voxel Size
    b. Voxel Size: x = 0.2, y = 0.2, z = 0.2
5. Create a label file of the resampled image by selecting segmentation
6. Segmentation
    a. Use a mask to define the cortical region
    b. Use lasso tool and holding ctrl delete unwanted noise and bumps around the inside section of the segmentation
    c. Click the cortex region and then add that to new material and that is material you want
7. Create a generate surface box
    a. Smoothing: constrained smoothing
    b. Smoothing: 5
    c. Check surface view
    d. Simplification editor: simplify faces: 100,000
    e. Click simplify now
8. Convex Hull
    a. Max Hull Points: 10000
    b. Epsilon: 0.0001
9. Check surface view of the convex hull with the generated surface
    a. Adjust the opacity of the convex hull
    b. Make note of any bends in the surface
    c. Make amendments to segmentation if the case
10. Export convex hull as a little-endian STL file

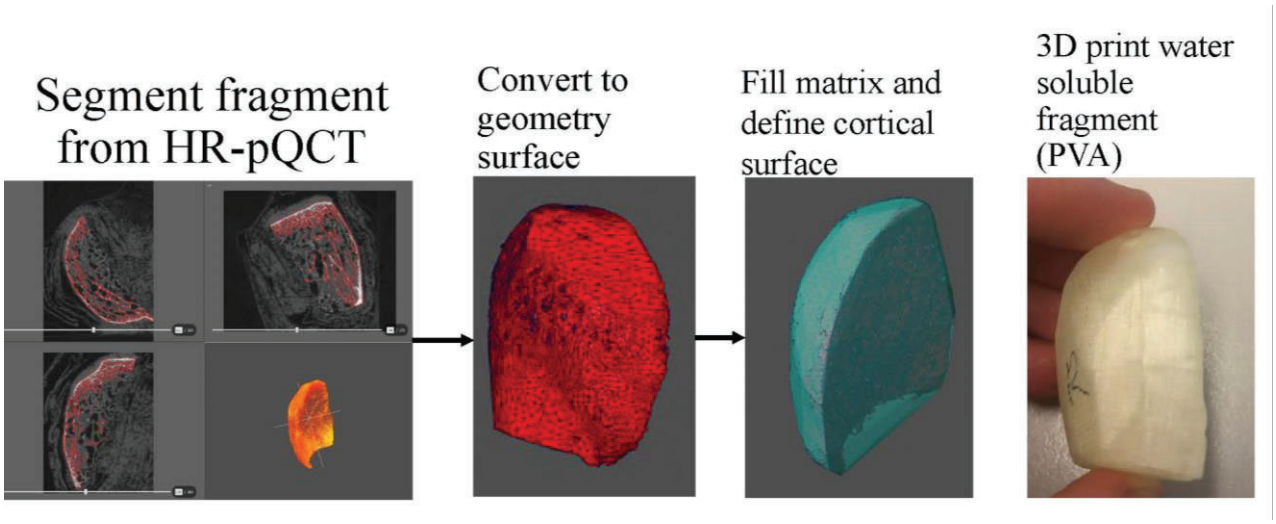

Figure B.1. Surrogate 3D printed GT fragment.

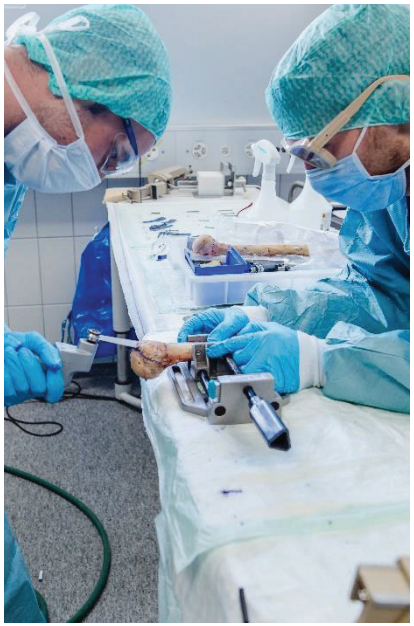

Figure B.3. *Photographs from osteotomy. The work was conducted with an upper extremity orthopaedic surgeon from Hadassah Medical Centre, Jerusalem, Israel.*

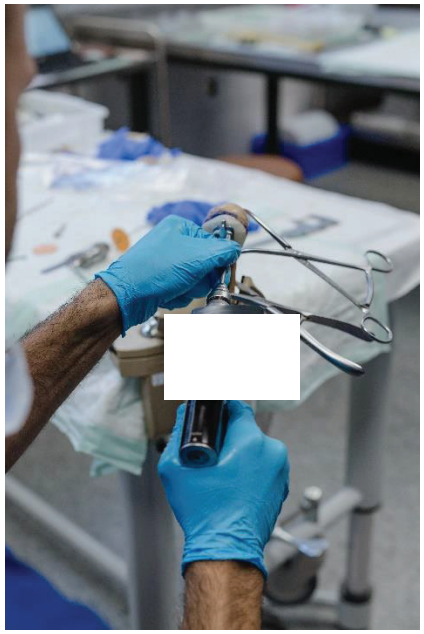

Figure B.2. *Photographs from instrumentation, device covered due to intellectual property sensitivity. The work was conducted with an upper extremity orthopaedic surgeon from Hadassah Medical Centre, Jerusalem, Israel.*

Appendix C.1: Experimental results

Table C.1. Experimental results: cycles, failure modes, mechanical properties.

AO Serial No:	Cycles to screw loosening	Cycles to failure	Screw(s) to perforate	Maximum displacement (mm)	Failure load (N)	Elastic stiffness (N/mm)
f07-1762r	14581	26190	8	-8.81	-1285.68	554.71
f07-1763l	16386	27977	8	-3.57	-1381.52	1052.56
f07-1766r	25676	33319	8	-4.54	-1622.58	1059.02
f07-1767l	14678	29166	8	-10.44	-1427.84	875.31
f10-1047l	3999	22165	8 and 9	-9.01	-1092.66	243.18
f10-1047r	10107	22196	8 and 9	-5.98	-1111.50	711.54
m07-1800r	9481	22785	8	-6.00	-1123.07	594.23
m07-1801l	5868	30506	8 and 9	-10.63	-1487.29	424.08
m07-1810r	17918	32573	8	-11.15	-1604.70	935.67
m07-1811l	21609	30123	9	-5.95	-1959.52	966.16
m07-1812r	30192	39694	9	-4.80	-2482.01	1677.25
m07-1813l	19169	46549	9	-12.26	-2924.24	1128.66
m10-1044l	12631	19929	9	-6.72	-990.14	636.63
m10-1044r	5290	20609	8	-9.73	-1021.10	258.22
m11-3000l	6024	29300	8 and 1	-10.63	-1487.29	427.18
m11-3000r	13034	26305	9	-6.72	-1389.89	756.38
m12-2200l	20065	31310	8	-6.23	-1534.12	1378.11
m12-2200r	13209	30869	8	-10.68	-1498.96	674.12
m12-2208l	16143	24860	8	-5.72	-1225.47	1063.65
m12-2208r	11769	19898	8	-8.37	-989.00	629.31

Table C.2. Image processing results: displacements and rotations of the humeral head.

AO Serial No:	Lateral displacement (mm)	Inferior Displacement (mm)	Infero-lateral displacement (mm)	Varus rotation (°)	Head Tilting (°)
f07-1762r	-9.91	-1.49	10.02	5.86	3.96
f07-1763l	-4.48	2.24	5.01	6.13	-0.16
f07-1766r	-3.34	-0.60	3.40	2.43	-2.36
f07-1767l	-8.97	-2.91	9.43	0.35	-2.56
f10-1047l	-11.66	0.74	11.68	9.77	2.81
f10-1047r	-6.28	-1.29	6.41	2.69	1.17
m07-1800r	-4.70	-0.76	4.76	1.90	-5.87
m07-1801l	-13.76	-1.06	13.80	8.28	8.61
m07-1810r	-12.46	-1.95	12.61	5.35	-4.25
m07-1811l	-5.85	-1.09	5.95	3.26	1.11
m07-1812r	-6.38	-0.51	6.40	6.01	-5.32
m07-1813l	-12.97	-0.24	12.97	7.80	-0.51
m10-1044l	-7.28	-0.45	7.29	4.82	0.05
m10-1044r	-13.06	-1.52	13.15	8.20	1.67
m11-3000l	-10.66	-1.69	10.80	0.04	11.44
m11-3000r	-6.68	-0.10	6.68	3.54	-5.20
m12-2200l	-5.33	-1.35	5.50	0.05	-5.25
m12-2200r	-8.38	-3.13	8.95	2.50	4.91
m12-2208l	-5.19	-0.72	5.24	1.50	0.33
m12-2208r	-7.38	-1.66	7.56	0.80	-0.02

Experimental protocol

1. Ensure that experimental set up is ready
    a. Turn on hydraulics
    b. Switch on computers
        i. First computer (closest to door)
        ii. The second computer (next to testing machine)
        iii. Turn on controllers (next to computer)
    c. Connect specimen mounting plate to X Y slider
    d. Connect X Y slider table to the adapter plate
    e. Position adapter plate so that the humeral head centre is in line with machine testing axis and x y sliders are in the neutral position
    f. Fix the adapter plate to the load cell plate using two clamps on either side
    g. Plug power supply into wall power
    h. Connect the negative signal (black wire)
    i. Connect positive signal (red wire)
    j. Check that the positive signal is connected to head piece
    k. Attach head piece to MTS machine
    l. Check all screws, bolts and clamps are secure
2. Take specimen out the refrigerator
3. Check screws of the specimen in X-Ray
4. Place specimen is designated unclean area (Metal trolley), ensure to keep wrapped in PBS until testing
5. Using the TRS, drill a k wire into the superior side of the humeral head placing a motion tracking marker for the head
6. Position motion tracking markers on to the drop head
7. Apply motion markers onto a plate
8. Load specimen on to testing apparatus with washers and bolts
9. Connect the negative electronic signal to the most inferior screw whole and bolt to plate
10. Turn on power supply 10 volts
11. Ensure that the switch on the power supply is set to a single channel (switch above connections)
12. Test connection of all screws, plate and drop head for the stop trigger
13. Position C-Arm to fire in the anteroposterior plane
14. Create a new patient folder
    a. Patient ID: specimen name
    b. Last Name: Systemfix2
    c. First Name: ScrwPerf_GR_No
    d. Date of Birth: Current date
15. Set C arm to following settings
    a. Voltage: 60 kV
    b. Current: 0.5 mA
16. Set up live feed camera
17. Load Matlab protocol
    a. WRITE PROTOCOL NAME HERE:

18. Create a new specimen test file
    a. "[specimen name]_GR_No"
19. In Test, parameter window enter the following parameters
    a. Initpause = 5 s Preload = -15 N
    b. Ramp = 10 s Rate = -3.5 N/s
    c. Final Ramp = 5 s 507.5 N/s
    d. Cycles = 50000 Freq = 4
    e. Sen.range = 4000 N Sample f = 1000 Hz

    f. Level 1: -15 N 0 N/cyc -15 N
    g. Level 2: -50 N -0.05 N/cyc -2550 N

    h. Trigger
        i. Qaulisys: On, St, Inc: 1000 cycles
        ii. X-Ray: On, C0, Inc: 250 cycles
        iii. Pause: On, C0, Inc: 250 cycles
20. Move drop head to the highest position and manually move MTS down
21. Displacement control drop head to be close to the specimen if required
22. Place the plastic cover in between drop head and humeral head because humeral holds a charge
23. Switch to load control mode
24. Zero load cell
25. Apply -15 N load and lift load cell to move machine so that it is contact with the specimen
26. Switch to displacement control
27. Switch back to load control and apply preload of -15 N
28. Take a test x-ray to check position and xray settings
29. Check circuitry by attaching a wire from plate and screws to head and checking on output voltage on computer
30. Begin test
    a. Unselect manual
31. Make sure to take note of the voltage and screw position in x-ray to ensure that test does not end prematurely

Image processing protocol for humeral head displacements and rotations

1. Import the instrumented (_PH)
2. rename
3. Resample to 0.2
4. Import the tested scan (_TEST)
5. rename
6. resample to 0.2
7. Rename to "SFII_[specimenname]_PH/TEST"
8. Import Philos STL which is set to zero on the global coordinate system
9. Resample transformed image WITH NO REFERENCE!
10. Segment the plate from the Instrumented scan
11. Generate Surface
12. simplification editor reduce faces to 18000
13. Adjust the position of STL file to match the Extracted surface file
14. Using the "Align surfaces" register the steel plate file with the extracted surface
    a. Surface_to_be_transformed: Philos.stl.am
    b. Reference_surface: ExtractedSurface
    c. Options: iterate
    d. Transformation: rigid
    e. Stop: Relative RMS: 0.001, max iter: 15
    f. Press surface until registered
15. Create "Apply to transform" block for Philos.Stl
16. copy the transform from the extracted iso-surface and paste onto the _PH
17. Resample transformed the image of the _PH to set its absolute coordinates back to zero
18. rename with _ZERO
19. Move manually _TEST to the _PH
20. Create register image block
    a. Set reference to _PH_ZERO
    b. Set histogram reference ranges from 5000 to 15000
    c. untick ignore the finest resolution
    d. Set optimizer step to 1 initial and 0.5 final
    e. finest levels 1, tolerance 0.0001
21. Resample transformed an image with no reference
22. Rename TEST_ZERO
23. Move manually the _PH to the _TEST HUMERAL HEAD, it makes more sense to move the original to the final position
24. Create register image block
    a. Set histogram reference ranges to 1 to 1500
    b. untick ignore the finest resolution
    c. Set optimizer step to 1 initial and 0.5 final
    d. finest levels 1, tolerance 0.0001
25. In the console type in "SFII_[specimenname]_TEST_RES" getTransform which provides you with the rotation and displacement matrix

Table C.3. Summary of statistical tests for the experimental results.

Parameter (Group: LSG/ SSG)	Normally distributed yes/ no	Statistical test
Global humeral head BMD (LSG)	Yes	Related-samples t-test
Global humeral head BMD (SSG)	Yes	
Humeral head radius (LSG)	No	Wilcoxen sign rank test
Humeral head radius (SSG)	No	
TJD (LSG)	No	Wilcoxen sign rank test
TJD (SSG)	Yes	
Peri-screw Row A BMD (LSG)	Yes	Related-samples t-test
Peri-screw Row A BMD (SSG)	Yes	
Peri-screw Row B BMD (LSG)	Yes	Related-samples t-test
Peri-screw Row B BMD (SSG)	Yes	
Peri-screw Row E BMD (LSG)	Yes	Related-samples t-test
Peri-screw Row E BMD (SSG)	Yes	
Screw loosening displacement (LSG)	Yes	Related-samples t-test
Screw loosening displacement (SSG)	Yes	
Cycles to failure (LSG)	Yes	Related-samples t-test
Cycles to failure (SSG)	Yes	
Cycles to screw loosening (LSG)	Yes	Related-samples t-test
Cycles to screw loosening (SSG)	Yes	
Varus rotation (LSG)	Yes	Related-samples t-test
Varus rotation (SSG)	Yes	
Humeral head tilt (LSG)	No	Wilcoxen sign rank test
Humeral head tilt (SSG)	Yes	
Lateral-inferior displacement (LSG)	Yes	Related-samples t-test
Lateral inferior displacement (SSG)	Yes	

Appendix C.2: Specimen sheets

AO Serial No: f07-1762r

X Ray stopped working during testing

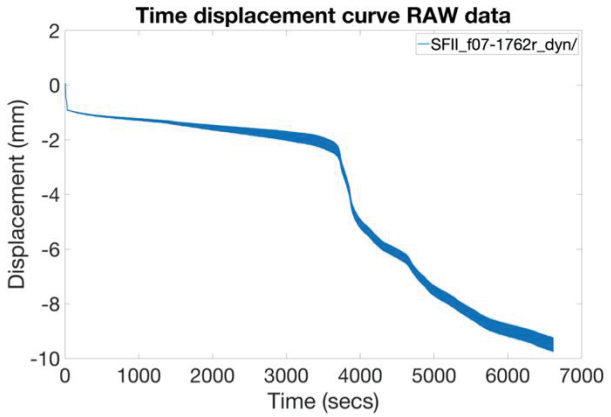

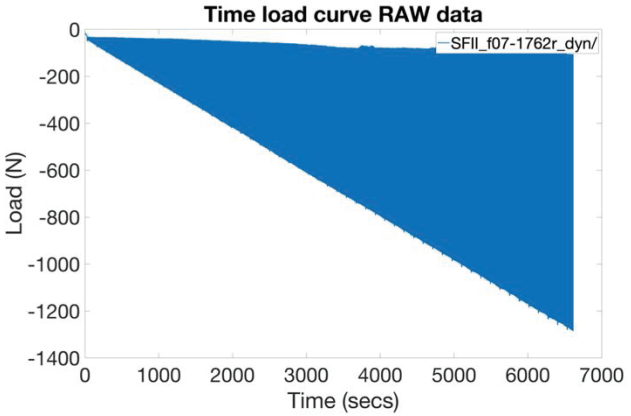

AO Serial No: f07-1763l

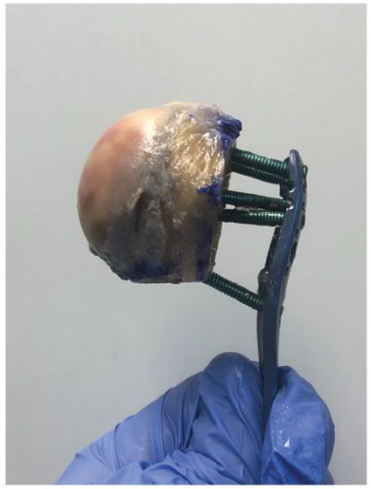

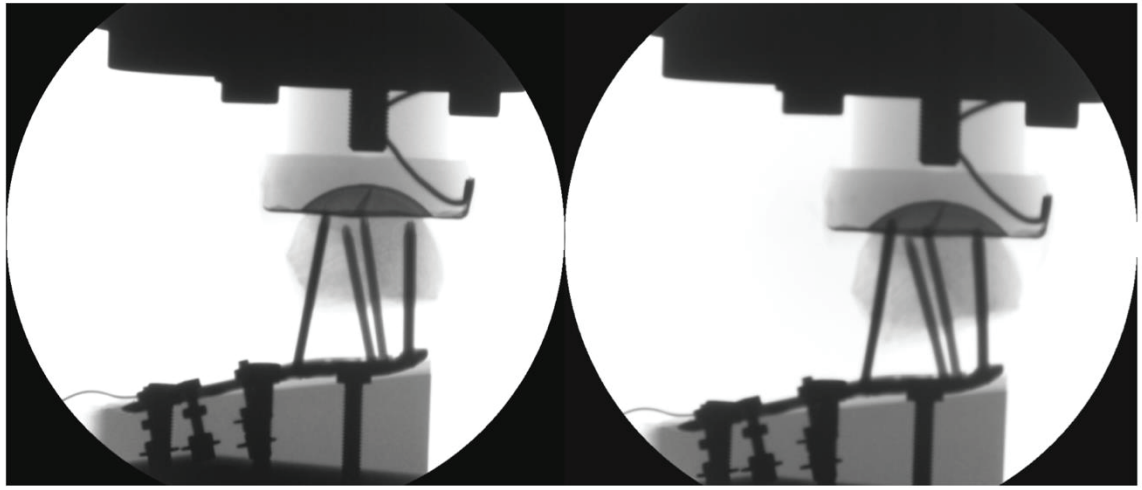

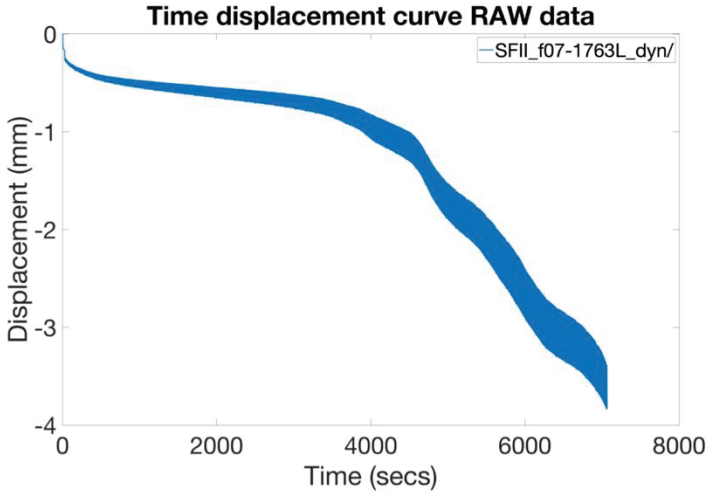

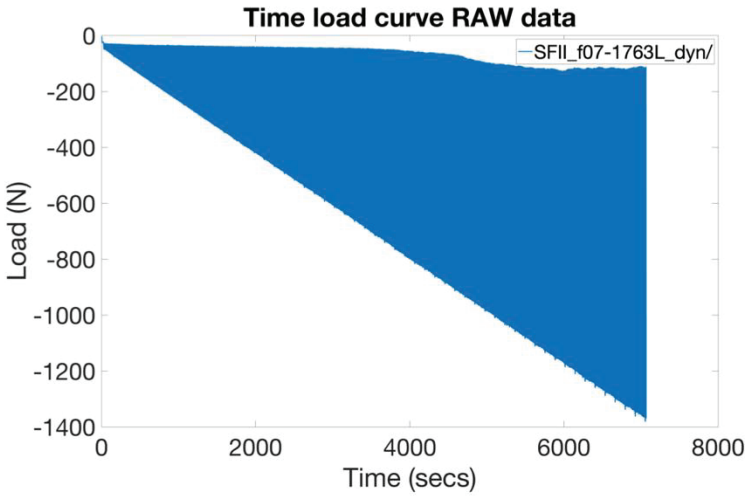

AO Serial No: f07-1766r

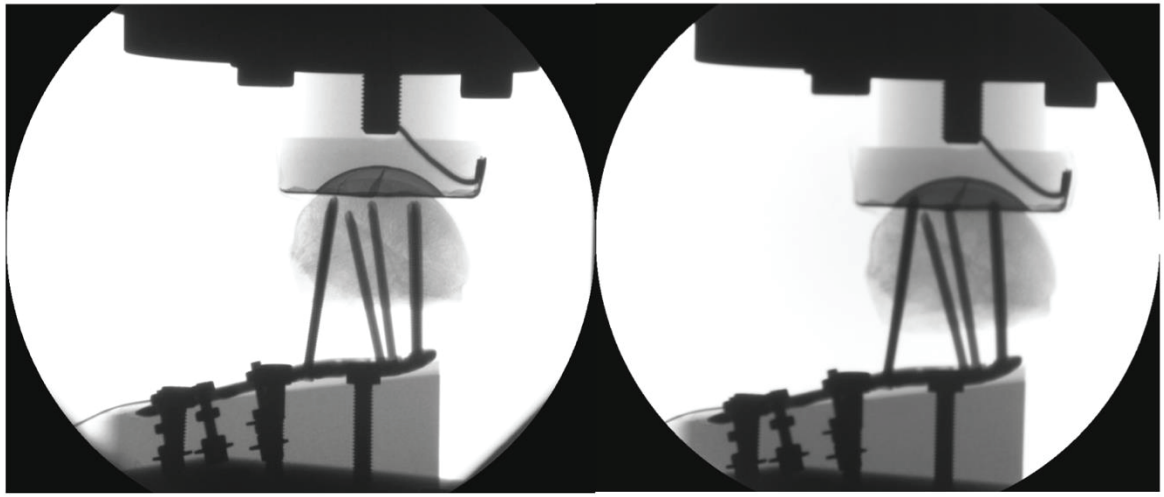

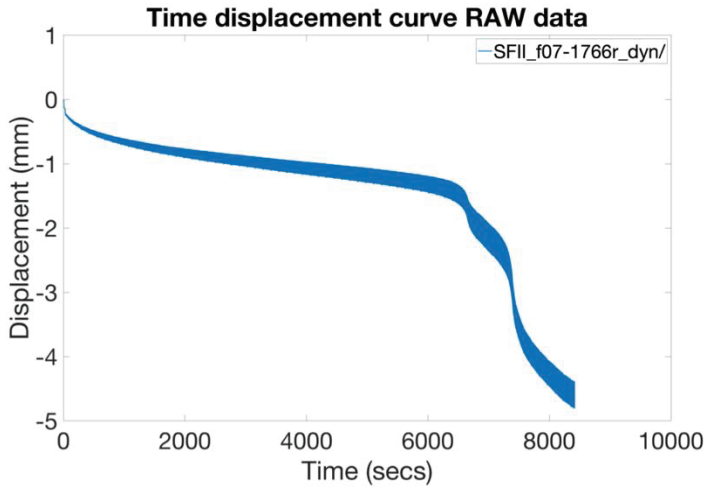

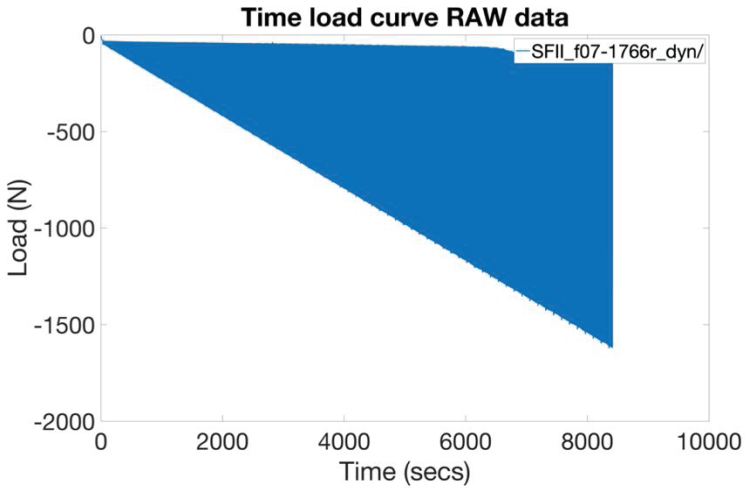

AO Serial No: 1767l

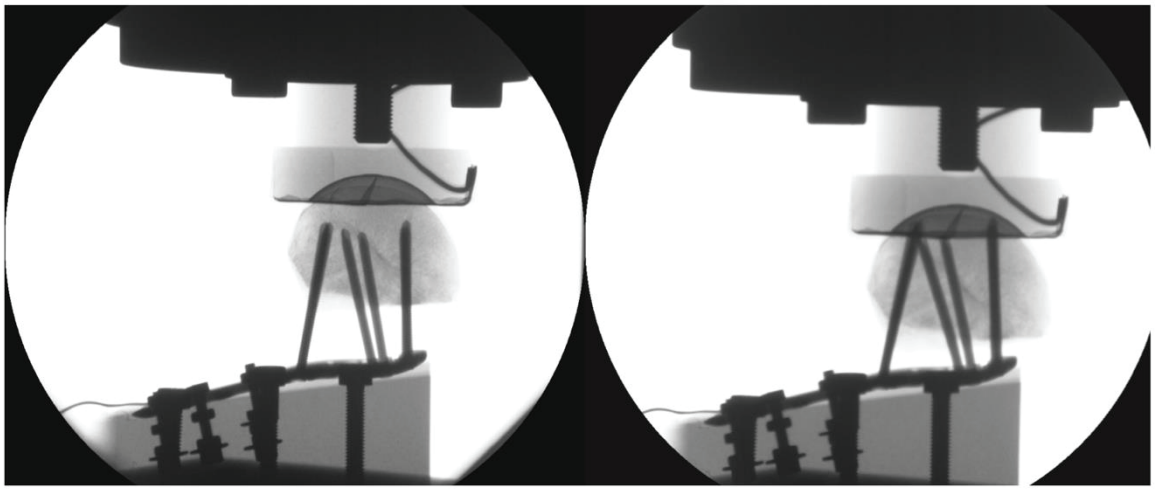

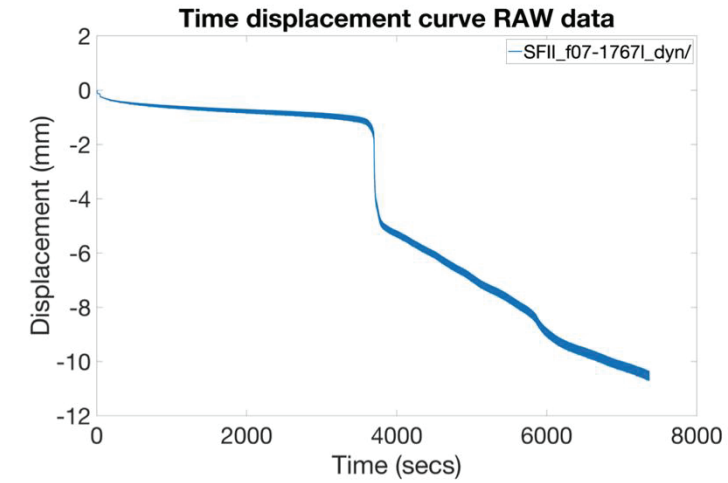

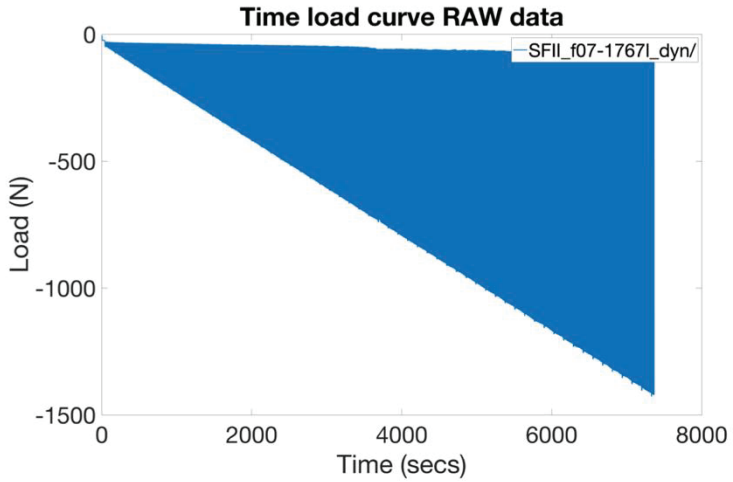

AO Serial No: f10-1047l

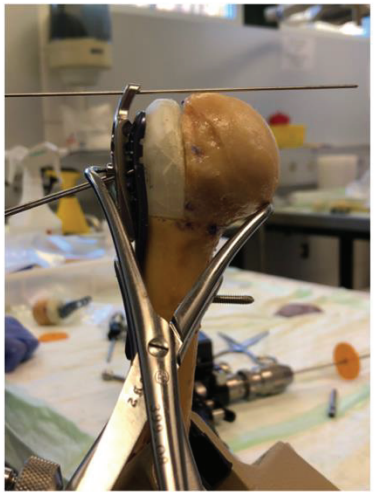

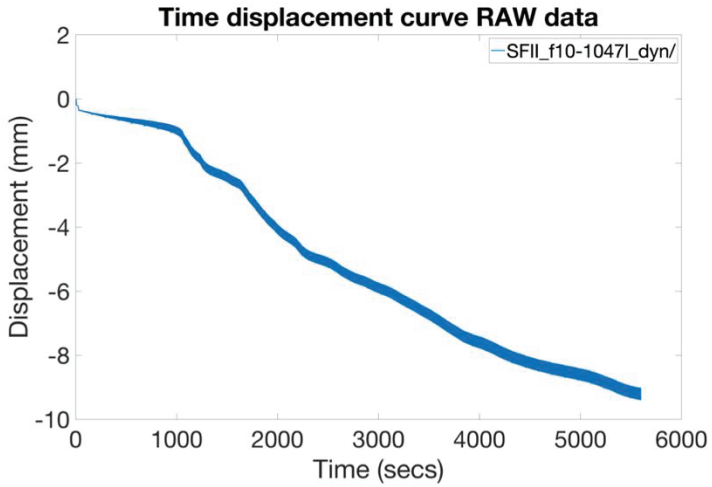

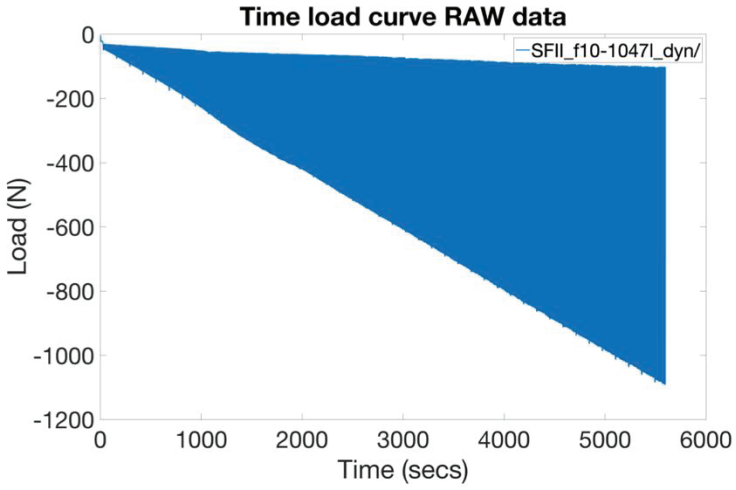

AO Serial No: f10-1047r

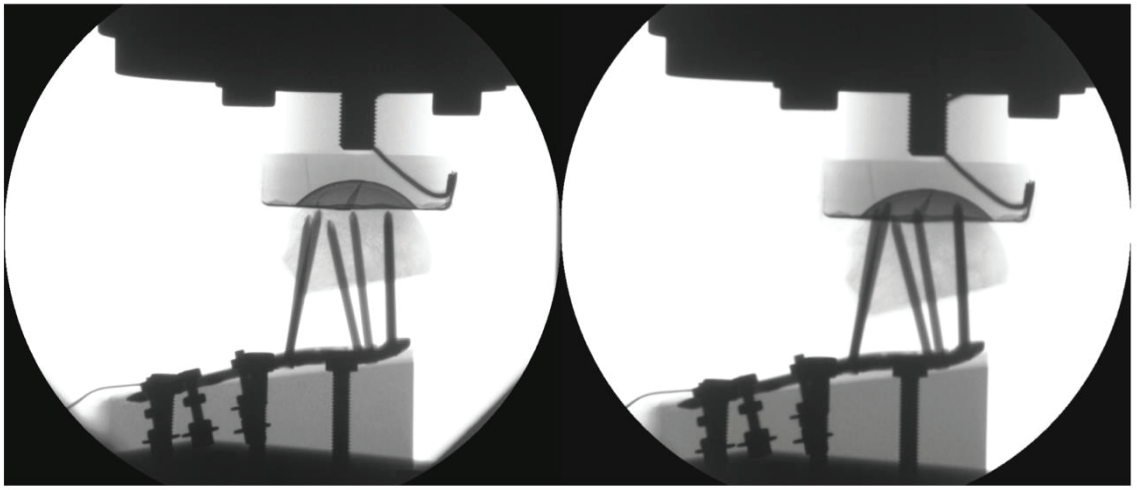

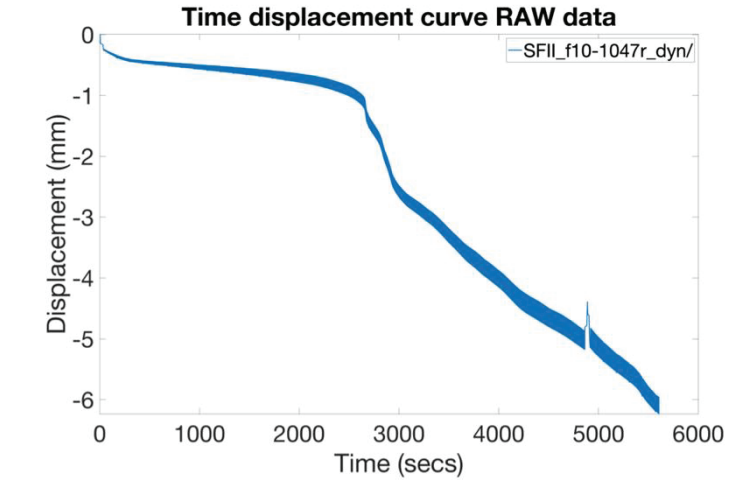

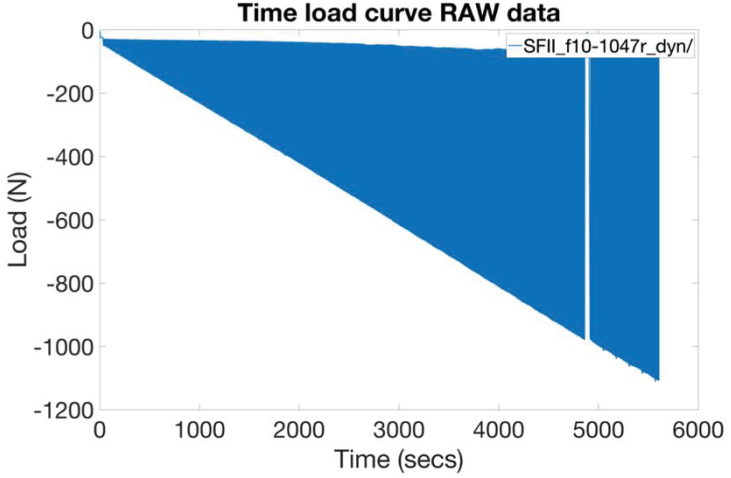

AO Serial No: m07-1800r

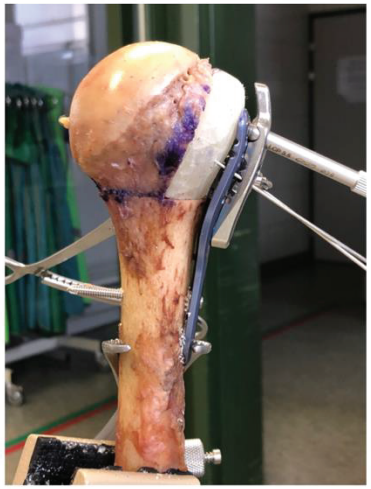

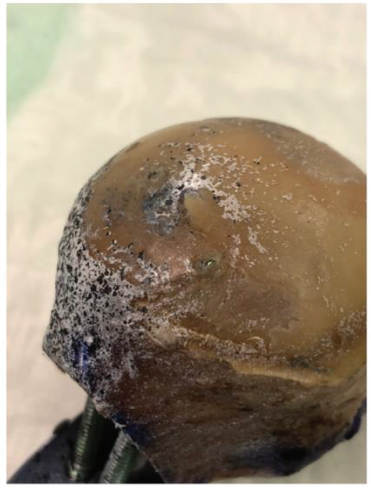

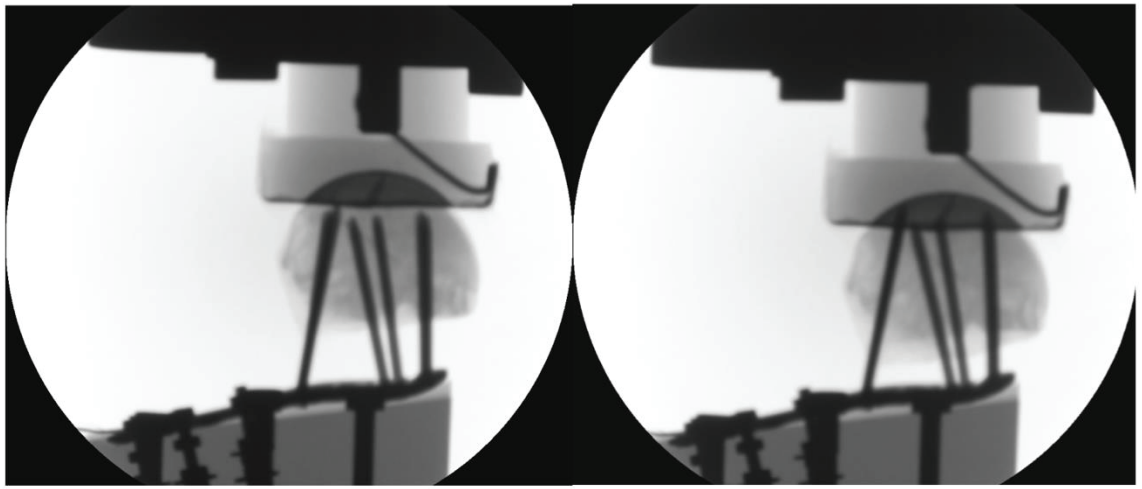

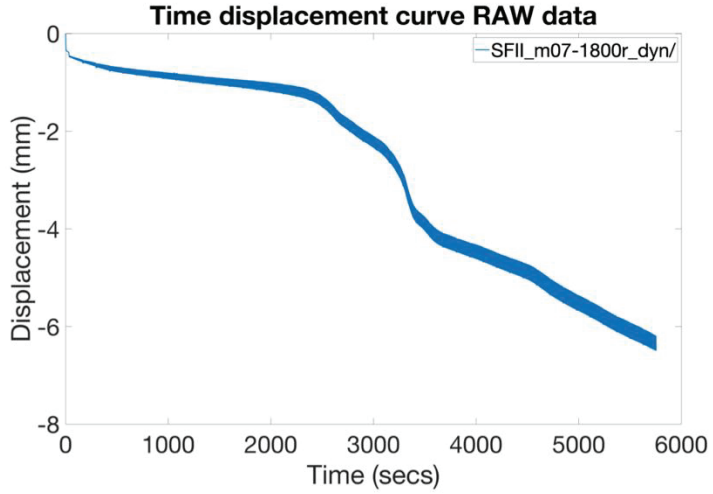

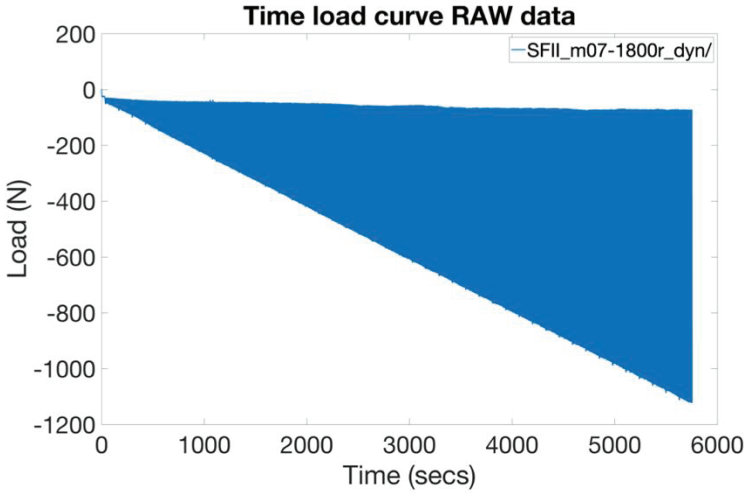

AO Serial No: m07-1801l

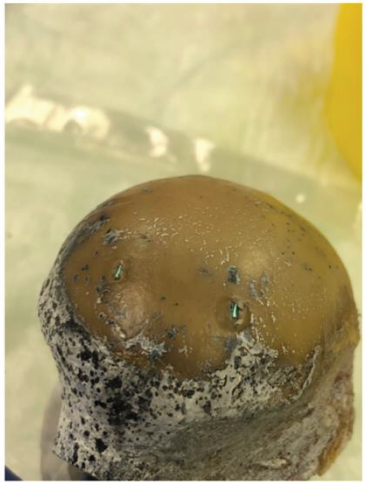

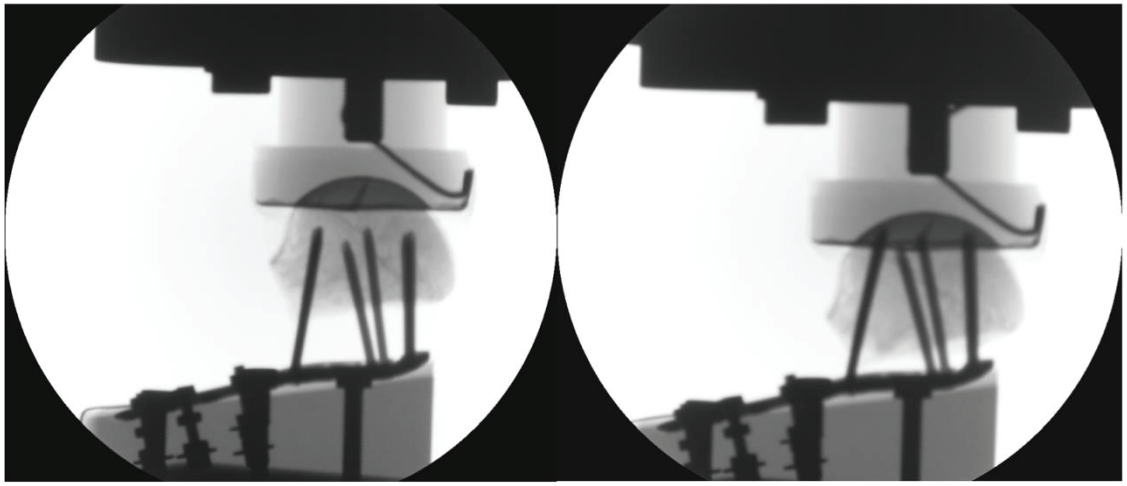

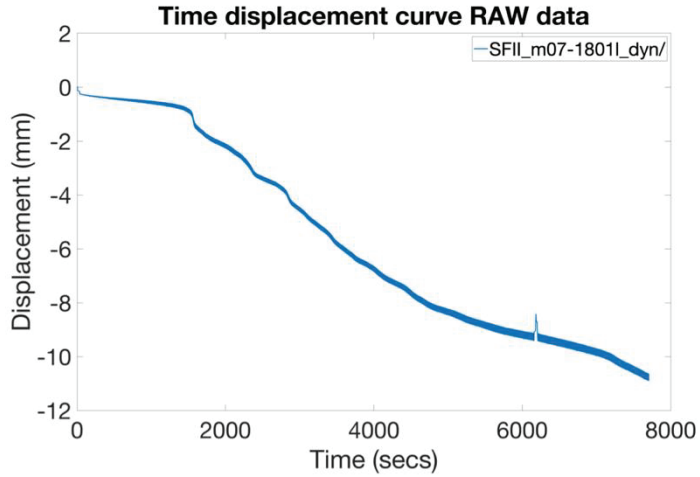

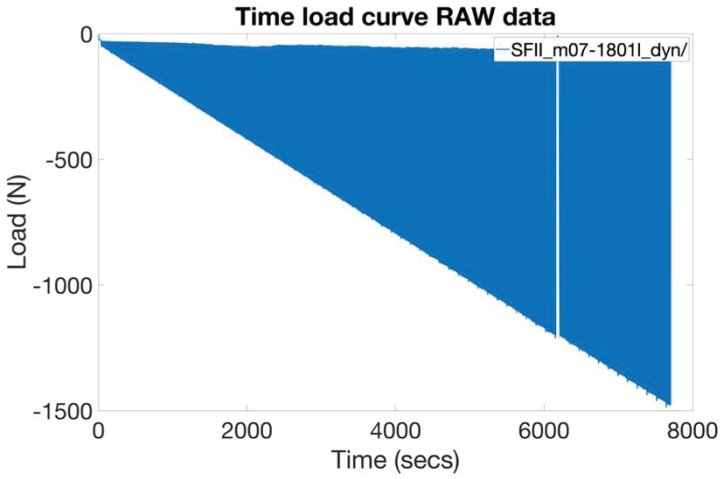

AO Serial No: m07-1810r

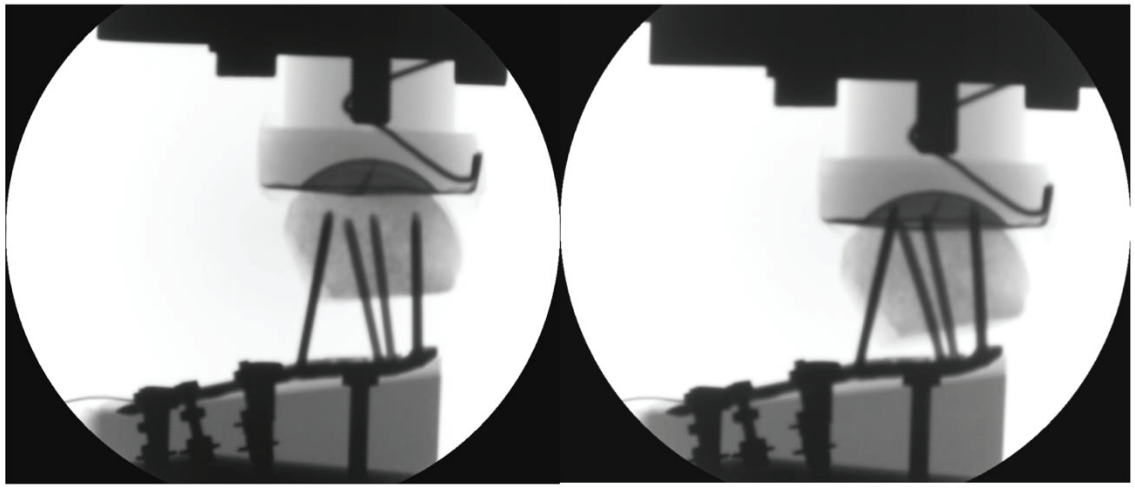

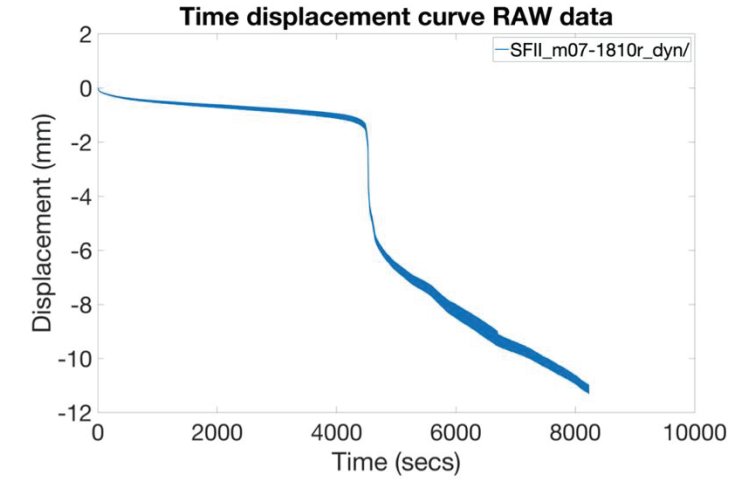

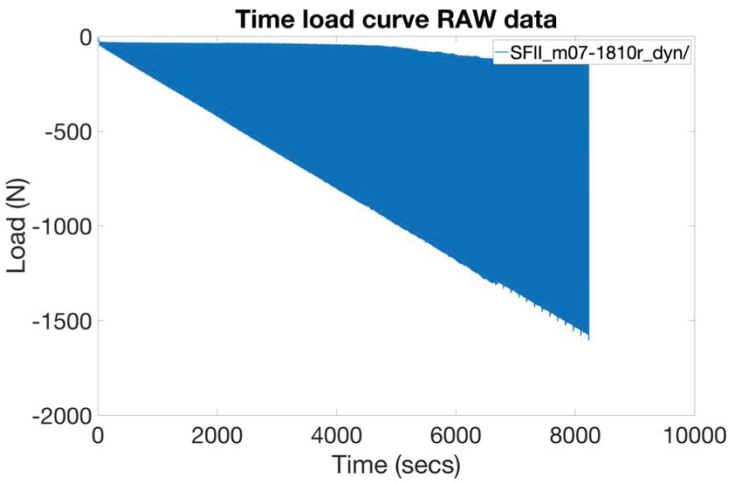

AO Serial No: m07-1811l

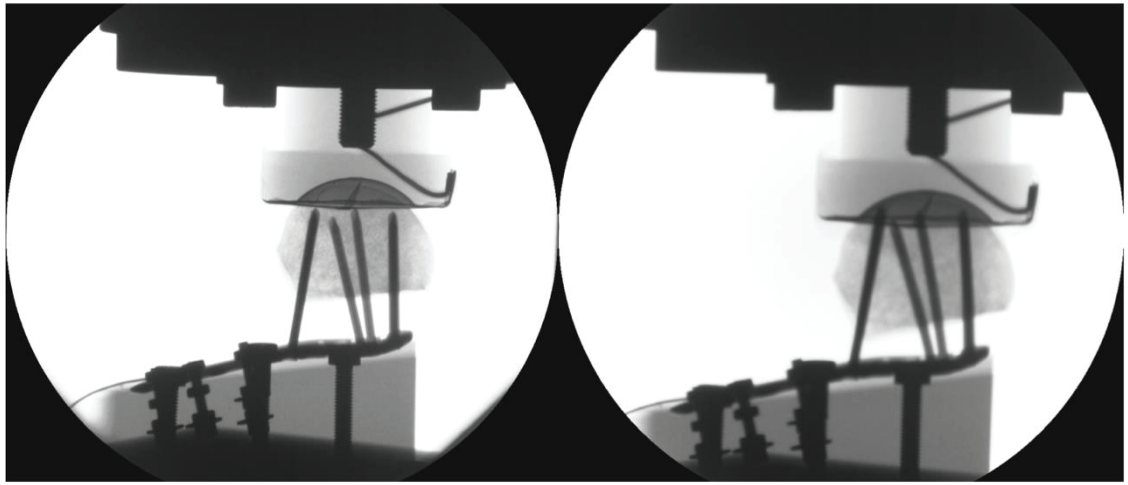

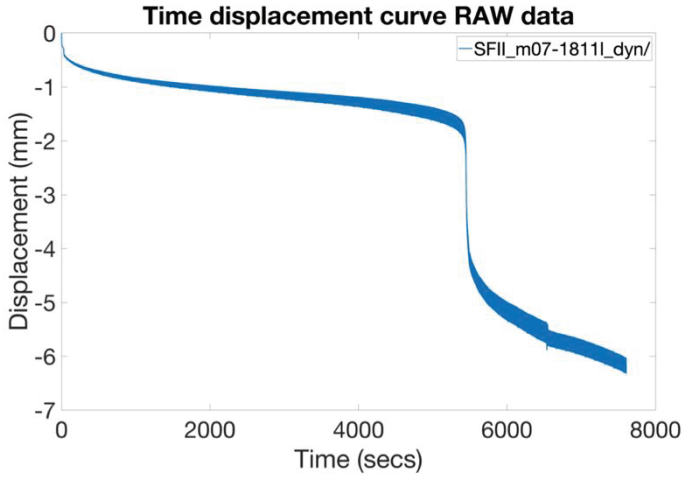

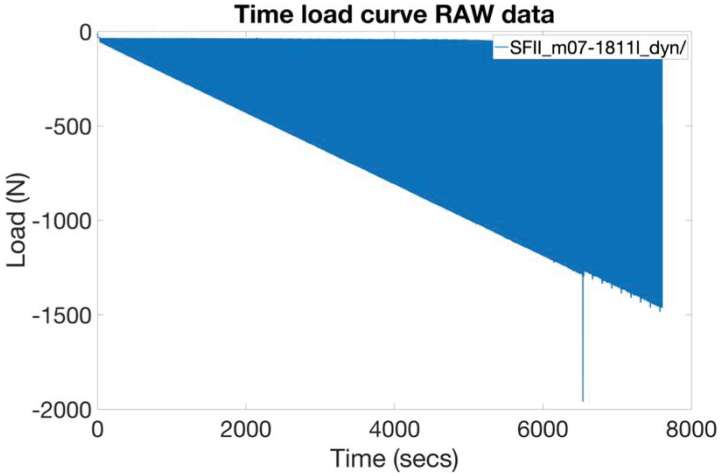

AO Serial No: m07-1812r

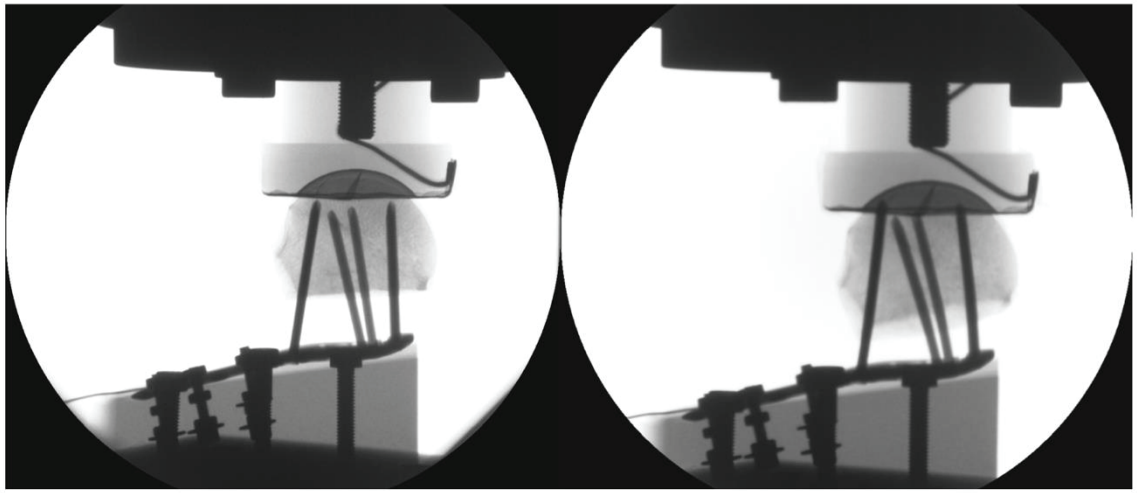

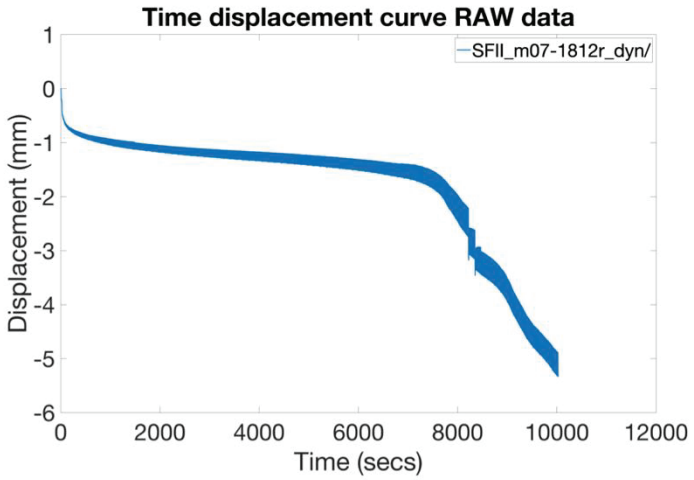

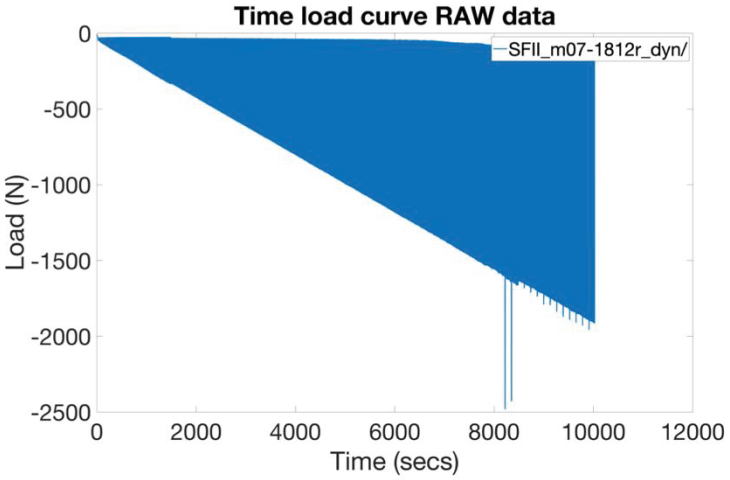

AO Serial No: m07-1813l

Instrumented image missing

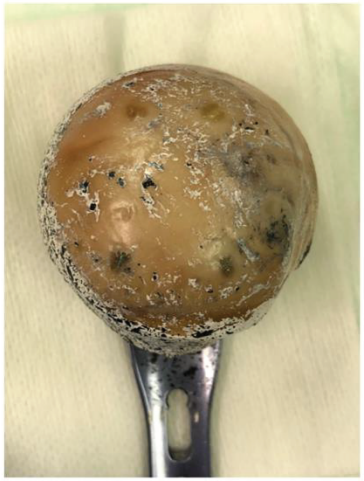

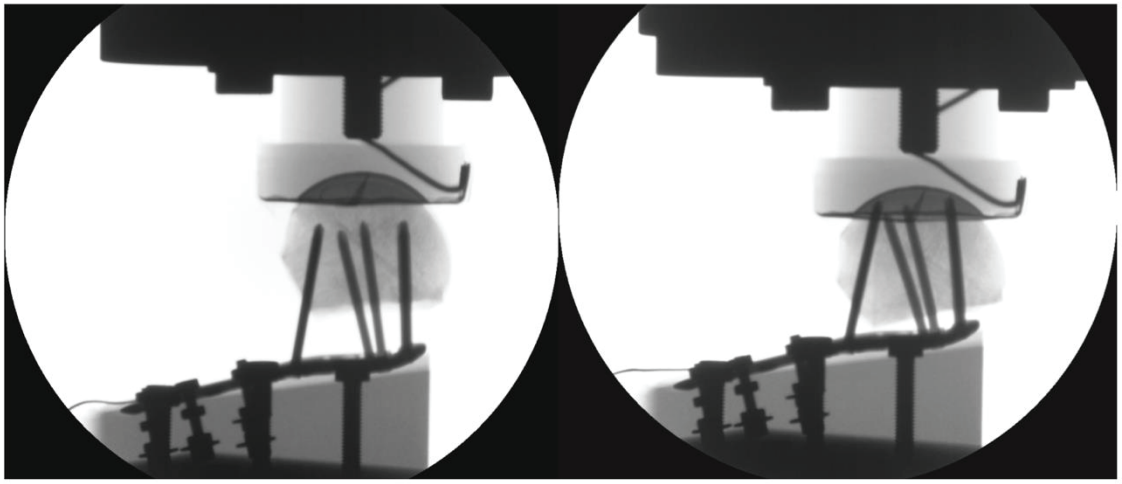

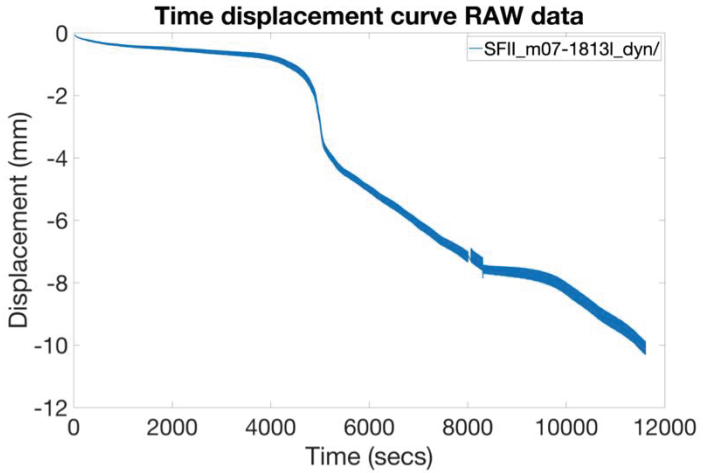

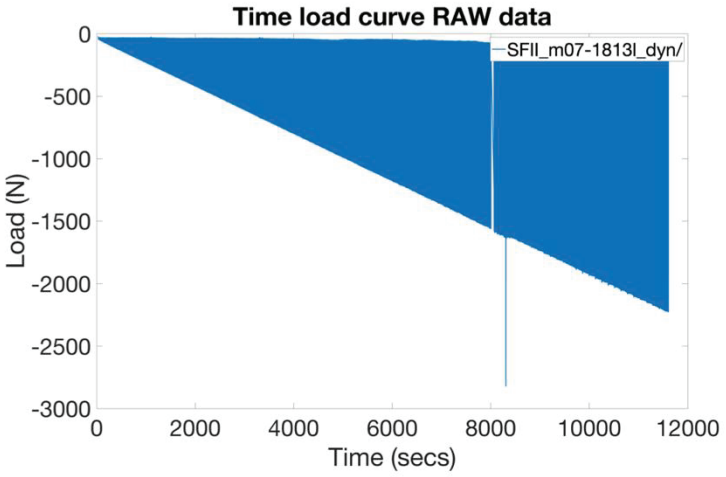

AO Serial No: m10-1044l

Instrumented image missing

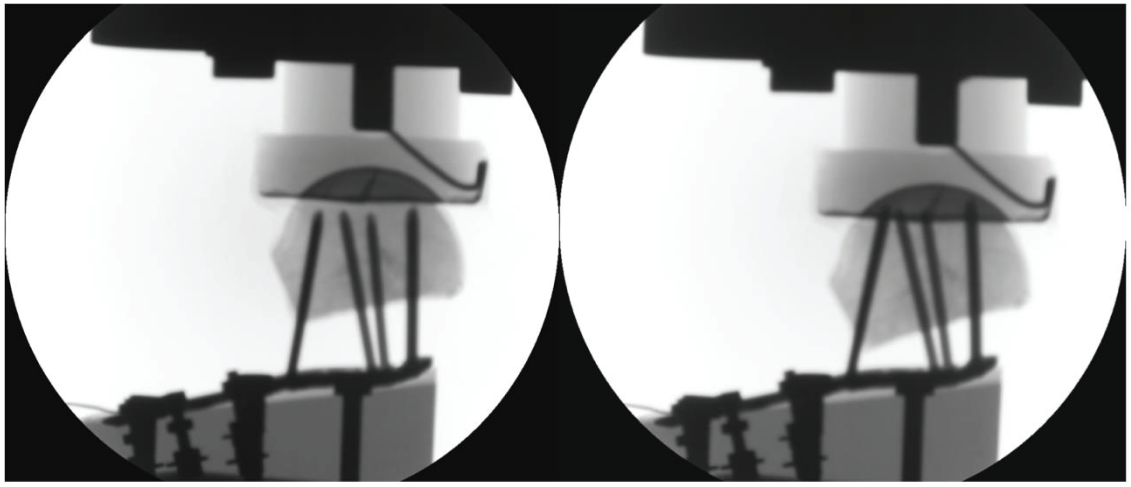

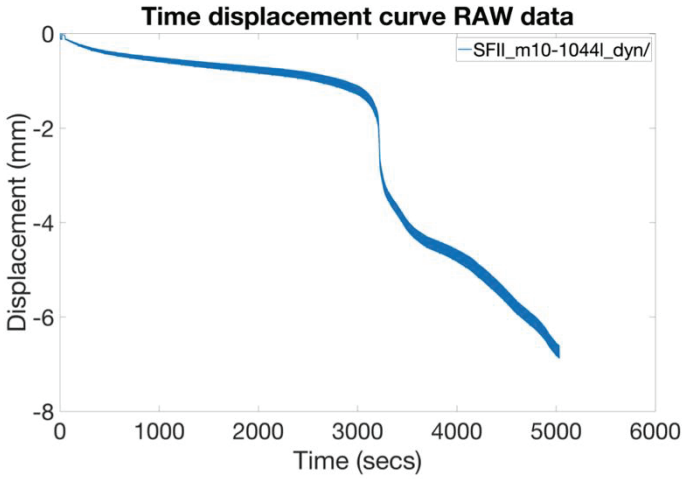

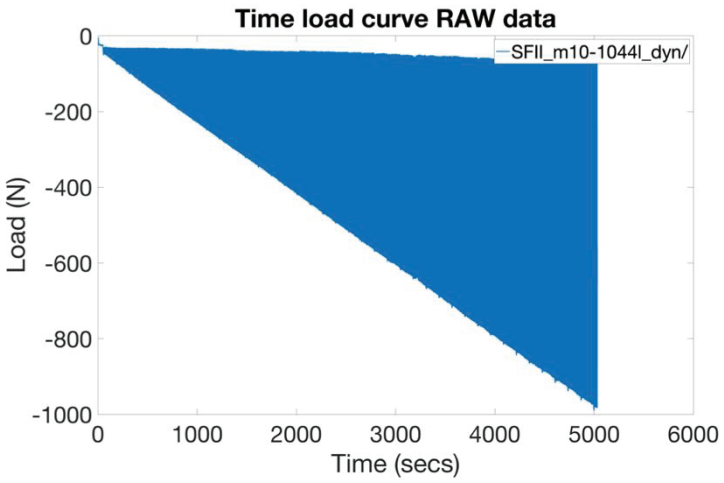

AO Serial No: m10-1044r

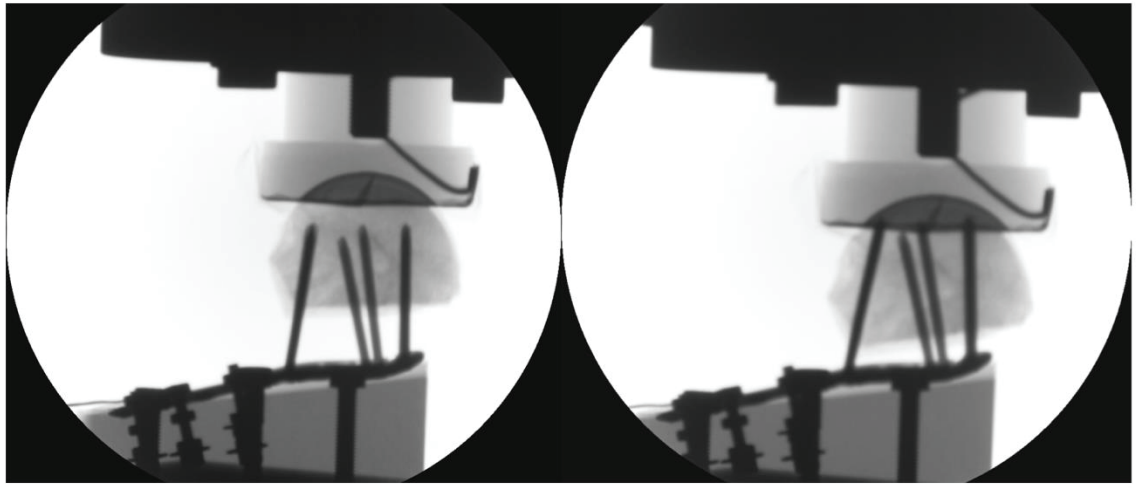

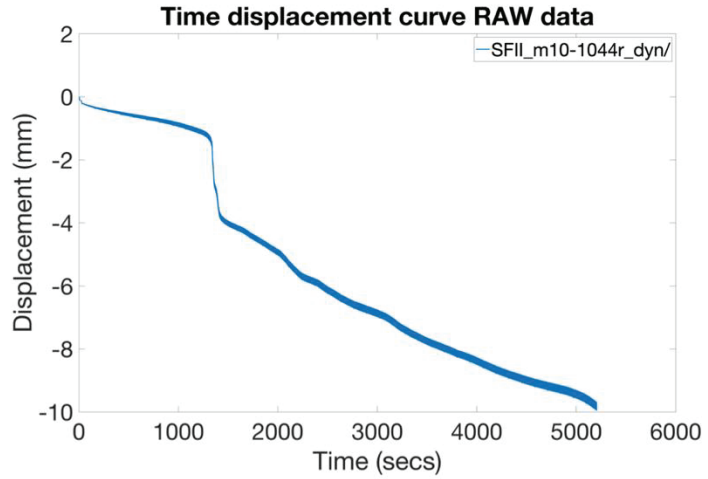

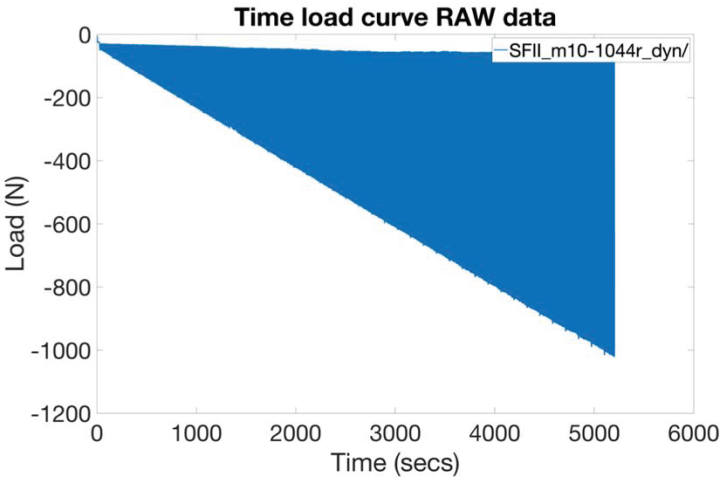

AO Serial No: m11-3000l

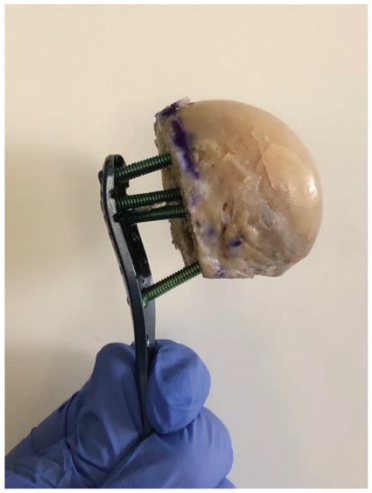

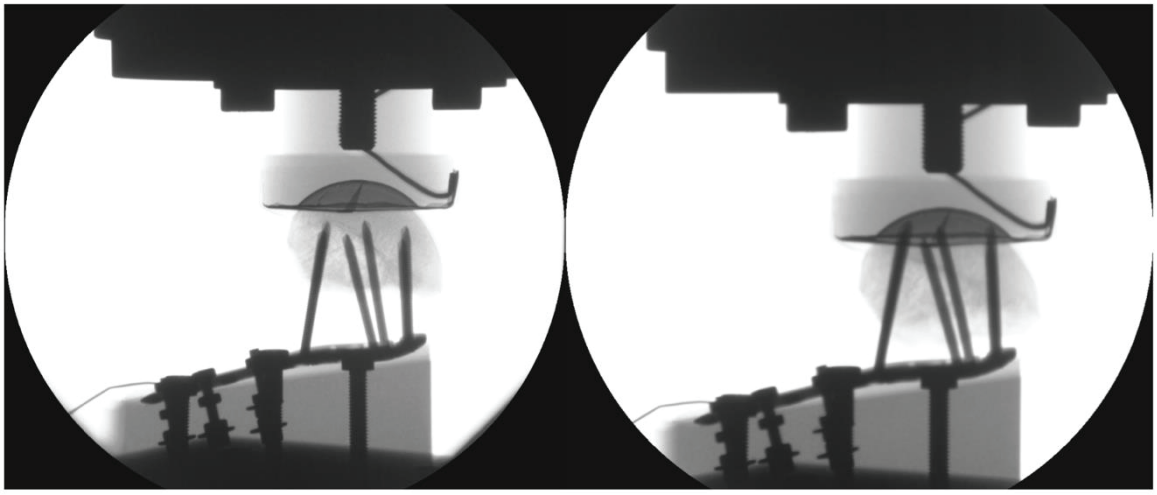

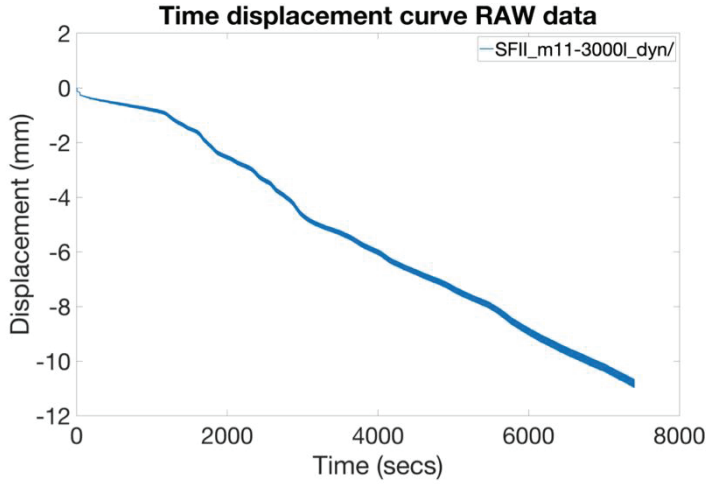

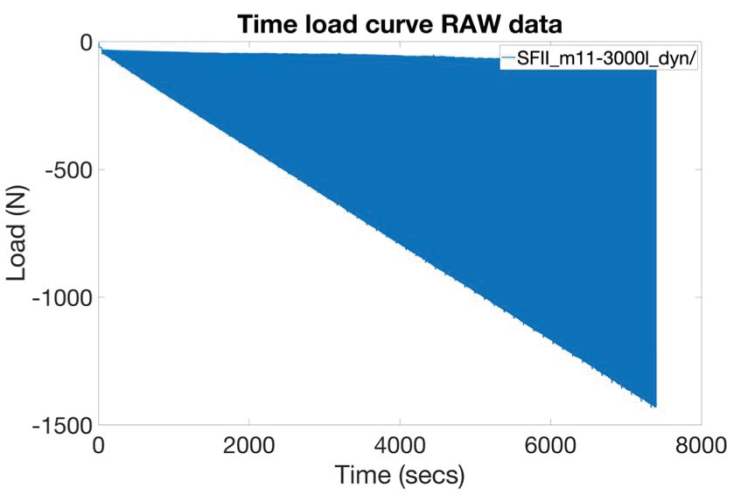

AO Serial No: m11-3000r

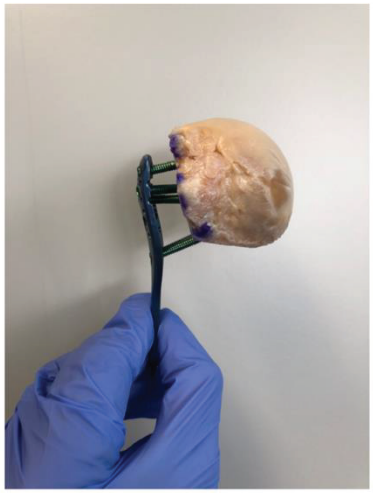

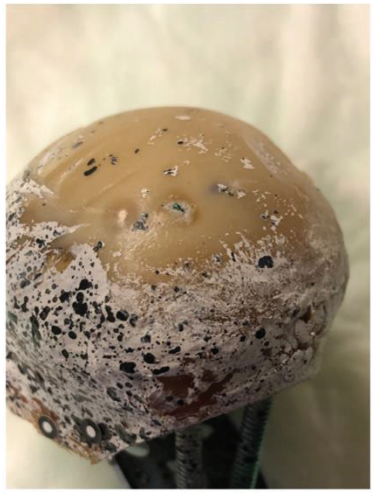

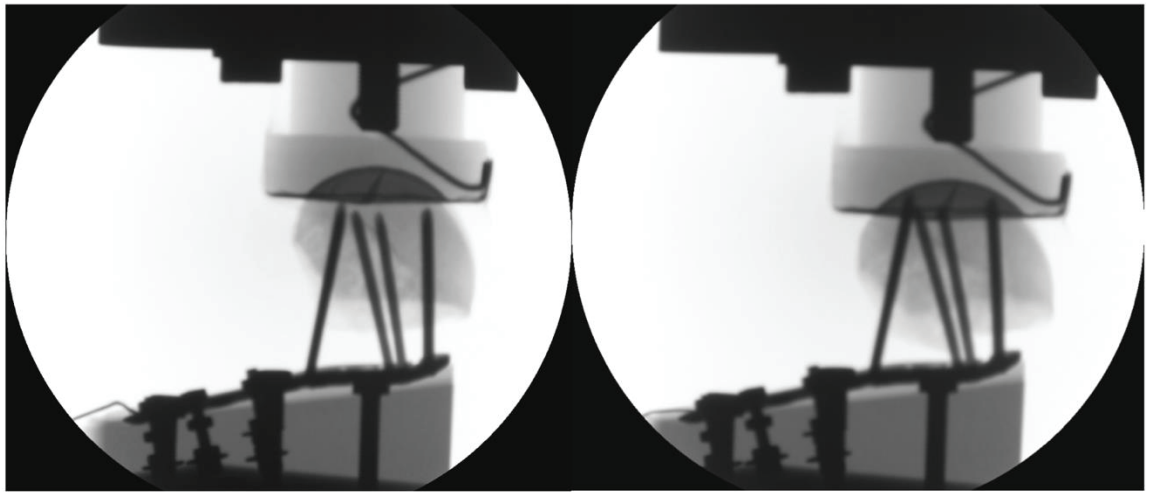

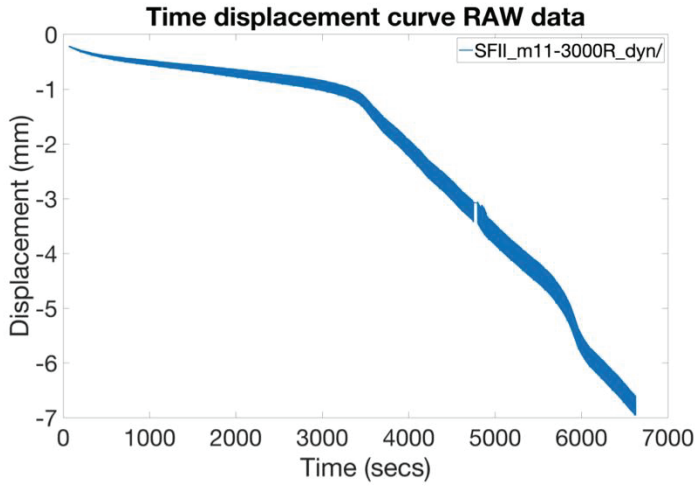

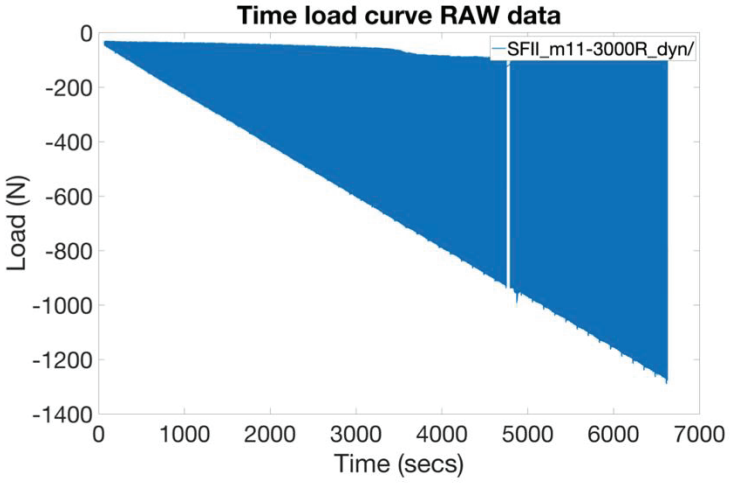

AO Serial No: m12-2200l

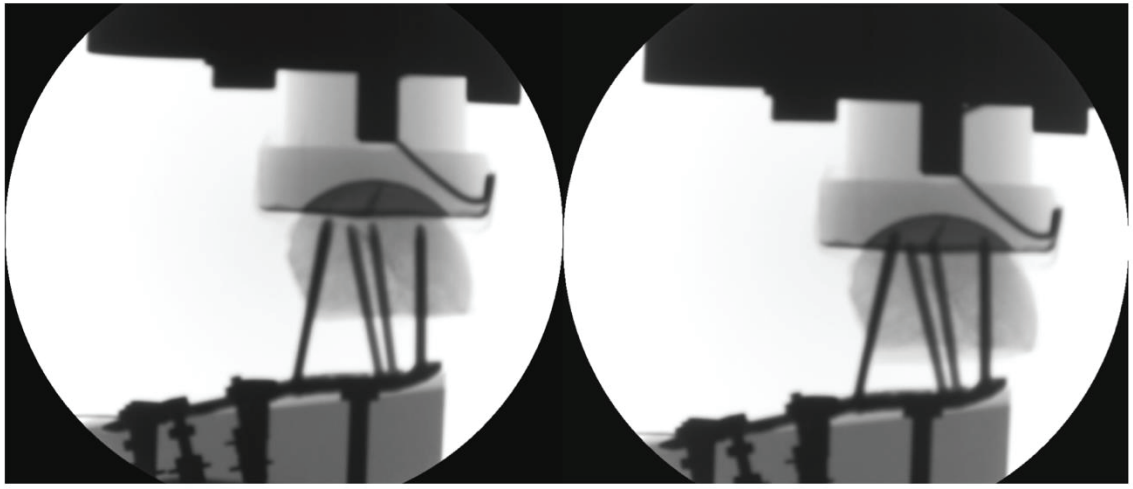

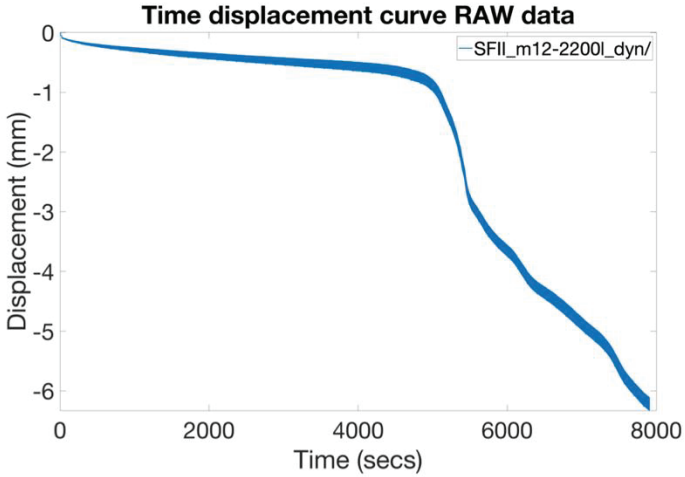

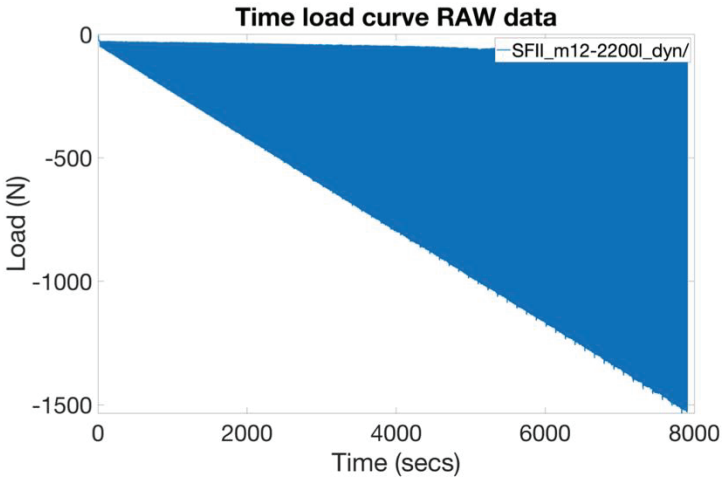

AO Serial No: m12-2200r

Failed image missing

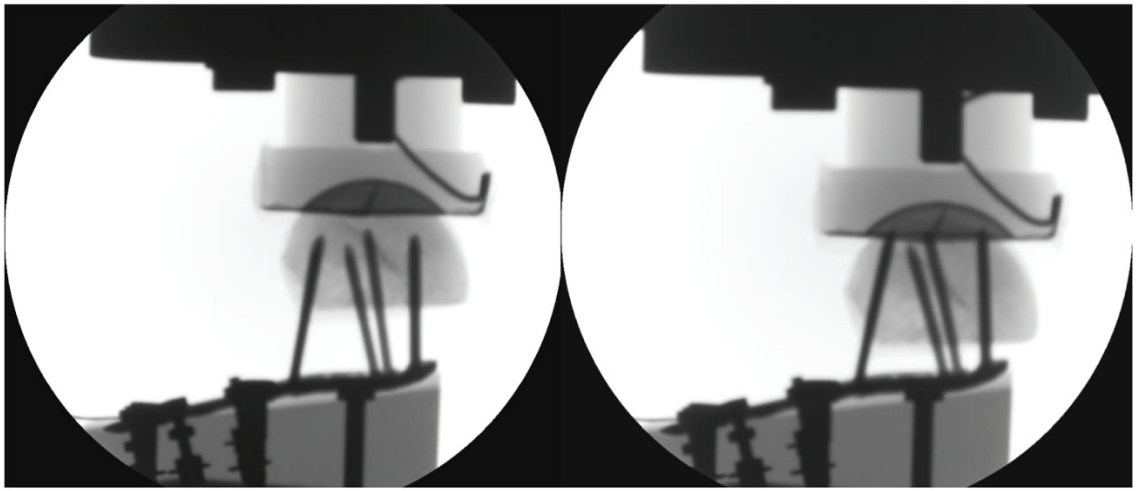

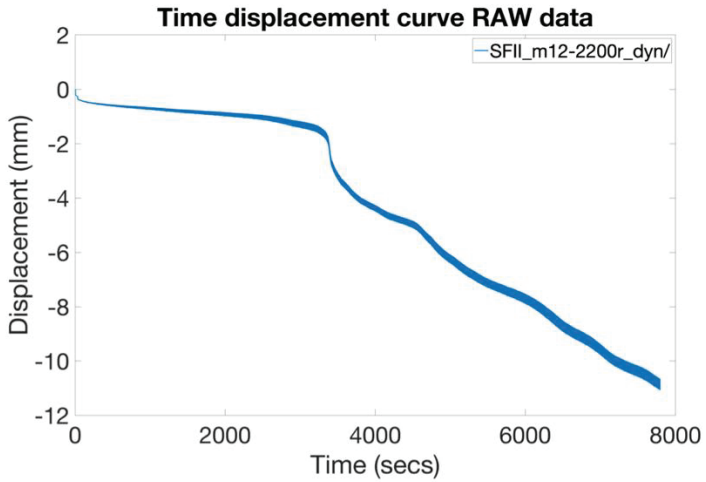

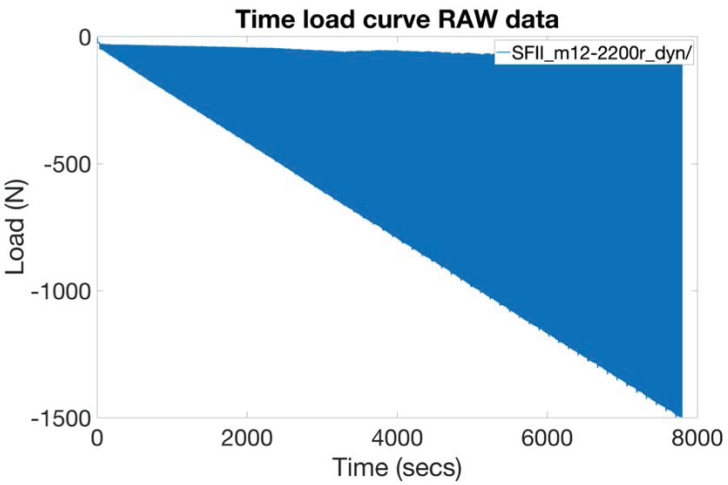

AO Serial No: m12-2208l

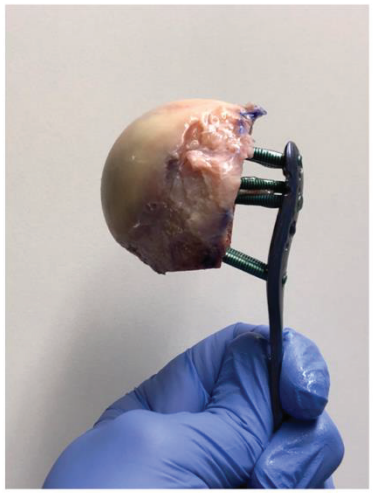

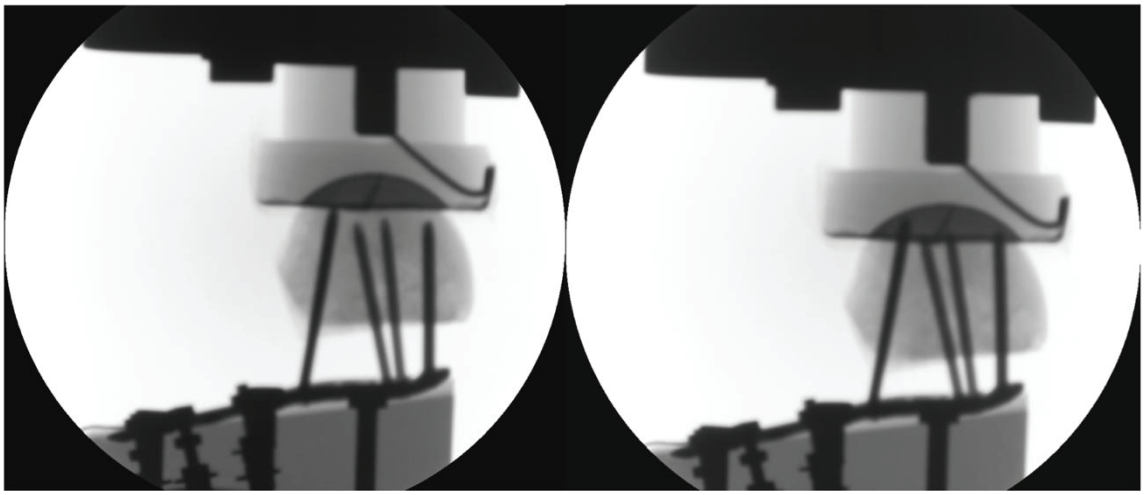

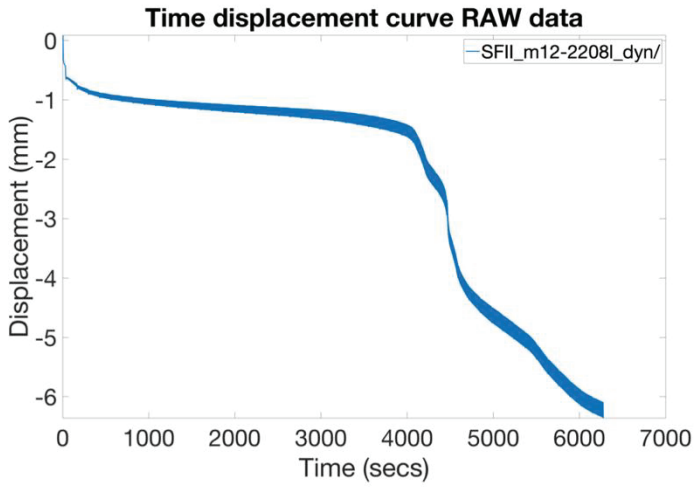

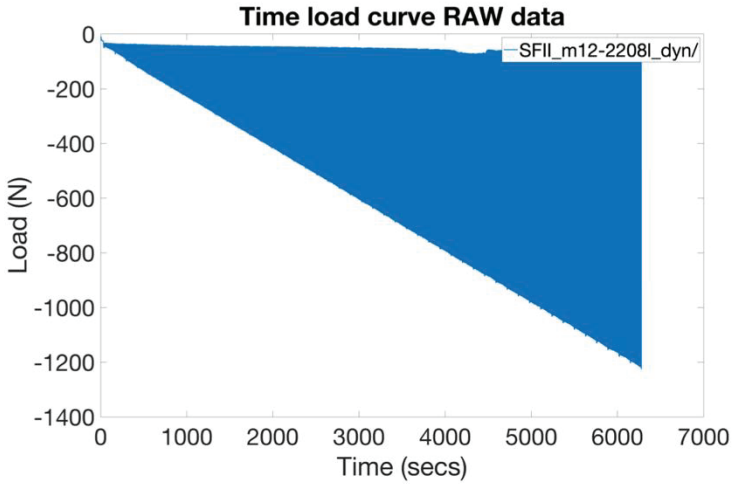

AO Serial No: m12-2208r

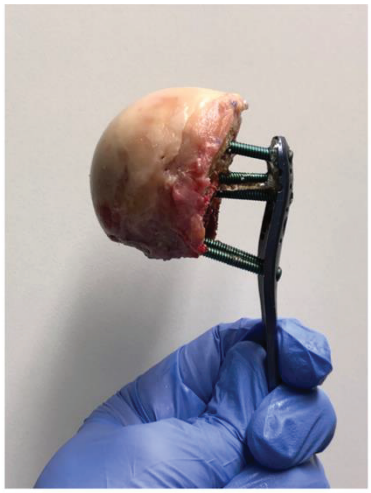

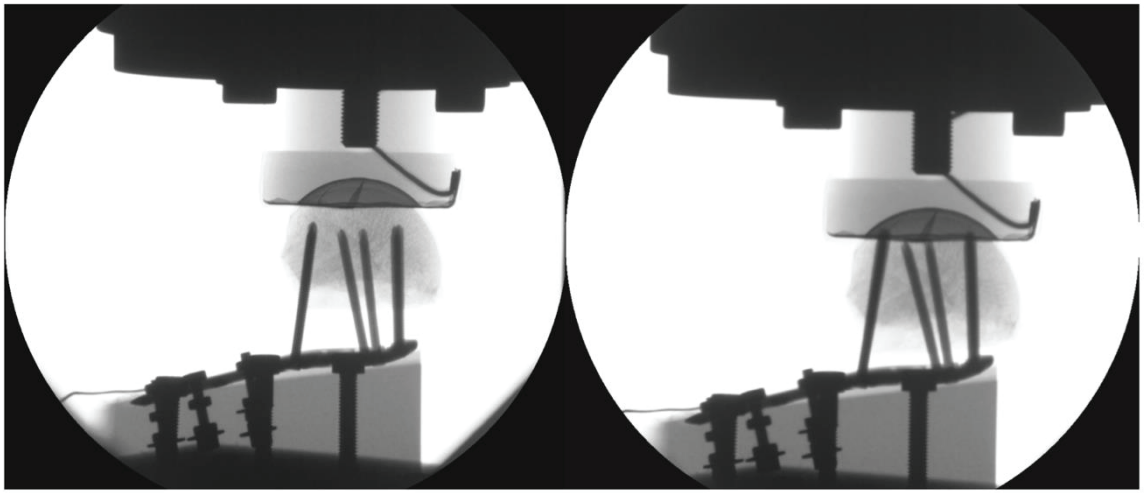

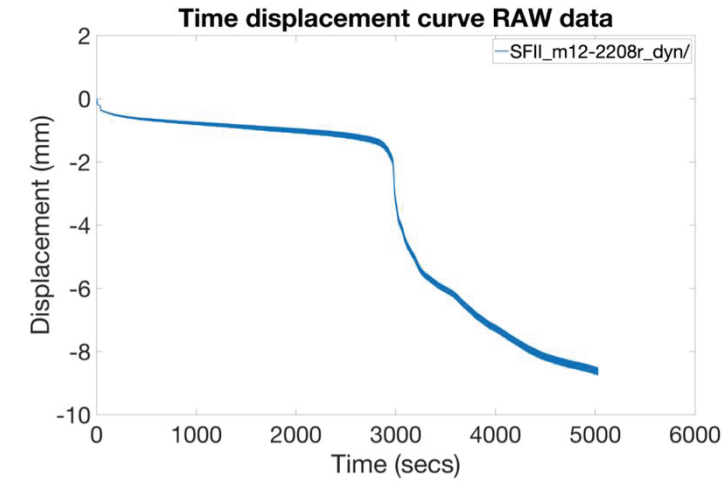

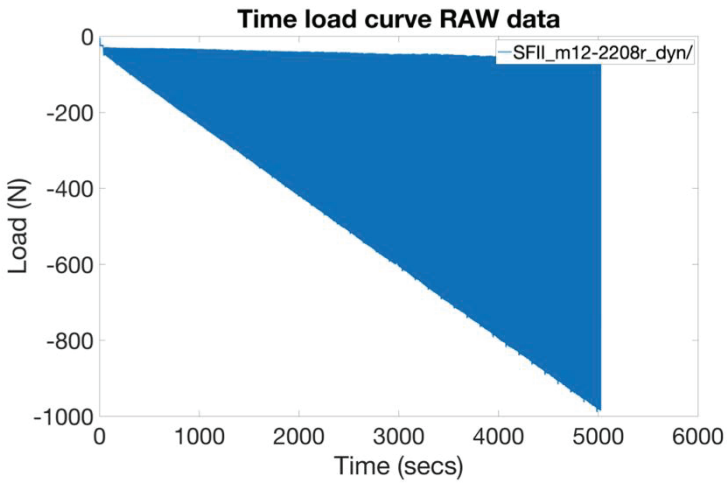

Appendix D: Specimen checklist

Table D.1. Specimen task checklist.

AO Serial No:	Tissue Removed	Intact CCT	Intact HR-pQCT	Osteotomised	CCT Osteotomy Scan	Instrumented	CCT Scanned (Instrumented)	Biomechanically tested	CCT Scanned (Tested)
f07-1762r	✓	✓	✓	✓	✓	✓	✓	✓	✓
f07-1763l	✓	✓	✓	✓	✓	✓	✓	✓	✓
f07-1766r	✓	✓	✓	✓	✓	✓	✓	✓	✓
f07-1767l	✓	✓	✓	✓	✓	✓	✓	✓	✓
f10-1047l	✓	✓	✓	✓	✓	✓	✓	✓	✓
f10-1047r	✓	✓	✓	✓	✓	✓	✓	✓	✓
m07-1800r	✓	✓	✓	✓	✓	✓	✓	✓	✓
m07-1801l	✓	✓	✓	✓	✓	✓	✓	✓	✓
m07-1810r	✓	✓	✓	✓	✓	✓	✓	✓	✓
m07-1811l	✓	✓	✓	✓	✓	✓	✓	✓	✓
m07-1812r	✓	✓	✓	✓	✓	✓	✓	✓	✓
m07-1813l	✓	✓	✓	✓	✓	✓	✓	✓	✓
m10-1044l	✓	✓	✓	✓	✓	✓	✓	✓	✓
m10-1044r	✓	✓	✓	✓	✓	✓	✓	✓	✓
m11-3000l	✓	✓	✓	✓	✓	✓	✓	✓	✓
m11-3000r	✓	✓	✓	✓	✓	✓	✓	✓	✓
m12-2200l	✓	✓	✓	✓	✓	✓	✓	✓	✓
m12-2200r	✓	✓	✓	✓	✓	✓	✓	✓	✓
m12-2208l	✓	✓	✓	✓	✓	✓	✓	✓	✓
m12-2208r	✓	✓	✓	✓	✓	✓	✓	✓	✓

Appendix E.1: FEA prediction model

Table E.1. Cylinder size parametric FEA study summary.

Cylinder size (radius, length above screw tip, length below screw tip) (mm)	Logarithmic correlation to cycles to screw loosening (R^2)	Logarithmic correlation to cycles to failure (R^2)
1.5, 5, 15	0.78	0.14
1.5, 10, 15	0.72	0.3
1.5, 15, 15	0.53	0.34
2, 5, 15	0.82	0.15
2, 10, 15	0.79	0.27
2, 15, 15	0.78	0.27
3, 5, 15	0.84	0.17
3, 10, 15	0.81	0.26
3, 15, 15	0.81	0.27
4, 5, 15	0.84	0.19
4, 10, 15	0.81	0.3
4, 15, 15	0.81	0.3

Table E.2. Summary of minimum compressive strains around screws for 100 N Gaussian loaded model.

AO Serial No:	Screw 1 (μstrain)	Screw 2 (μstrain)	Screw 3 (μstrain)	Screw 4 (μstrain)	Screw 8 (μstrain)	Screw 9 (μstrain)	Average (μstrain)
f07-1762r	-51.67	-27.58	-42.69	-116.48	-59.98	-43.99	-55.05
f07-1763l	-14.37	-13.02	-23.85	-31.32	-28.28	-31.05	-22.73
f07-1766r	-21.57	-12.73	-29.55	-35.21	-39.17	-22.96	-27.05
f07-1767l	-73.09	-56.83	-72.69	-53.59	-20.77	-30.70	-48.30
f10-1047l	-113.39	-67.91	-167.91	-256.80	-205.91	-145.91	-152.80
f10-1047r	-62.69	-38.95	-73.09	-100.38	-100.15	-29.71	-68.81
m07-1800r	-16.15	-77.11	-47.79	-70.77	-20.72	-81.97	-50.24
m07-1801l	-85.34	-25.63	-130.48	-122.09	-149.45	-65.95	-96.84
m07-1810r	-23.52	-38.48	-59.60	-87.37	-76.67	-72.25	-58.15
m07-1811l	-41.36	-17.06	-41.60	-47.78	-55.97	-49.54	-42.24
m07-1812r	-13.09	-27.57	-16.00	-43.97	-19.73	-26.65	-23.63
m07-1813l	-40.69	-23.03	-76.44	-47.89	-46.51	-29.26	-42.26
m10-1044l	-20.42	-57.39	-68.78	-118.86	-45.53	-125.94	-70.98
m10-1044r	-59.99	-137.94	-135.17	-243.54	-63.72	-110.84	-113.60
m11-3000L	-108.96	-25.81	-168.60	-112.04	-163.55	-53.38	-98.77
m11-3000R	-15.85	-41.48	-43.60	-65.50	-42.64	-57.36	-42.71
m12-2200l	-14.92	-37.27	-26.27	-54.32	-14.03	-55.05	-33.65
m12-2200r	-87.19	-23.79	-61.67	-109.61	-57.02	-17.05	-57.19
m12-2208l	-53.22	-12.08	-46.34	-41.79	-41.63	-19.91	-35.16
m12-2208r	-36.15	-64.39	-88.88	-94.25	-38.53	-42.23	-55.01

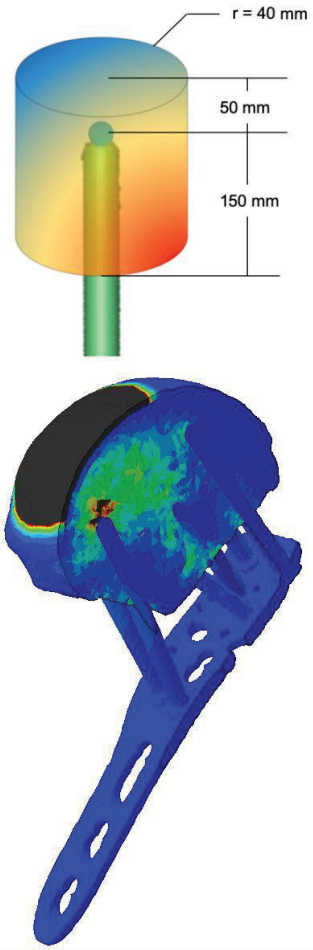

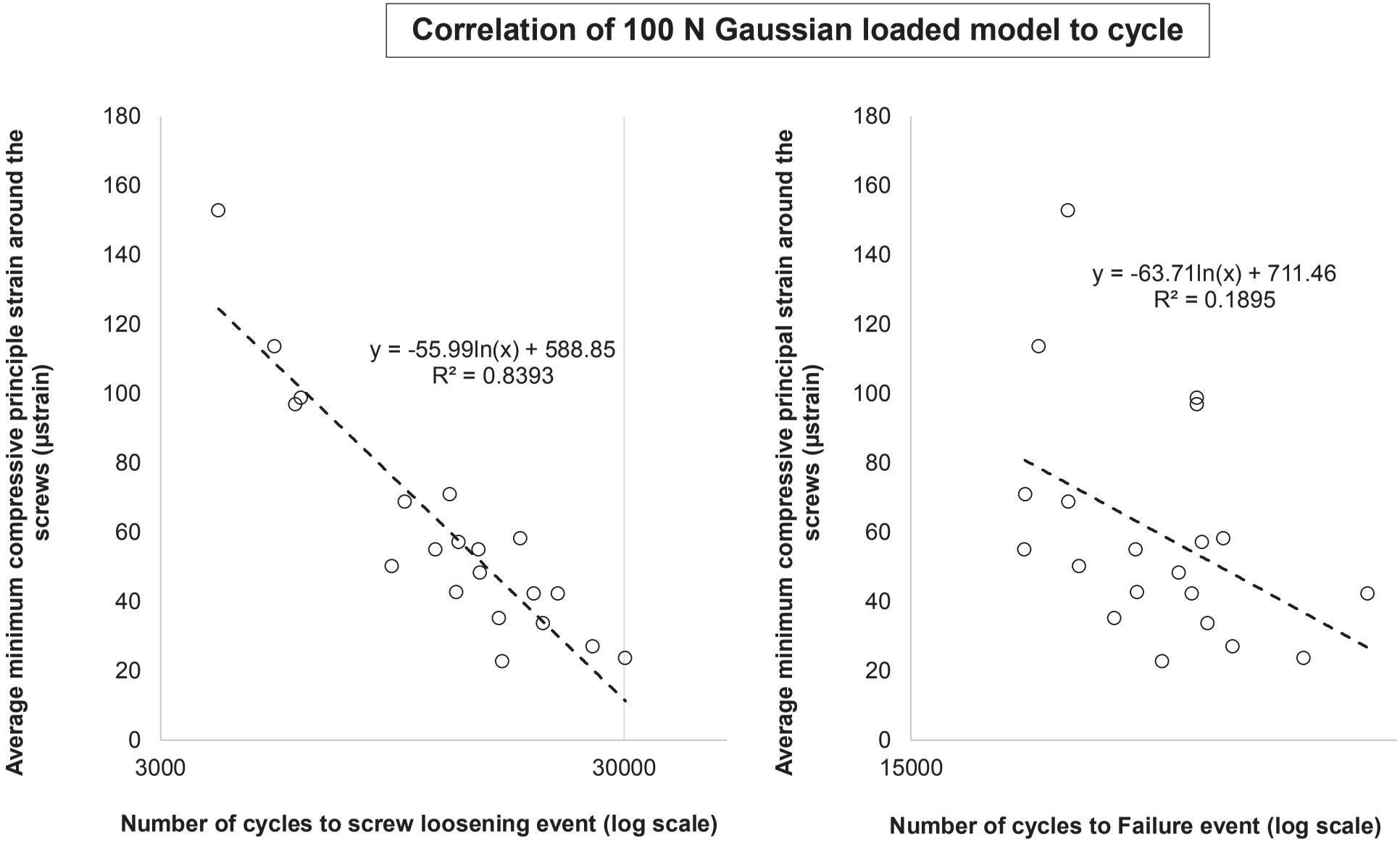

Figure E.1. *Logarithmic correlation of 100 N Gaussian loaded model to cycle events, each point represents a specimen.*

Table E.3. Summary of minimum compressive strains around screws for screw extended model.

AO Serial No:	Screw 1 (μstrain)	Screw 2 (μstrain)	Screw 3 (μstrain)	Screw 4 (μstrain)	Screw 8 (μstrain)	Screw 9 (μstrain)	Average (μstrain)
f07-1762r	-17.42	-12.23	-20.23	-45.58	-35.08	-19.30	-24.15
f07-1763l	-12.91	-11.57	-23.01	-23.80	-31.65	-31.35	-21.86
f07-1766r	-16.56	-8.53	-25.00	-24.68	-38.01	-20.00	-22.07
f07-1767l	-23.34	-23.77	-36.46	-21.52	-25.01	-28.63	-26.42
f10-1047l	-24.06	-13.73	-45.82	-64.17	-66.06	-118.79	-56.72
f10-1047r	-31.95	-21.65	-53.69	-79.06	-89.38	-28.84	-52.00
m07-1800r	-12.30	-52.87	-36.93	-56.00	-20.28	-62.03	-38.71
m07-1801l	-26.33	-11.58	-39.46	-29.55	-45.98	-28.00	-29.54
m07-1810r	-12.39	-14.93	-27.14	-34.38	-46.93	-43.34	-29.92
m07-1811l	-21.43	-15.83	-30.46	-35.99	-49.07	-44.03	-32.29
m07-1812r	-10.49	-17.96	-12.60	-28.89	-17.86	-22.44	-17.72
m07-1813l	-17.14	-13.37	-23.94	-19.83	-21.33	-22.86	-19.59
m10-1044l	-14.54	-45.59	-61.42	-115.00	-57.43	-92.11	-64.06
m10-1044r	-21.68	-35.92	-53.61	-145.25	-113.22	-111.83	-77.78
m11-3000L	-49.27	-14.99	-48.41	-42.09	-49.07	-21.66	-36.97
m11-3000R	-14.08	-32.20	-39.97	-45.56	-31.14	-38.77	-32.88
m12-2200l	-11.38	-30.48	-21.84	-45.26	-13.79	-41.57	-27.56
m12-2200r	-33.34	-14.47	-28.72	-27.99	-35.96	-11.81	-25.94
m12-2208l	-39.74	-9.00	-30.87	-29.59	-33.02	-18.08	-26.38
m12-2208r	-15.82	-21.34	-59.18	-35.62	-47.21	-33.50	-35.94

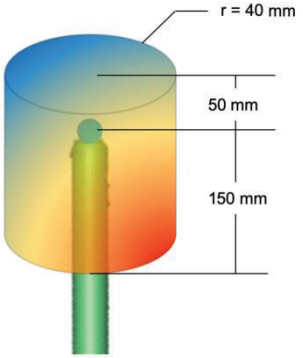

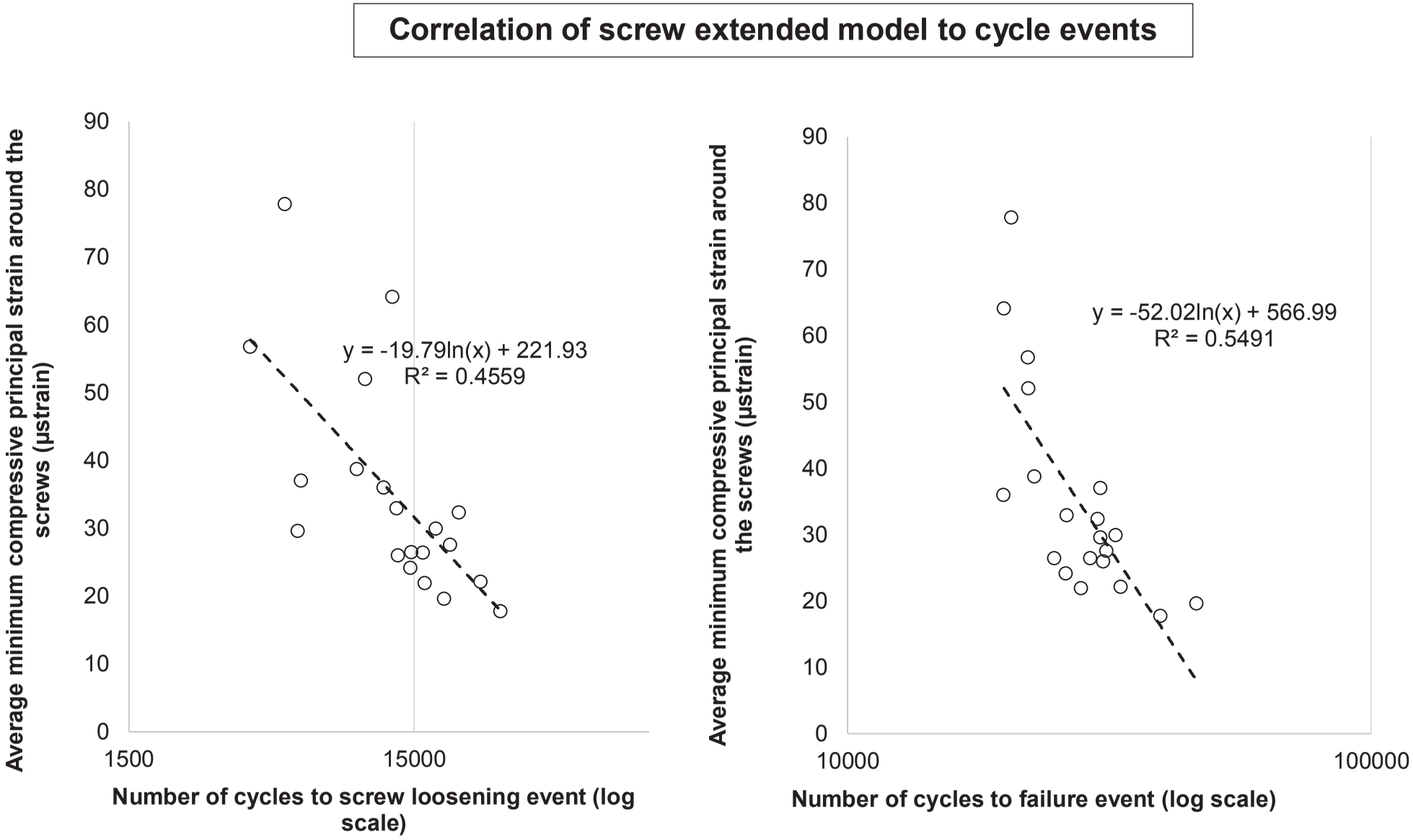

Figure E.2. Logarithmic correlation of screw extended model to cycle events, each point represents a specimen.

Table E.4. Summary of minimum compressive strains around screws for cup loaded model.

AO Serial No:	Screw 1 (μstrain)	Screw 2 (μstrain)	Screw 3 (μstrain)	Screw 4 (μstrain)	Screw 8 (μstrain)	Screw 9 (μstrain)	Average (μstrain)
f07-1762r	-61.55	-23.53	-42.05	-114.45	-66.98	-36.85	-54.66
f07-1763l	-15.30	-14.25	-22.67	-30.23	-27.64	-28.45	-22.34
f07-1766r	-	-	-	-	-	-	-
f07-1767l	-84.25	-45.03	-71.37	-53.48	-29.52	-46.37	-52.29
f10-1047l	-	-	-	-	-	-	-
f10-1047r	-60.12	-43.42	-67.16	-98.28	-77.25	-35.52	-63.59
m07-1800r	-	-	-	-	-	-	-
m07-1801l	-72.08	-10.43	-62.70	-48.46	-96.06	-61.11	-57.23
m07-1810r	-16.50	-33.76	-56.37	-63.99	-52.44	-83.35	-50.87
m07-1811l	-52.92	-11.91	-43.80	-54.60	-49.20	-44.62	-42.80
m07-1812r	-11.76	-32.86	-14.70	-45.17	-18.68	-22.91	-23.39
m07-1813l	-50.79	-13.91	-71.00	-45.55	-56.89	-29.10	-43.14
m10-1044l	-49.38	-33.92	-72.18	-69.65	-83.07	-105.26	-69.04
m10-1044r	-	-	-	-	-	-	-
m11-3000L	-125.79	-30.55	-164.80	-112.10	-184.20	-56.80	-105.85
m11-3000R	-	-	-	-	-	-	-
m12-2200l	-14.32	-33.85	-27.13	-46.20	-25.55	-43.12	-31.80
m12-2200r	-56.95	-40.80	-51.70	-114.73	-47.39	-46.45	-57.68
m12-2208l	-	-	-	-	-	-	-
m12-2208r	-44.09	-77.08	-77.05	-89.09	-29.04	-58.30	-55.10

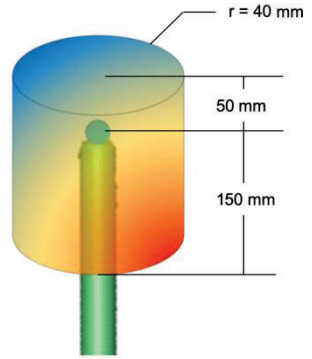

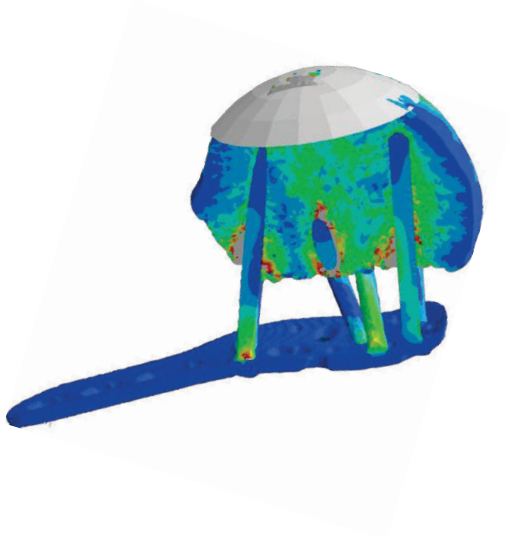

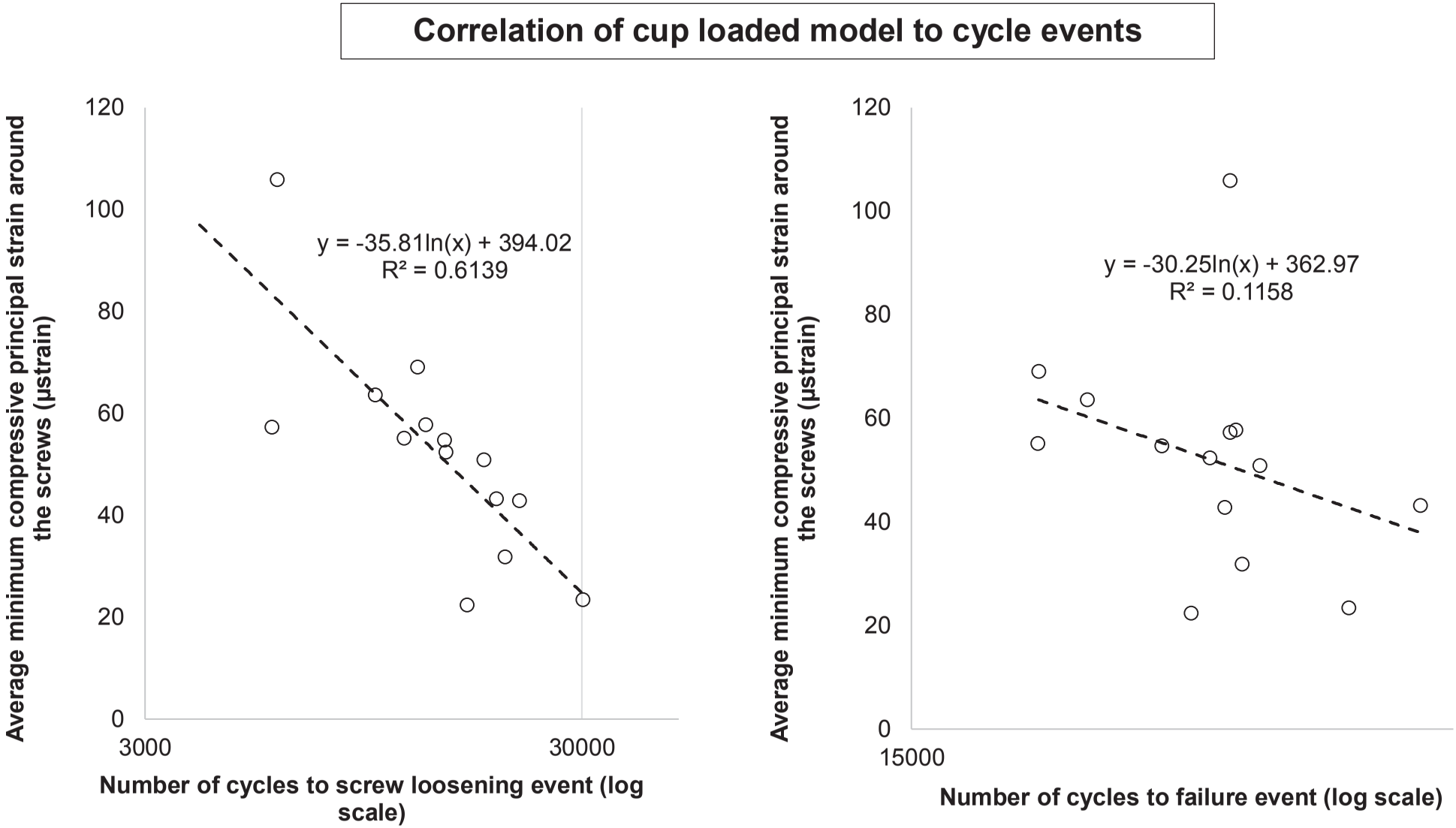

Figure E.3. Logarithmic correlation of cup loaded model to cycle events, each point represents a specimen.

Appendix E.2: Mesh convergence study

Table E.5. Summary of minimum compressive strains around screws for coarse mesh 100 Gaussian loaded model.

AO Serial No:	Screw 1 (μstrain)	Screw 2 (μstrain)	Screw 3 (μstrain)	Screw 4 (μstrain)	Screw 8 (μstrain)	Screw 9 (μstrain)	Average (μstrain)
f07-1762r	-29.22	-16.23	-32.67	-70.11	-57.18	-30.64	-37.93
f07-1763l	-13.26	-11.90	-23.98	-29.10	-30.64	-31.88	-21.37
f07-1766r	-16.79	-15.13	-27.24	-31.58	-34.43	-26.47	-25.58
f07-1767l	-32.20	-51.97	-28.88	-31.68	-13.23	-36.19	-32.85
f10-1047l	-36.67	-55.82	-102.69	-179.60	-113.24	-180.96	-111.44
f10-1047r	-52.72	-29.36	-74.71	-87.38	-115.83	-32.62	-67.22
m07-1800r	-20.23	-40.77	-47.96	-49.98	-33.96	-73.00	-43.59
m07-1801l	-39.98	-20.75	-80.54	-66.93	-105.71	-57.14	-59.26
m07-1810r	-14.43	-33.85	-39.61	-56.99	-64.28	-81.64	-47.15
m07-1811l	-31.49	-19.97	-42.79	-46.06	-48.10	-49.37	-39.31
m07-1812r	-8.70	-24.18	-14.36	-35.92	-21.97	-32.39	-20.74
m07-1813l	-45.43	-8.97	-49.62	-28.16	-53.27	-23.33	-34.28
m10-1044l	-17.90	-49.17	-61.36	-112.73	-49.82	-110.78	-65.24
m10-1044r	-39.77	-55.53	-79.92	-163.94	-87.41	-114.19	-85.56
m11-3000L	-65.87	-13.31	-104.43	-70.37	-100.43	-42.26	-62.33
m11-3000R	-11.92	-44.38	-43.43	-55.72	-34.65	-61.75	-39.57
m12-2200l	-16.06	-32.42	-21.03	-42.29	-13.22	-39.89	-27.98
m12-2208l	-26.68	-15.09	-36.95	-35.11	-32.48	-29.42	-28.99
m12-2208r	-19.99	-51.35	-51.81	-44.75	-40.87	-46.08	-43.03

Table E.6. Summary of minimum compressive strains around screws for default mesh 100 Gaussian loaded model.

AO Serial No:	Screw 1 (μstrain)	Screw 2 (μstrain)	Screw 3 (μstrain)	Screw 4 (μstrain)	Screw 8 (μstrain)	Screw 9 (μstrain)	Average (μstrain)
f07-1762r	-51.67	-27.58	-42.69	-116.48	-59.98	-43.99	-55.05
f07-1763l	-14.37	-13.02	-23.85	-31.32	-28.28	-31.05	-22.73
f07-1766r	-21.57	-12.73	-29.55	-35.21	-39.17	-22.96	-27.05
f07-1767l	-73.09	-56.83	-72.69	-53.59	-20.77	-30.70	-48.30
f10-1047l	-113.39	-67.91	-167.91	-256.80	-205.91	-145.91	-152.80
f10-1047r	-62.69	-38.95	-73.09	-100.38	-100.15	-29.71	-68.81
m07-1800r	-16.15	-77.11	-47.79	-70.77	-20.72	-81.97	-50.24
m07-1801l	-85.34	-25.63	-130.48	-122.09	-149.45	-65.95	-96.84
m07-1810r	-23.52	-38.48	-59.60	-87.37	-76.67	-72.25	-58.15
m07-1811l	-41.36	-17.06	-41.60	-47.78	-55.97	-49.54	-42.24
m07-1812r	-13.09	-27.57	-16.00	-43.97	-19.73	-26.65	-23.63
m07-1813l	-40.69	-23.03	-76.44	-47.89	-46.51	-29.26	-42.26
m10-1044l	-20.42	-57.39	-68.78	-118.86	-45.53	-125.94	-70.98
m10-1044r	-59.99	-137.94	-135.17	-243.54	-63.72	-110.84	-113.60
m11-3000L	-108.96	-25.81	-168.60	-112.04	-163.55	-53.38	-98.77
m11-3000R	-15.85	-41.48	-43.60	-65.50	-42.64	-57.36	-42.71
m12-2200l	-14.92	-37.27	-26.27	-54.32	-14.03	-55.05	-33.65
m12-2208l	-53.22	-12.08	-46.34	-41.79	-41.63	-19.91	-35.16
m12-2208r	-36.15	-64.39	-88.88	-94.25	-38.53	-42.23	-55.01

Table E.7. Summary of minimum compressive strains around screws for fine mesh 100 Gaussian loaded model.

AO Serial No:	Screw 1 (μstrain)	Screw 2 (μstrain)	Screw 3 (μstrain)	Screw 4 (μstrain)	Screw 8 (μstrain)	Screw 9 (μstrain)	Average (μstrain)
f07-1762r	-26.92	-16.26	-30.96	-74.00	-60.14	-42.82	-40.92
f07-1763l	-14.40	-12.47	-26.54	-27.37	-30.24	-32.29	-23.06
f07-1766r	-21.17	-16.25	-29.29	-32.41	-34.56	-22.05	-26.23
f07-1767l	-39.32	-54.93	-35.98	-31.64	-17.55	-35.63	-35.97
f10-1047l	-70.24	-24.74	-117.76	-159.98	-160.60	-160.62	-114.73
f10-1047r	-56.91	-34.47	-77.71	-111.06	-117.22	-34.59	-72.95
m07-1800r	-17.07	-71.23	-44.40	-66.50	-23.79	-96.19	-51.46
m07-1801l	-54.80	-19.18	-92.30	-53.60	-132.14	-65.47	-70.48
m07-1810r	-24.17	-23.95	-47.60	-54.13	-86.68	-68.37	-50.40
m07-1811l	-36.10	-18.62	-44.35	-46.76	-63.41	-57.02	-44.19
m07-1812r	-12.98	-25.57	-14.72	-39.71	-19.60	-28.05	-22.84
m07-1813l	-27.84	-19.35	-45.65	-30.73	-38.93	-34.63	-32.78
m10-1044l	-17.46	-52.87	-67.04	-132.96	-58.44	-145.38	-77.65
m10-1044r	-45.22	-78.14	-85.21	-203.15	-78.94	-144.67	-102.07
m11-3000L	-87.29	-15.98	-107.93	-81.39	-109.55	-38.57	-72.05
m11-3000R	-17.28	-39.91	-46.41	-60.14	-42.79	-58.81	-42.79
m12-2200l	-12.68	-33.14	-24.47	-50.34	-16.38	-50.78	-31.79
m12-2208l	-51.47	-11.66	-46.91	-39.29	-40.75	-21.42	-34.69
m12-2208r	-23.87	-32.91	-69.78	-46.23	-60.02	-47.30	-47.82

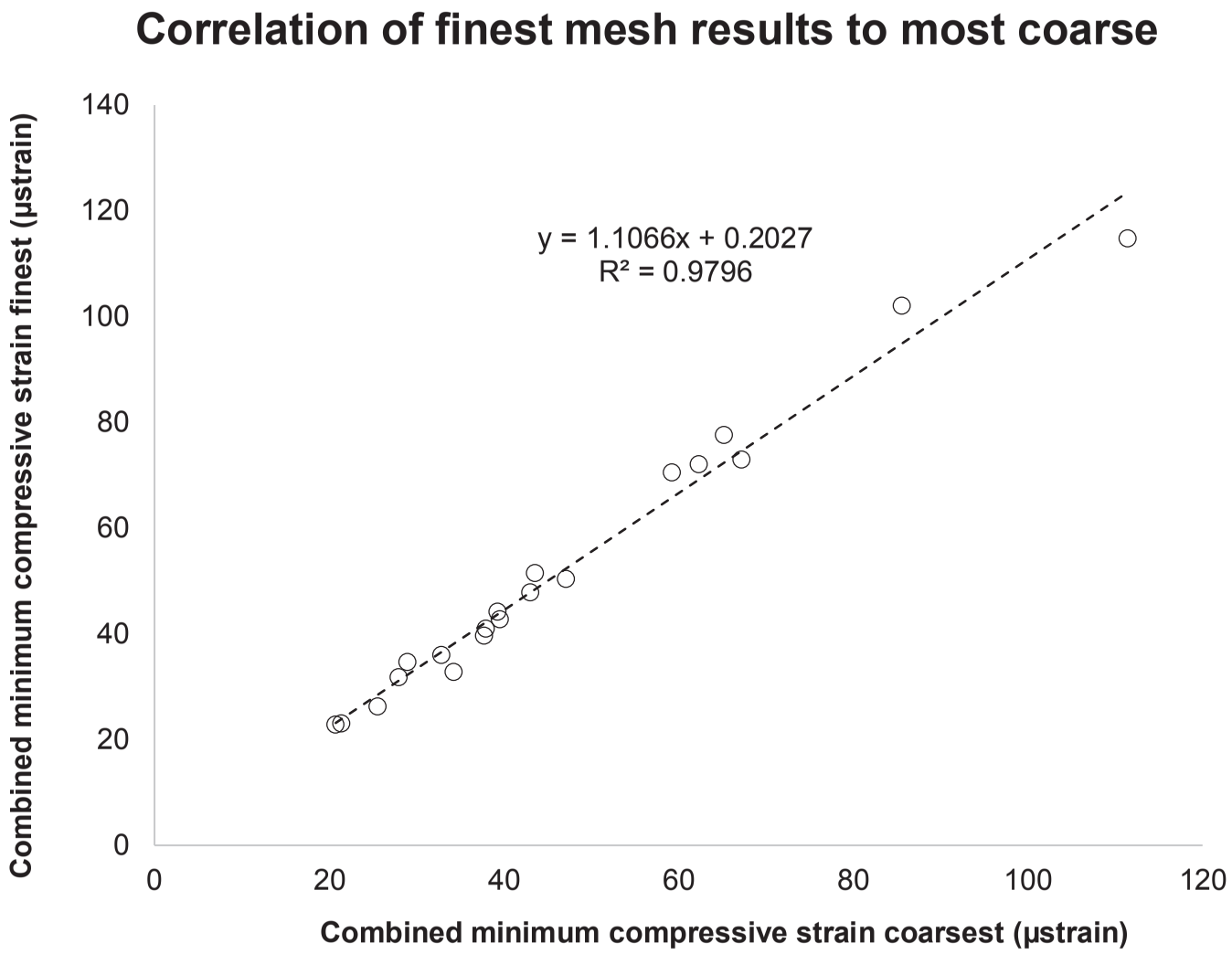

Figure E.4. *Linear correlation of finest mesh results to most coarse, each point represents a specimen.*

Table E.8. Summary of FE model mesh.

	Course		Default		Fine	
Average amongst specimens	**Mean**	**STD**	**Mean**	**STD**	**Mean**	**STD**
Number of nodes	62474	6127	183117	17034	321463	30796
Number of elements	301147	30554	909943	88760	1630859	165383
Mean edge length (mm)	1.09	0.02	0.77	0.02	0.66	0.01
Mean edge standard deviation (mm)	0.75	0.09	0.48	0.04	0.35	0.05
Mean element volume (mm^3)	0.18	0.01	0.06	0.0003	0.03	0.0002

Appendix F: Density prediction model

Table F.1. Summary of linear correlations for density-based predictions from cylinder size parametric study.

	Average BMD		Total BMC	
Cylinder size (radius, length above screw tip, length below screw tip) (mm)	Linear correlation to cycles to screw loosening (R^2)	Linear correlation to cycles to failure (R^2)	Linear correlation to cycles to screw loosening (R^2)	Linear correlation to cycles to failure (R^2)
4, 5, 20	0.81	0.4	0.75	0.55
3, 5, 20	0.79	0.27	0.83	0.34
4, 15, 20	0.69	0.42	0.02	0.44
4, 15, 30	0.77	0.52	0.31	0.64
3, 15, 30	0.77	0.53	0.4	0.71
1.5, 15, 30	0.77	0.56	0.43	0.75
1, 15, 30	0.76	0.56	0.43	0.74

Table F.2. Summary of results for BMD for cylinder size 3, 5,20.

AO Serial No:	Screw 1 (HAmg/cm³)	Screw 2 (HAmg/cm³)	Screw 3 (HAmg/cm³)	Screw 4 (HAmg/cm³)	Screw 8 (HAmg/cm³)	Screw 9 (HAmg/cm³)	Average (HAmg/cm³)
f07-1762r	155.26	95.25	195.80	72.77	118.40	79.44	119.49
f07-1763l	183.16	242.04	170.26	186.42	142.38	155.38	179.94
f07-1766r	268.51	197.82	201.36	159.39	159.15	172.23	193.08
f07-1767l	86.55	171.43	83.71	121.45	115.15	121.54	116.64
f10-1047l	77.13	102.25	58.11	38.86	62.49	61.84	66.78
f10-1047r	155.21	151.15	100.92	68.28	93.12	111.54	113.37
m07-1800r	186.58	147.70	140.53	101.36	119.37	109.72	134.21
m07-1801l	104.12	159.77	81.36	83.18	58.71	97.99	97.52
m07-1810r	171.95	127.90	110.31	94.55	113.83	95.95	119.08
m07-1811l	142.87	216.07	137.53	124.75	106.36	128.28	142.65
m07-1812r	279.75	185.01	234.36	129.93	220.96	169.15	203.19
m07-1813l	155.22	198.76	105.42	133.67	100.85	153.39	141.22
m10-1044l	138.98	159.39	71.54	83.48	75.84	87.65	102.81
m10-1044r	116.22	97.24	63.67	43.54	63.88	61.39	74.32
m11-3000L	96.63	127.67	70.78	75.40	81.12	71.44	87.17
m11-3000R	187.60	144.64	124.52	106.46	117.68	126.68	134.60
m12-2200l	155.27	210.51	155.70	119.38	157.03	135.43	155.56
m12-2200r	165.78	97.19	140.39	88.58	121.27	108.82	120.34
m12-2208l	127.35	195.07	136.58	138.01	174.66	160.17	155.31
m12-2208r	135.83	95.93	91.78	88.90	127.55	120.56	110.09

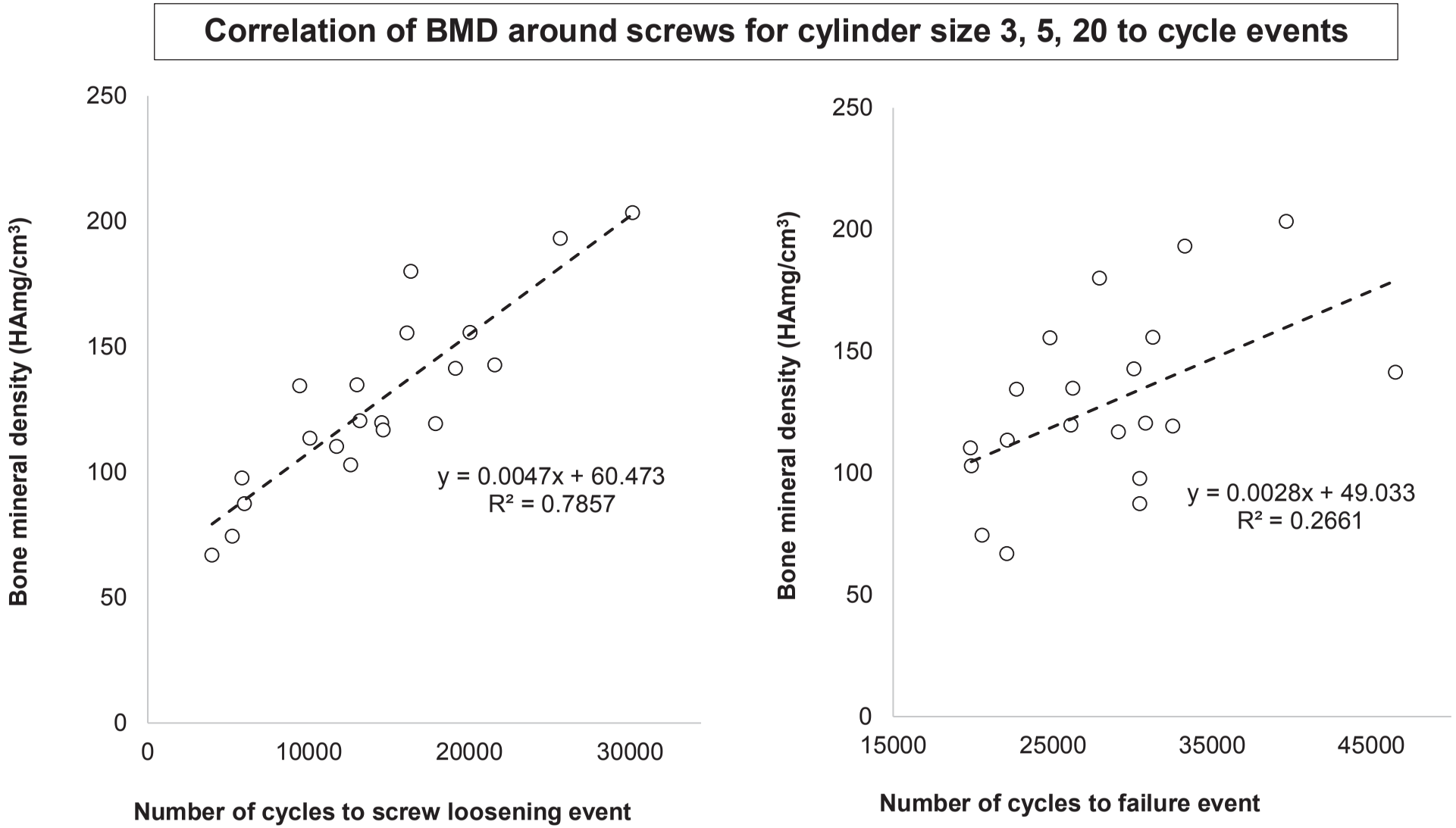

Figure F.1. Linear correlation of BMD around screws for cylinder size 3, 5, 20 to cycle events, each point represents a specimen.

Table F.3. Summary of results for BMC for cylinder size 3, 5,20.

AO Serial No:	Screw 1 (mg)	Screw 2 (mg)	Screw 3 (mg)	Screw 4 (mg)	Screw 8 (mg)	Screw 9 (mg)	Total (mg)
f07-1762r	100.51	61.60	125.60	45.29	76.15	51.11	460.3
f07-1763l	102.52	138.70	97.47	119.68	80.14	89.99	628.5
f07-1766r	155.18	118.50	111.91	98.57	82.00	97.21	663.4
f07-1767l	56.15	111.31	54.44	77.99	74.76	78.78	453.4
f10-1047l	46.67	63.02	37.79	24.74	40.48	39.64	252.3
f10-1047r	98.15	91.57	58.58	40.86	52.30	64.66	406.1
m07-1800r	114.99	90.57	86.37	64.52	66.93	67.86	491.2
m07-1801l	67.01	103.00	52.78	51.88	38.01	63.03	375.7
m07-1810r	110.97	82.70	71.24	60.45	73.97	62.23	461.6
m07-1811l	89.78	133.09	89.47	77.97	66.80	78.65	535.8
m07-1812r	170.45	114.90	142.11	83.66	124.57	101.34	737.0
m07-1813l	99.77	127.87	68.30	85.36	65.41	99.23	545.9
m10-1044l	83.97	98.15	46.21	48.27	44.58	53.98	375.2
m10-1044r	74.35	62.29	40.90	28.12	40.03	39.15	284.8
m11-3000L	62.43	82.98	46.08	48.65	52.87	46.49	339.5
m11-3000R	102.19	83.82	74.96	68.65	73.10	79.15	481.9
m12-2200l	95.70	130.30	93.85	75.55	90.37	83.23	569.0
m12-2200r	106.59	62.45	89.66	57.39	78.17	70.45	464.7
m12-2208l	77.67	116.18	88.64	87.59	102.72	91.15	564.0
m12-2208r	87.15	61.48	58.74	56.81	78.26	77.58	420.0

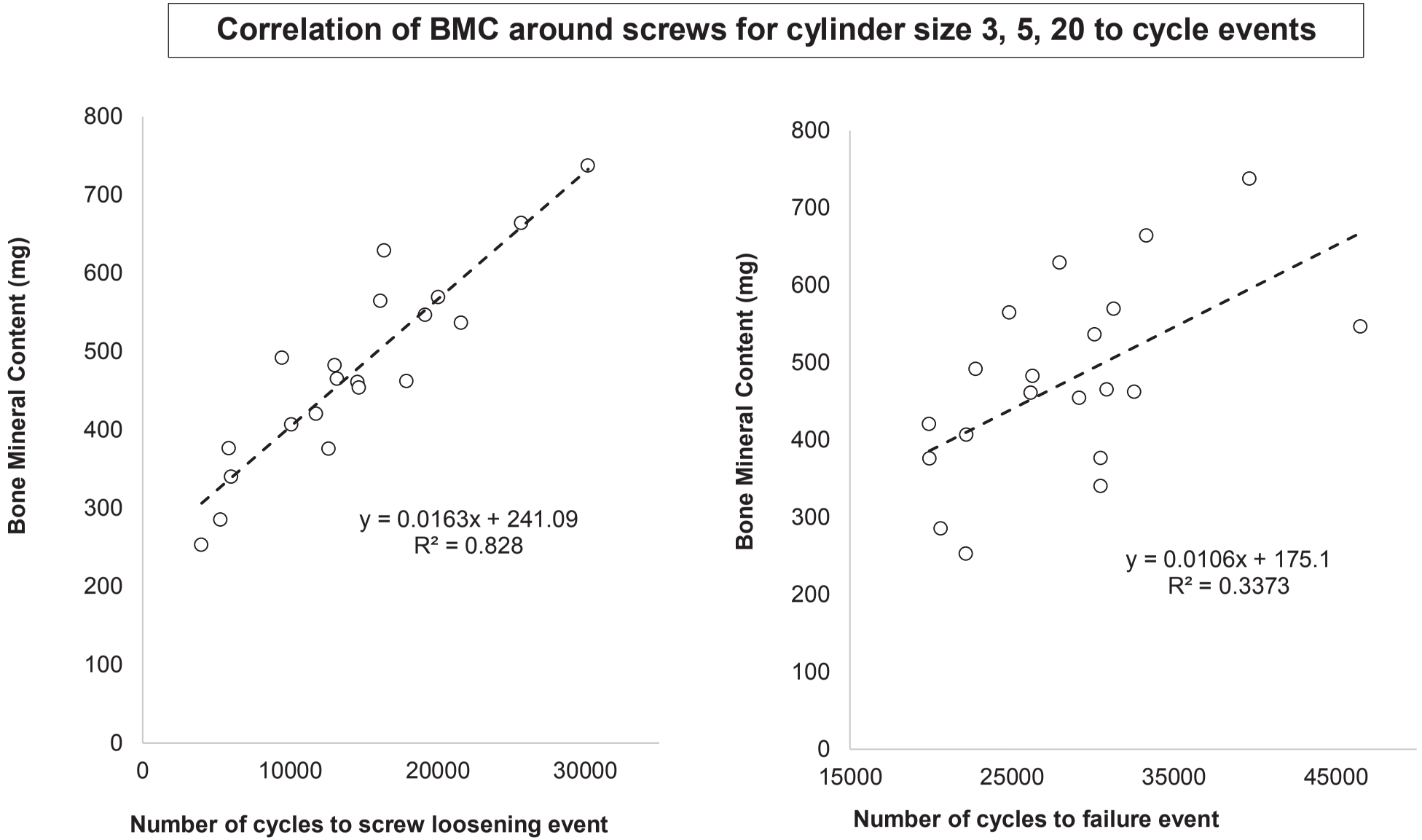

Figure F.2. *Linear Correlation of BMC around screws for cylinder size 3, 5, 20 to cycle events, each point represents a specimen.*

Table F.4. Summary of results for BMD for cylinder size 1.5, 15, 30.

AO Serial No:	Screw 1 (HAmg/cm³)	Screw 2 (HAmg/cm³)	Screw 3 (HAmg/cm³)	Screw 4 (HAmg/cm³)	Screw 8 (HAmg/cm³)	Screw 9 (HAmg/cm³)	Average (HAmg/cm³)
f07-1762r	201.15	121.52	224.52	100.97	133.91	102.43	147.4
f07-1763l	183.59	241.74	165.78	192.19	144.51	157.64	180.9
f07-1766r	276.83	198.67	201.28	155.29	154.20	176.34	193.8
f07-1767l	135.91	200.20	108.20	153.28	133.62	143.83	145.8
f10-1047l	112.03	149.59	98.76	75.53	89.54	65.68	98.5
f10-1047r	169.60	152.81	101.23	66.90	86.10	102.14	113.1
m07-1800r	185.54	138.87	140.40	101.01	114.04	112.83	132.1
m07-1801l	152.52	203.74	121.28	126.26	85.29	124.68	135.6
m07-1810r	194.67	186.34	145.50	116.91	117.22	112.99	145.6
m07-1811l	149.96	215.16	157.13	126.46	112.22	130.17	148.5
m07-1812r	287.10	183.29	242.93	131.87	226.34	170.37	207.0
m07-1813l	190.23	234.91	148.85	169.56	144.64	181.87	178.3
m10-1044l	138.95	160.57	83.63	79.19	79.75	96.99	106.5
m10-1044r	155.72	133.56	83.43	50.67	66.84	66.14	92.7
m11-3000L	110.71	165.72	107.96	98.69	120.51	100.87	117.4
m11-3000R	185.34	147.62	128.38	108.73	117.92	129.75	136.3
m12-2200l	153.41	213.47	152.69	118.83	162.71	134.47	155.9
m12-2200r	186.37	117.24	159.62	118.07	138.42	135.02	142.5
m12-2208l	127.26	194.06	142.76	133.79	171.05	151.72	153.4
m12-2208r	164.96	136.89	108.76	114.59	110.99	132.35	128.1

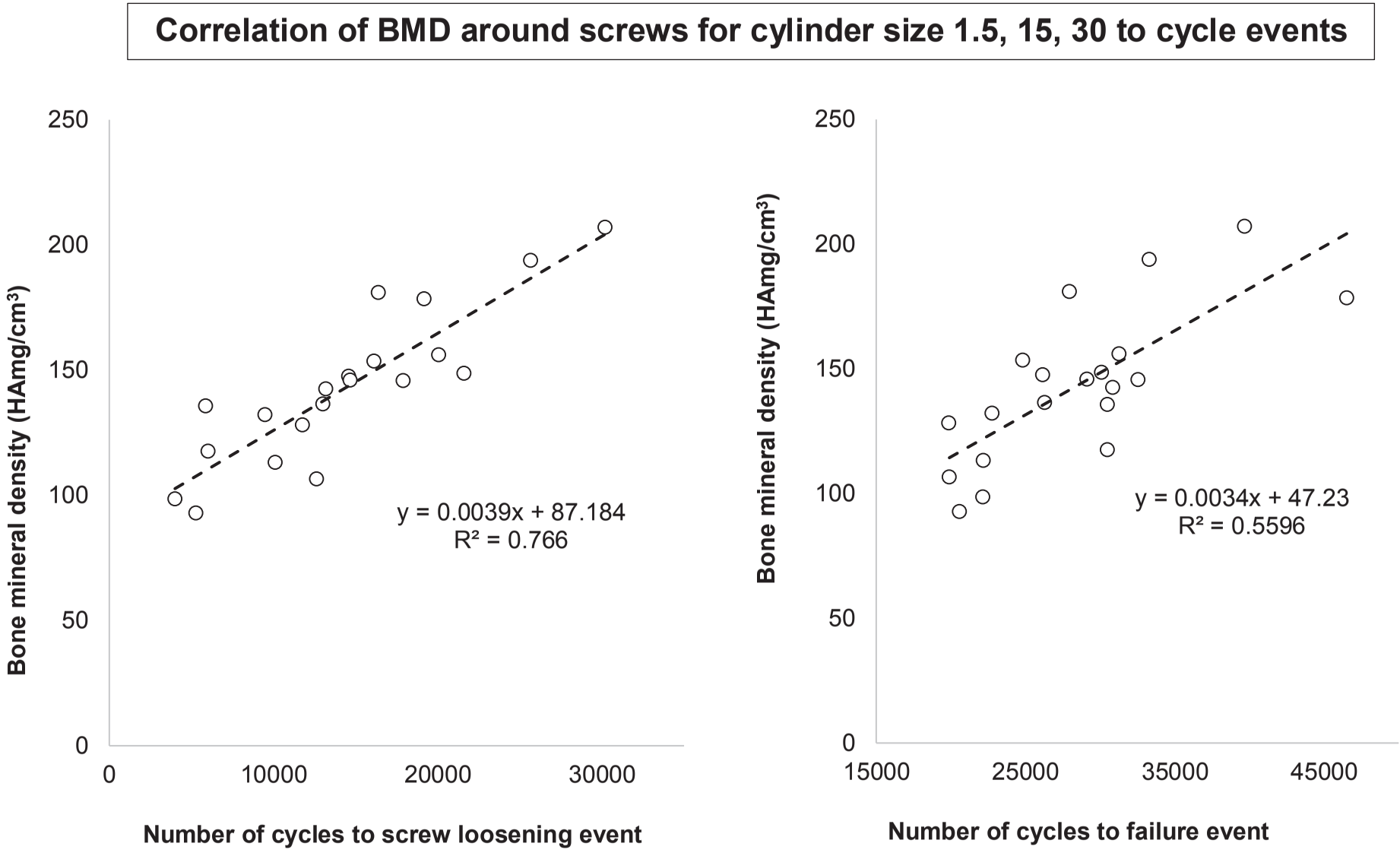

Figure F.3. *Linear Correlation of BMD around screws for cylinder size 1.5, 15, 30 to cycle events, each point represents a specimen.*

Table F.5. Summary of results for BMC for cylinder size 1.5, 15, 30.

AO Serial No:	Screw 1 (mg)	Screw 2 (mg)	Screw 3 (mg)	Screw 4 (mg)	Screw 8 (mg)	Screw 9 (mg)	Total (mg)
f07-1762r	43.76	25.45	45.02	21.18	26.47	21.32	183.2
f07-1763l	29.61	39.87	27.26	35.64	23.36	26.28	182.0
f07-1766r	45.81	34.08	31.75	27.35	20.92	28.51	188.4
f07-1767l	31.43	42.05	24.04	33.80	27.48	31.51	190.3
f10-1047l	23.08	31.36	22.55	16.39	18.86	12.91	125.2
f10-1047r	31.29	26.24	16.57	11.42	13.78	17.05	116.4
m07-1800r	32.68	24.23	24.30	18.45	18.17	20.00	137.8
m07-1801l	33.13	43.90	27.59	27.83	18.78	27.21	178.5
m07-1810r	38.30	39.29	30.56	25.30	25.18	25.05	183.7
m07-1811l	27.32	38.26	30.47	22.46	20.82	23.17	162.5
m07-1812r	49.74	32.73	41.58	24.47	36.40	29.28	214.2
m07-1813l	39.87	47.63	33.53	36.23	32.60	39.97	229.8
m10-1044l	23.76	28.04	15.85	12.98	13.33	17.22	111.2
m10-1044r	31.94	27.26	17.50	11.53	12.40	12.82	113.5
m11-3000L	21.94	35.86	24.43	19.88	27.21	21.46	150.8
m11-3000R	28.80	24.43	21.92	20.19	21.24	23.32	139.9
m12-2200l	27.11	37.64	26.31	21.34	26.57	23.78	162.7
m12-2200r	38.95	23.86	32.02	25.74	28.57	28.33	177.5
m12-2208l	22.37	33.25	27.35	24.30	28.92	24.73	160.9
m12-2208r	33.68	28.42	22.56	24.67	20.06	26.34	155.7

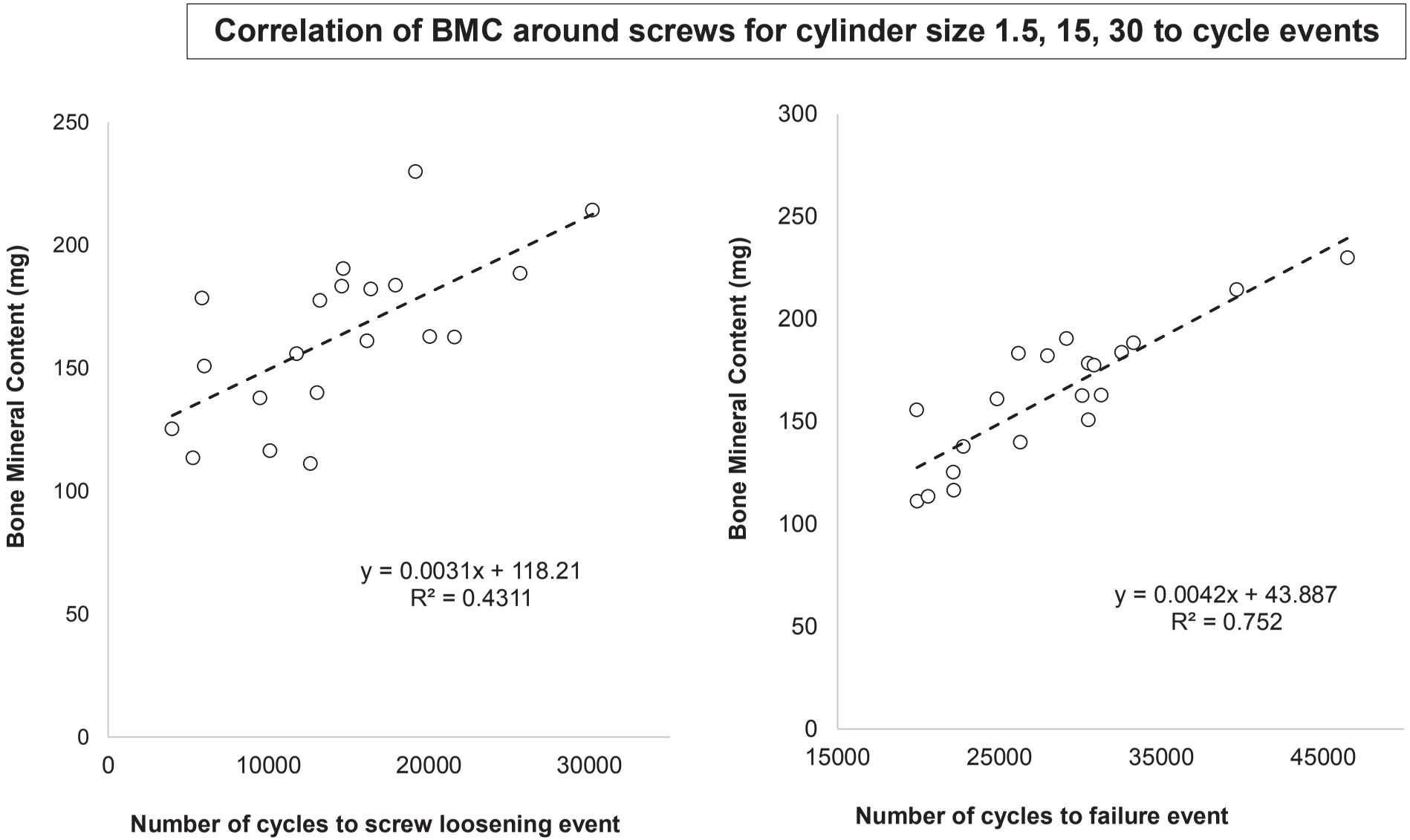

Figure F.4. *Linear correlation of BMC around screws for cylinder size 1.5, 15, 30 to cycle events, each point represents a specimen.*